HOKKAIDO UNIVERSITY

Title	Studies on land-use/land-cover change and forest fragmentation with the implications for landslide occurrence in the Garhwal Himalaya, India
Author(s)	Batar, Amit Kumar
Citation	. ( ) 12859
Issue Date	2017-09-25
DOI	10.14943/doctoral.k12859
Doc URL	http://hdl.handle.net/2115/87114
Type	theses (doctoral)
File Information	Amit_BATAR.pdf

Instructions for use

Studies on land-use/land-cover change and forest fragmentation with the implications for landslide occurrence in the Garhwal Himalaya, India

Ph.D.
Thesis

Submitted to Graduate School of Environmental Science,
Hokkaido University, Sapporo, Japan

In Partial Fulfillment of the Requirements for the Degree of
Doctor of Philosophy

By
Amit Kumar BATAR

Sapporo, Japan
August, 2017

Abstract

The Garhwal Himalaya is believed to have experienced extensive deforestation and forest fragmentation due to anthropogenic and natural drivers, but the data and documentation detailing this transformation are limited. Previous studies have examined forest fragmentation and landslide occurrence separately, and forest fragmentation has been believed to cause landslides. However, there is no study to understand the correlation between forest fragmentation and landslide occurrence. Therefore, understanding the link between forest fragmentation and landslide occurrence is important in the mountains such as the Himalaya.

Remote sensing satellite data are suitable for poorly researched area with less data availability, and can provide detailed assessment. This study, therefore, used satellite remote sensing and geographic information system (GIS) to create a spatial inventory of land-use and land-cover (LULC), and to examine forest fragmentation and landslides in the Garhwal Himalaya. Then, an evaluation on how potential change of forest fragmentation would result in changes of landslide susceptibility and vice versa. Three images from Landsat 2 Multispectral Scanner System (MSS), Landsat 5 Thematic Mapper (TM), and Landsat 8 Operational Land Imager (OLI) were used to extract land cover. A cross-tabulation detection method in a GIS module was used to detect land cover changes during the 1st period (1976–1998) and the 2nd period (1998–2014). The landscape fragmentation tool LFT v2.0 was used to prepare a forest fragmentation map and to analyze the patterns and changes of the forest fragmentation during the 1st period (1976–1998) and the 2nd period (1998–2014). Using the weight-of-evidence (WOE) model, the relationship between the forest fragmentation and the landslide occurrence was established to identify the potential change of forest fragmentation and landslide susceptibility in the study area.

The results of this research showed that the overall annual rate of decreasing change in the forest cover was 0.22% and 0.27% in the 1st period (1976–1998) and the 2nd period (1998–2014), respectively. Non-forest area, i.e., agriculture land, built-up area, scrub land and barren land, had increased in both periods of time. An increase in the areas of scrub land and barren land also contributed to the accumulation of wasteland in the area. The forest fragmentation analysis showed that a large core forest has decreased throughout the study period. The results of forest fragmentation showed that the increased non-forest and perforated areas were the main cause of the decline in the large core forest. The total

area of the forest patches also increased during the study period (1976–2014).

The result of the weighted contrast value showed that the forest fragmentation probability was primarily observed near built-up area (less than 500 m), agriculture land (less than 500 m), roads (less than 1000 m), and streams (less than 500 m) with very gentle and gentle slopes (less than 25 degree) at the lower to middle altitude zone (less than 2000 m). The probability map of the forest fragmentation showed that medium to high probabilities are primarily concentrated near the roads and agriculture land area on very gentle to gentle slopes at the lower altitudes. The probability map of the forest fragmentation also showed that the role of higher altitude zone (more than 2000 m) is less significant, and that factors such as distance to roads, distance to agriculture land, distance to built-up area and slopes are more important. The analysis of the forest fragmentation probability suggested that the area would experience more forest fragmentation in the future due to the increased areas of patch forest and perforated forest, meaning the increase in the forest degradation.

Regarding the landslide susceptibility, the result clearly showed that medium to high landslide susceptibilities had occurred mainly in the non-forest area. The result of the weighted contrast value showed that most of the medium to high landslide susceptibilities are primarily concentrated in the areas adjacent to higher altitudes, steep slopes, and the non-forest area such as scrub land, barren land, and pasture land.

Regarding potential change in the forest fragmentation probability and the landslide susceptibility, the result demonstrated that the forest fragmentation probability was observed in the areas where landslides are less likely to occur. The probability of landslides would not give a major influence on forest fragmentation and vice versa, which was suggested for the first time by the approach with the combination of both forest fragmentation and landslide occurrence.

Acknowledgements

Table of contents

2.4 Methods

List of tables

List of appendices

Chapter 1
Introduction

1.1 Background information

Mountains are among the most fragile environments on earth. Ecosystems in many mountains, including the Himalaya, which is one of the most unstable and fragile mountain areas in the world, are strongly affected by drivers of global change such as land use and climate change (Ives and Messerli, 1989; Lambin et al., 2001; Miehe, 2009; Macchi and ICIMOD, 2010; Shrestha, 2012; Joshi et al., 2012). Environmental degradation such as deforestation and forest degradation of the Himalayan region are the major environmental issues of global significance and some of the most intensively studied land use change processes (Ives and Messerli, 1989; Singh and Singh, 1991; Tiwari, 2008). Despite the fact that the Indian Himalayas are recognized as one of the global biodiversity hotspots, forest cover is under pressure from extensive and rapid land cover change due to anthropogenic and natural drivers (Meyer and Turner, 1992; Gupta, 2013; Tiwari and Joshi, 2014). At the same time, the Himalayan region is vulnerable to numerous types of hazards, such as landslides, extreme rainfall events, flood, and forest fire, which further deteriorate the mountain landscape and forest ecosystem (Lasch et al., 2002; Jasrotia and Singh, 2006).

From an ecological perspective, mountain forest ecosystems are of particular significance, as they not only provide goods and services that are essential to maintain life-support on both local and global scale but also play defining role for greenhouse gas regulation, nutrient cycling, genetic and species diversity. (Beniston, 2003; Nagendra et al., 2004; Sivrikaya et al., 2007). Mountain ecosystems are continuously experiencing extensive land-use and land-cover (LULC) changes, due to natural and anthropogenic processes (Klein, 2001; Agarwal et al., 2002; Liu et al., 2003). These changes have not only led to modifications in forest ecosystem, but also to the conversion of land cover, with serious environmental implications (Hansen et al., 2001; Lung and Schaab, 2010). Changes in forest cover can result in a variety of negative environmental consequences (Malek et al., 2015). For example, deforestation can affect the vegetation composition and water balance and can increase erosion rates (Glade, 2003; Ghimire et al., 2013). This leads to increased environmental risks, such as landslide occurrence, and can have strong impacts on the human well-being on a larger scale (Tasser et al., 2003; Papathoma-Kohle and Glade, 2013). Landslide triggered by natural factors such as rain/snow or earthquake

(Keefer, 1984; Dai et al., 2002; Malamud et al., 2004; Dahal et al., 2006), as well as human activities such as built-up expansion, agriculture expansion, deforestation, unplanned and poor road construction or inadequate road maintenance (Glade, 2003; Tropeano and Turconi, 2004; Van Beek and Van Asch, 2004; Gorsevski et al., 2006; Wang and Niu, 2009; Raghuvanshi et al., 2014). Dai et al., (2002) and Glade, (2003) studied that deforestation and construction of road and buildings in the mountainous terrain are the major triggering factors for landslide occurrence. It is also important to understand that these landslides have not only caused large-scale human tragedies and material damage, (Schuster and Fleming, 1986; Keefer, 2000; Mario and Jibson, 2000; Dai et al., 2002; Kanungo et al., 2006; Pan et al., 2008) but also, resulted negative effects on forests, protected areas leading to LULC change, especially in landslide-prone areas (Greenway, 1987; Glade, 2003; Vanacker et al., 2003; Meusburger and Alewell, 2008; Karsli et al., 2009; Van Den et al., 2009; Yi et al., 2010; Bruschi et al., 2013).

In Indian Himalayan region (IHR), forests are one of the most important natural resources (Zeng et al., 2008), being recognized for having vital benefits in socio-economic development and conservation of biodiversity (Li et al., 2009; Cabral et al., 2010). Also, forests have an important role in maintaining the volume of river water in dry seasons, replenishing ground-water and supporting agriculture (Singh, 2006; Singh and Sharma, 2009). Forests are mainly used for fuel wood and fodder (Bazilian et al., 2011), timber for construction (Pandit and Kumar 2013), livestock grazing, and medicinal and recreational purposes in this region (Rasul, 2010). Overexploitation of these forest products have caused severe degradation to natural forest ecosystems and rich biodiversity of the region (Ives and Messerli, 1989). The degradation can be represented by alteration in forest landscape patterns, including reduction of forest patches (Onojeghuo and Blackburn, 2011), fragmentation of forest into small sizes (Coops et al., 2004; Tang et al., 2008) and the isolation of forest areas (Sharma et al.,2001; Sharma and Roy, 2007).

Forest loss and fragmentation are distinct but related phenomena. Forest loss is simply the conversion of forestland to some other land use, but forest fragmentation occurs when a large region of forest is broken down, or fragmented, into a collection of smaller patches of forest habitat (Fahrig, 2003; Collingham and Huntley, 2013). Forest landscape is at high risk of forest fragmentation because of changes in LULC due to processes such as agricultural intensification, logging, and infrastructure development. These changes have led not only to the loss of habitat and biodiversity, but also to the modification of natural

2

landscape and ecosystem functions (Lambin et al., 2003; Foley, 2005; Fischer and Lindenmayer, 2007; Lele and Joshi, 2009; Leal et al., 2012; Biswas and Khan, 2013). The anthropogenic drivers and their impact on natural resources such are widely documented across the Hindu Kush Himalayan (HKH) region (Sundriyal and Sharma, 1996; Chettri et al., 2002; Bawa et al., 2007; Khan et al., 2012; Tiwari and Joshi, 2014), although non-anthropogenic drivers such as natural hazards also contribute to forest fragmentation (Huebner and Randolph, 1995). However, very few studies have been conducted to understand the correlation between natural hazards and forest fragmentation. Therefore, understanding the link between natural hazards and forest fragmentation at different scales is also important for implementing conservation strategies for proper land management in mountain region such as the Himalayas.

1.2 Research objectives

The objectives of this study are:

1. To understand the spatial-temporal trends in land-use and land-cover (LULC) change from 1976 to 2014,
2. To evaluate the forest fragmentation due to the LULC change from 1976 to 2014,
3. To establish the relationship between forest fragmentation and the occurrence of landslides, and,
4. To identify the potential change of forest fragmentation with implication for landslide occurrence.

1.3 Study area

1.3.1   Background issues of the Garhwal Himalaya and the study area

The Garhwal Himalaya situated in the western part of the Uttarakhand Himalaya is one of the hotspots of biodiversity (Chandra et al., 2010). Extensive deforestation and forest fragmentation in the Garhwal Himalaya have caused serious environmental degradation (Ives and Messerli, 1989; Roy and Tomar, 2000), which is a critical issue in the Uttarakhand Himalaya and the basic reason for biodiversity loss (Sharma and Roy, 2007). During the three decades from 1967 to 1997, the forest cover in the Garhwal Himalaya has altered drastically due to increasing population pressure, increased agricultural activities and extraction of natural resources (Wakeel et al., 2005). Natural resource

3

extraction from the forests have exceeded sustainable limits and this has become a cause of serious concern for the government and the people of India (FSI, 2004). According to data from the Ministry of Environment and Forests (MoEF), 44,868 hectares of forest land have been changed to non-forest use in Uttarakhand since 1980, 9500 hectares of which have been converted for the construction of roads, followed by 5500 hectares for hydro-projects and 3100 hectares for transmission lines. Agriculture is the main occupation of the people of the Garhwal Himalaya. About 70% of the population is directly or indirectly employed in the agriculture sector (Sati, 2012), which may lead to the overexploitation of natural resources in the region. Not surprisingly, the fragile nature of the Garhwal Himalaya, coupled with increasing human activity, poses a serious threat to the natural landscape, especially for the forest ecosystem. Therefore, forest cover has been under pressure over the past few decades in the region.

The present study focuses on the Rudraprayag district of the Uttarakhand state, situated in the Garhwal Himalaya (Figure 1.1). The Rudraprayag district has been continuously experiencing extensive forest loss, due to agriculture expansion and infrastructure development. The forest in this area has been utilized for hydroelectric projects (62.93 hectares), roads (187.52 hectares), and other activities (299.08 hectares) (Srivastava, 2017). On the other hand, natural hazards such as floods, landslides, and forest fires have increased over the last few decades and may lead to further deterioration of the forest landscape in the study area (Gupta et al., 2013). For example, a vegetation cover mapping was done at the National Remote Sensing Centre (NRSC) for the flood affected area in the Mandakini river between Kedarnath to Rudraprayag during the 16th and 17th of June 2013. The assessment shows that vegetation cover has changed at 50 locations. The loss of forest cover was 46 hectares and the loss of grassland cover was 124.9 hectares in the Rudraprayag district. Recently, in 2016, a study was conducted by the Forest Department of Uttarakhand, which was related to the forest fire in Uttarakhand. According to the report, 79 locations experienced forest fires, and the loss of forest cover was 157.20 hectares between April and May 2016.

The Rudraprayag district is also a part of high earthquake zone because the main central thrust passing this region and one of the most visited pilgrim site (Kedarnath Temple) in India. The Rudraprayag district, where Kedarnath is situated has already faced the problem of natural disasters 8 times in the last 34 years (Rautela and Thakur, 1999; Rautela et al., 2014). In the monsoon period (June–September), the highways, which are the important main routes to the pilgrim site (Kedarnath Temple) are influenced by

4

landslides. Some of the major natural hazards includes landslides that occurred in Agastmuni (2005 and 2006), Jakholi (2010), Ukhimath (2010, 2012 and 2013); floods occurred in Vijaynagar (2005) and Kedarnath (2013).

1.3.2 Baseline information

As per the report of Central Ground Water Board (CGWB), the Rudraprayag district did not existed as a separate entity but was comprised in Chamoli and Pauri districts before 1997. On 18th September 1997, the Rudraprayag district was established, which includes Okhimath tehsil, Jakholi sub-tehsil from Tehri district and Bacchansyon and Dhanpur Patti of Srinagar tehsil of Pauri district. The study area, i.e., the Rudraprayag district is a part of a vulnerable zone in the Garhwal Himalaya of the Uttarakhand state of India. It extends from 30° 12' 58" N to 30° 48' 47" N latitude and 78° 50' 07" E to 79° 22' 34" E longitude. The geographical area of the Rudraprayag district is around 1936.06 km^2. The district is bounded by Uttarkashi in the north, Chamoli in the east, Tehri Garhwal in the west and Pauri Garhwal in the south (Figure 1.1).

The altitude varies from 546 to 6840 m above sea level (Figure 1.1). As per the report of Disaster Mitigation and Management Centre (DMMC), the Rudraprayag district is a land of deep valleys, high ridges, and steep mountains. It is comprised of two main tectonic units, viz. Garhwal group and Central Crystalline group, and covers two sections of the Himalaya: the Lesser Himalaya and Greater Himalaya (Kumar and Agrawal, 1975; Kumar, 2005).

Mandakini is the major river of the Rudraprayag district, with a catchment area of 1641.64 km^2, and it has many tributaries. It originates from the Chorabari glacier (3895 m) (Figure 1.1). The mean air temperature in winter (December to February) varies from 8.32 to 13.15°C and that in summer (May to July) from 27.75 to 32.54°C (Rautela et al., 2014).
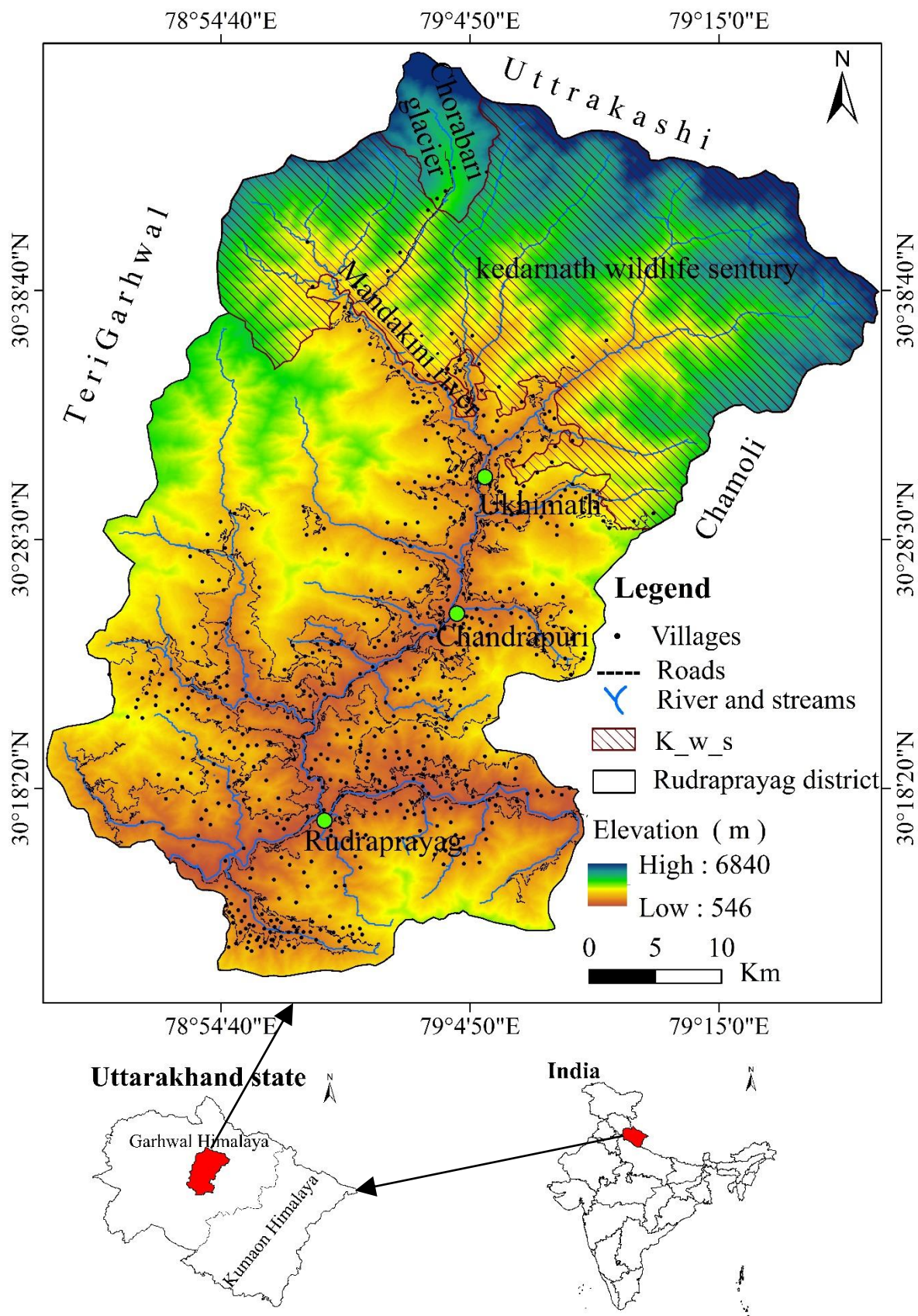
Figure 1.1. Location and extent of the Rudraprayag district, Uttarakhand, India.

In the study area, rainfall is highly variable depending upon the altitude. In the southern part of the district at Rudraprayag, the average annual rainfall is around 1220 mm, while in the central part at Chandrapuri, the average annual rainfall is 1751 mm, and the rainfall in the northern higher part at Ukhimath is 1995 mm (Rautela et al., 2014). The overall average rainfall in the district is 1485 mm. Most of the rainfall (70–80% of annual precipitation) occurs from June to September.

The major crops and horticulture of the Rudraprayag district are given in Table 1.1. Agricultural activities are restricted on river terraces, gentle hill slopes, and intermountain valleys. Most of the population are engaged in agricultural activity in order to earn their livelihood. Therefore, agriculture is the primary occupation of the people. The Rudraprayag district is famous for an important pilgrim site (Kedarnath Temple) in India. Therefore, tourism is another important livelihood option for the local people during the tourist season in the Rudraprayag district.

Table 1.1. Major field crops and horticulture of the Rudraprayag district

Season		Major field crops cultivated
Kharif	Cereals	Paddy, Figermillet, Barnyard millet, Maize, Amaranthus
	Pulses	Black gram, Horse gram, Pigeon pea, French bean, Soybean (Black)
	Oil Seeds	Soybean, Sesame
Rabi	Cereals	Wheat, Barely
	Pulses	Gram, Pea, Lentil
	Oil Seeds	Mustard
	Horticulture crop-fruits	Temperate fruits (Apple, Plum, Pear, Peach etc.)
		Citrus (Malta, Orange etc.)
		Dry fruits (Walnut, Almond etc.)
		Other (Mango, Litchi, Guava, Anar etc.)
	Other Horticulture crops	Vegetables
		Spices
		Flowers

Source: National Innovations in Climate Resilient Agriculture (NICRA) (2009).

The Kedarnath wildlife sanctuary has a total area of 975 km^2, out of which 645 km^2 is covered by the Rudraprayag district (Figure 1.1). It had been a notified reserve forest between 1916 and 1920. Its status was changed to a sanctuary on 21 January, 1972 and now falls under management category IV (Managed Nature Reserve) of the International Union for Conservation of Nature (IUCN). It is one of the largest protected areas in the Uttarakhand (Bhat et al., 2013). Over 175 villages are located along the southern boundary of the sanctuary, whose inhabitants depend substantially on its resources for fuel wood, fodder, medicinal plants and pastures for livestock grazing (Kittur and Sathyakumar, 2010). IUCN has reported that 44.4% to 48.8% of the sanctuary is forest, 7.7% comprises alpine meadows and scrub, 42.1% is rocky or under glaciers and permanent snow, and 1.5% represents formerly forested areas that have been degraded.

The population of the Rudraprayag district is increasing, but, compared to the other district of Uttarakhand, it is low. According to the 1991, 2001 and 2011 census, the Rudraprayag district had populations of 198,672 persons, 227,439 persons, and 236,857 persons, respectively, and its population growth rate over the decades of 1991 to 2001 and 2001 to 2011 was 14.4% and 4.14%, respectively. According to the 2001 and 2011 census, the population density was 115 persons per km^2 and 119 persons per km^2, respectively. Figure 1.2 shows the population density of the Rudrapryag district from 1990–2015 through Socioeconomic Data and Applications Center (SEDAC) online (http://sedac.ciesin.columbia.edu) data portal provided by National Aeronautics and Space Administration (NASA).

Roy et al., (2015) prepared vegetation type of India (Scale 1:50,000) using medium-resolution (spatial resolution 23.5 m) IRS (Indian Remote Sensing) LISS-III (Linear Imaging Self Scanning Sensor) images. The digital map is now available through a web portal (http://bis.iirs.gov.in). The vegetation type map of the Rudraprayag district is shown in Figure 1.3.

Figures 1.4 and 1.5 show the forestline in 2014 in the Rudraprayag district. The relation to their elevation range is shown in Figure 1.6. The forestline in 2014 in elevation range was found to be 3000–4000 m.
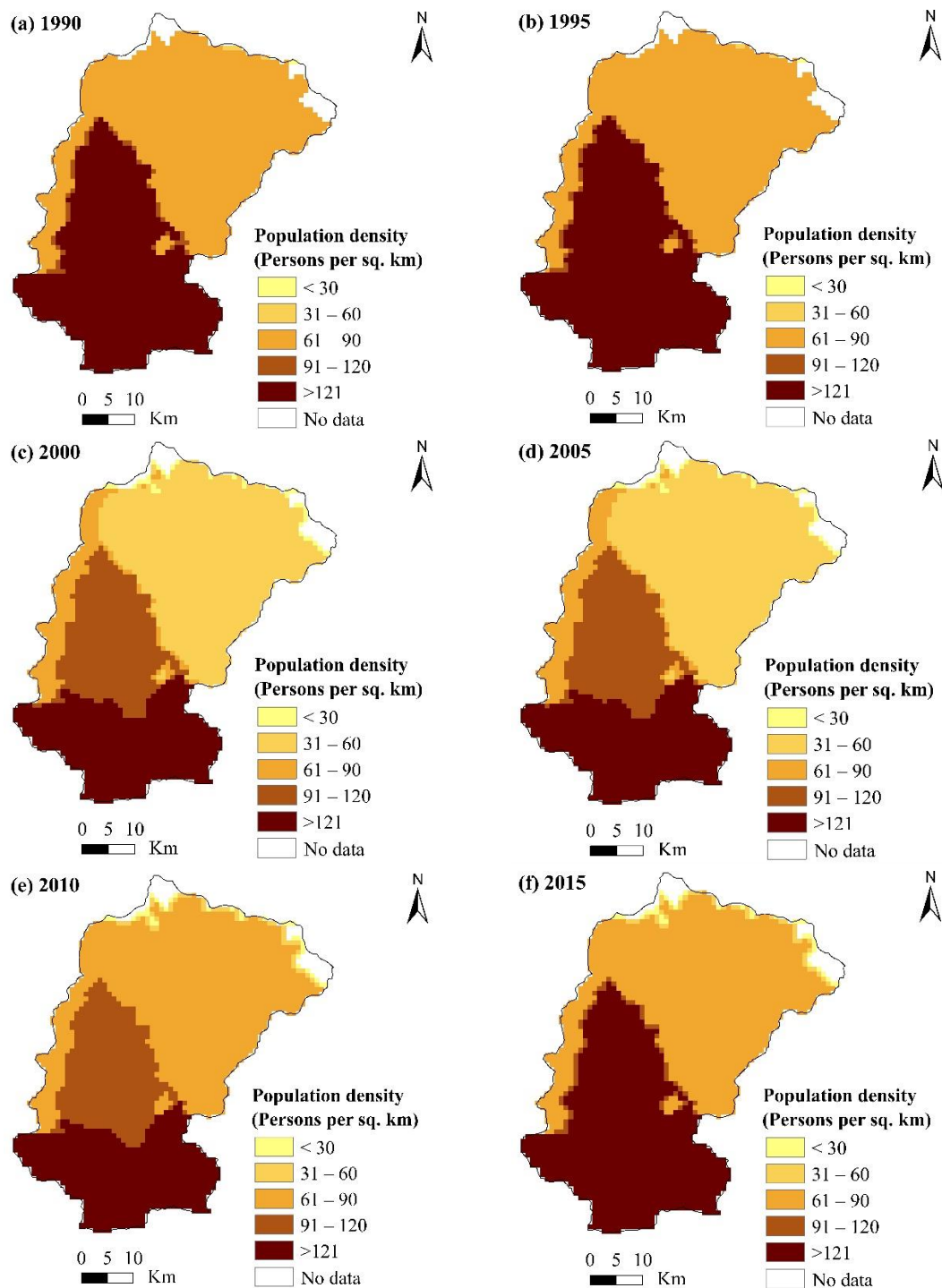
Figure 1.2. Population density for the years **a)** 1990, **b)** 1995, **c)** 2000, **d)** 2005, **e)** 2010, **f)** 2015. The data are gridded at a resolution of 30 arc-seconds.

Source: Central for International Earth Science Information Centre (CIESIN), International Food Policy Research Institute (IFPRI), the World Bank, and Centro International de Agriculture Tropical (CIAT). Global rural-urban mapping project (GRUMPv1 & GPWv4): Socioeconomic Data and Applications Center (SEDAC), NASA.

Legend

■	Himalayan moist temperate	■	Degraded forest	■	Agriculture
■	Sub alpine	■	Scrub	■	Barren land
■	Tropical sal mixed moist deciduous	■	Dry evergreen scrub	■	River bad
■	Temperate coniferous	■	Dry deciduous scrub	■	Water bodies
■	Sal.	■	Ziziphus sp.	■	Settlement
■	Pine	■	Dry alpine scrub	■	Snow
■	Oak	■	Wet grasslands		
■	Mixed plantation	■	Moist alpine pasture		
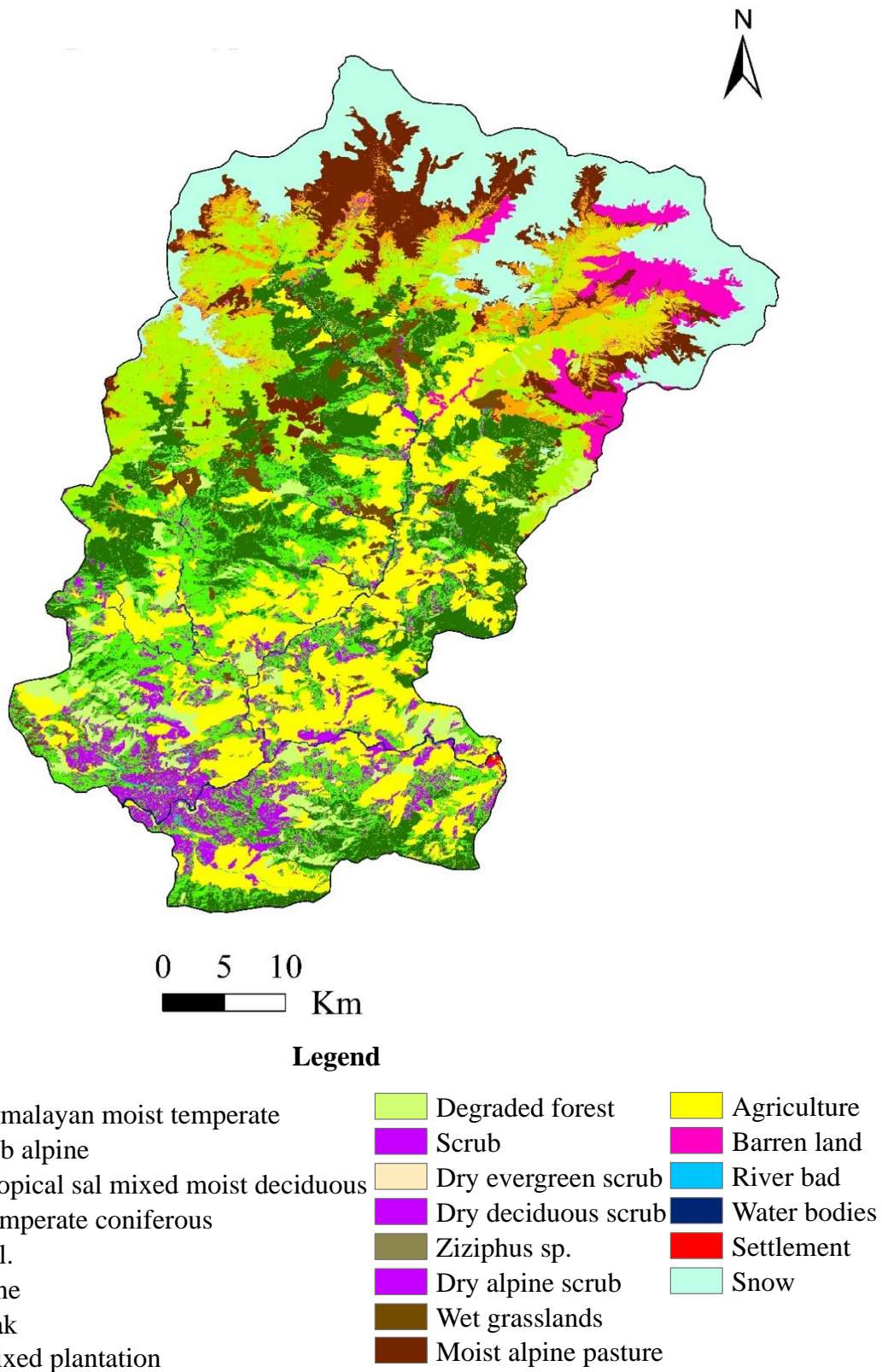
Figure 1.3. Vegetation type map of the Rudraprayag district, 2015.

Source: Roy et al., (2015) (available at http://bis.iirs.gov.in).

10

Figure 1.4. Forestline of the Rudraprayag district in 2014. The forestline was derived using land-cover map 2014, digital elevation model (DEM), slope angle and slope aspect. Base map: prepared by the author.
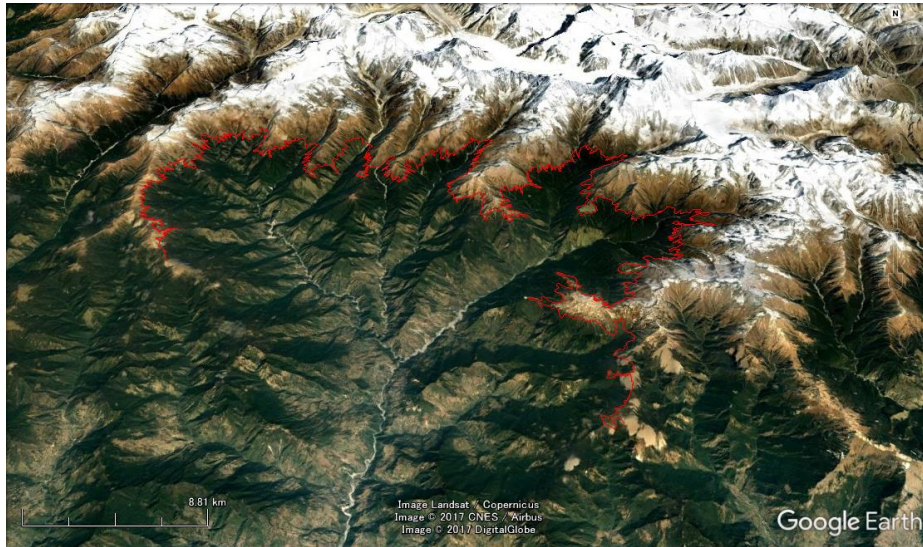
Figure 1.5. The distribution of forestline in 2014 shown in red line (Base image: Google Earth®).
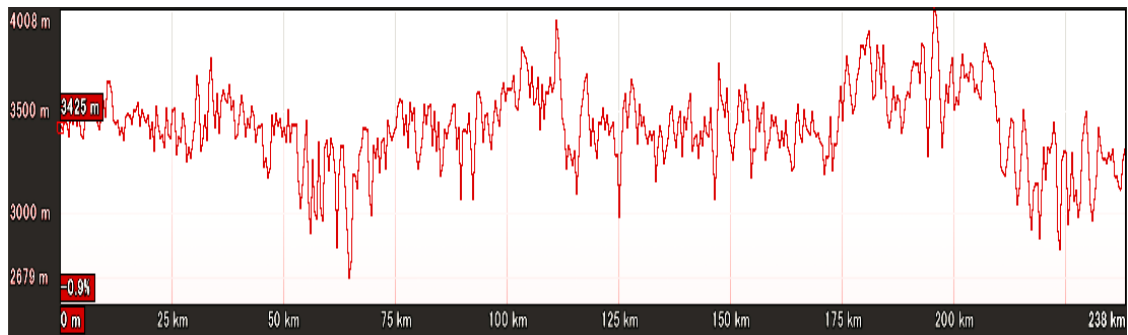
Figure 1.6. The forestline in 2014 in relation to elevation range of the Rudraprayag district.

1.4 Justification and significance of the study

Studying how human-environment interactions change forest cover is essential. The dynamics of land-use and land-cover (LULC) change, forest cover change and the forest fragmentation process and their drivers in the Himalayan region are well documented as described in the previous section (1.3.1). However to our knowledge no study has been conducted to understand the correlation between natural hazards and forest fragmentation. Therefore, understanding the link between natural hazards and forest fragmentation is needed for implementing conservation strategies for proper land management in mountain regions such as the Himalayas. So far, very few attempts have been made to characterize the processes of LULC change in the study area. This study contributes to

12

the understanding of the spatio-temporal trends in LULC change, pattern of forest fragmentation, changes of the forest fragmentation pattern caused by LULC change as well as potential change of forest fragmentation in the zone of landslide susceptibility and vice versa. Finding the areas where changes have occurred in term of LULC and forest fragmentation will help to fill the gap that leads to prioritization in forest management, conservation, and biodiversity policies.

1.5 Outline of the thesis

This thesis contains eight chapters. Chapter 1 describes the background information of the research, objectives, study area, justification and significance of the study, and outline of the thesis itself. Chapter 2 presents methodologies employed in this study, which includes: the remote sensing data used, methods for land-cover mapping, forest fragmentation mapping, data preparation and methods for forest fragmentation probability and landslides susceptibility as well as the validation of forest fragmentation probability and landslides susceptibility. Chapter 3 examines the status of land-cover in the study area, and change of LULC from 1976 to 2014, as well as change trajectories, gain and loss of LULC from 1976 to 2014. Chapter 4 examines the status of forest and non-forest area and forest fragmentation and change of forest and non-forest and forest fragmentation from 1976 to 2014 in the study area. Chapter 5 focuses on forest fragmentation probability mapping and validation of forest fragmentation probability map, as well as analysis of forest fragmentation probability. Chapter 6 focuses on landslide susceptibility mapping and validation of landslide susceptibility map, as well as analysis of landslide susceptibility. Chapter 7 discusses the discussion on the work presented the previous chapters, with LULC change, forest fragmentation, forest fragmentation probability, landslide susceptibility and observed potential change of forest fragmentation in zone of landslide susceptibility classes. Finally, Chapter 8 presents the general conclusions of the study.

Chapter 2
Research methodology

2.1 Data preparation for land-use and land-cover (LULC) change and forest fragmentation

2.1.1 Satellite remote sensing

Satellite remote sensing and geographical information system (GIS) have emerged as a powerful tools to create spatial inventory on natural resources and play crucial roles in monitoring and analyzing of spatial and dynamic assessment of an area (Mondal et al., 2015). In this study, three cloud-free satellite images from Landsat 2 (MSS), Landsat 5 (TM), and Landsat 8 (OLI) from the USGS server were used for land cover maps (Figure 2.1). These images were selected on the basis of their availability and the quality of the datasets for the study area. Table 2.1 summarizes the details of the satellite data used in this study.

Table 2.1. Details of satellite data used in this study

Satellite	Sensor	Path/Row	Spatial Resolution (Meters)	Date of Acquisition	Sources
Landsat 2	MSS	156/39	60	11/19/1976	USGS**
Landsat 5	TM	146/39	30	11/12/1998	USGS
Landsat 8	OLI*	146/39	30	11/24/2014	USGS

* OLI: Operational Land Imager, **USGS: United States Geological Survey.

14

（a）

N

Legend

RGB

Red: Band_3

Green: Band_2

Blue: Band_1

0   5   10
Km
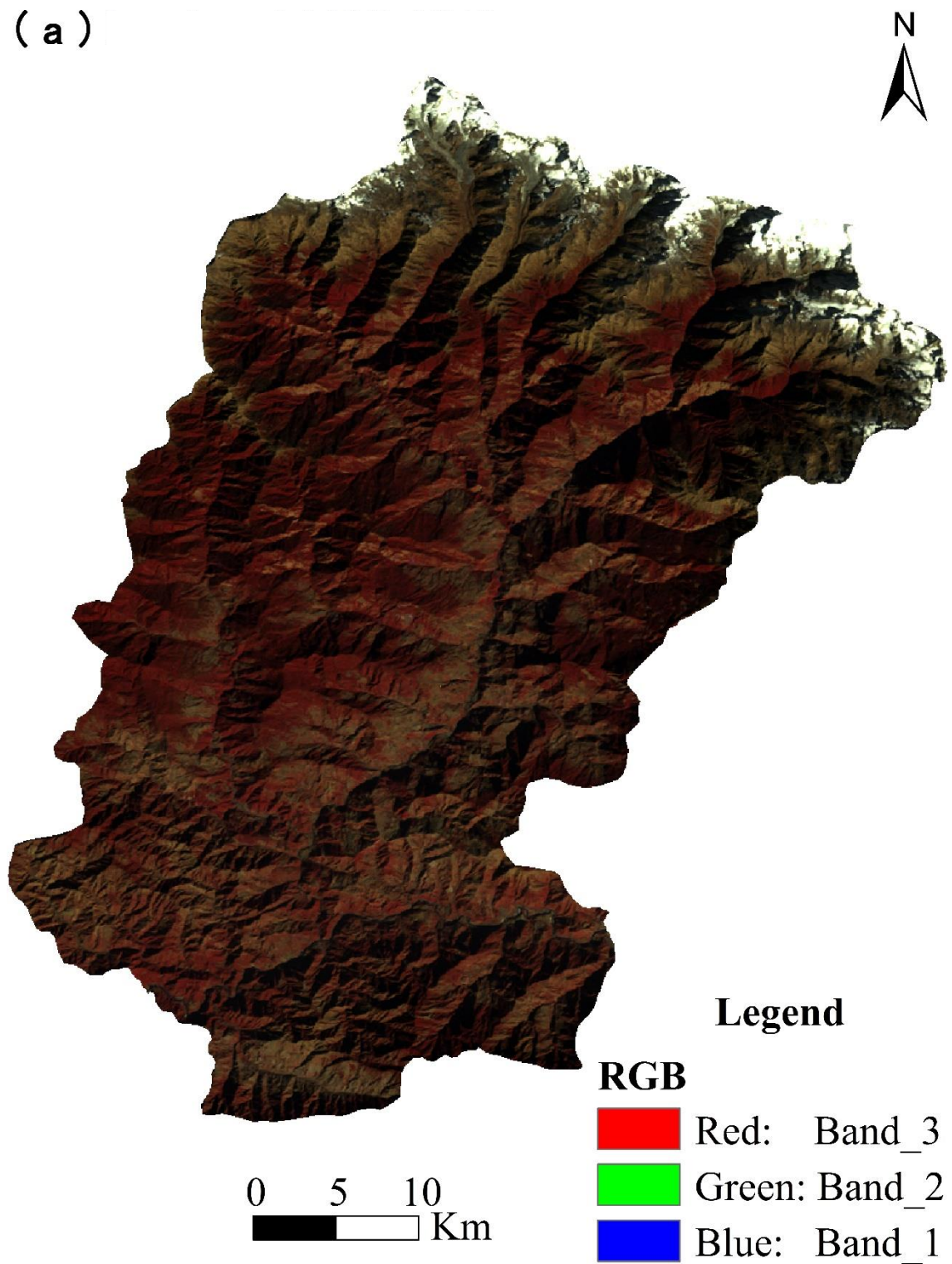
Figure 2.1. Temporal satellite image of study area: **(a)** Landsat 2 MSS of 1976.
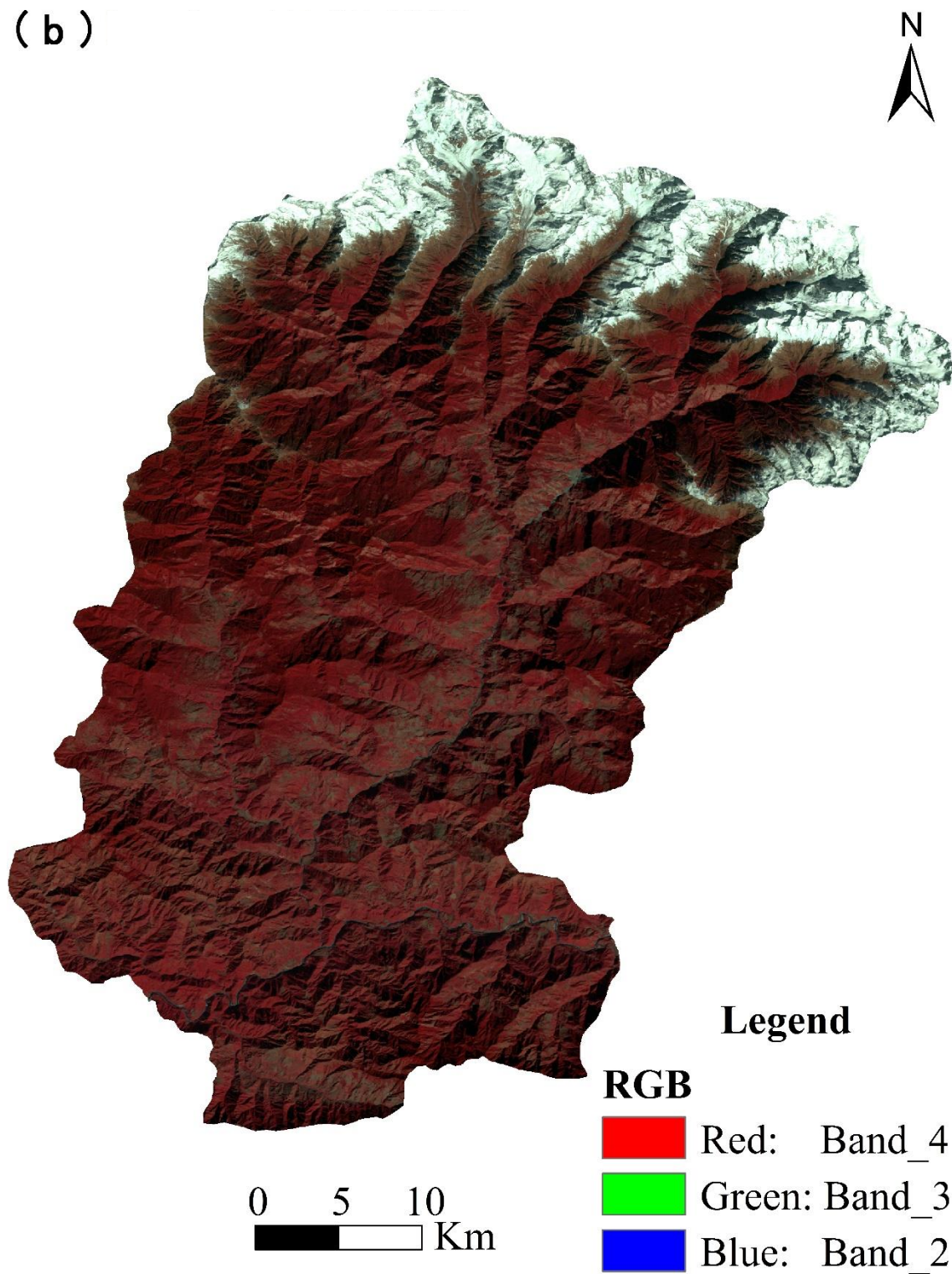
Figure 2.1 (continued). Temporal satellite image of study area: **(b)** Landsat 5 TM of 1998.

（c）

N

Legend

RGB

Red: Band_5

Green: Band_4

Blue: Band_3

0   5   10
Km
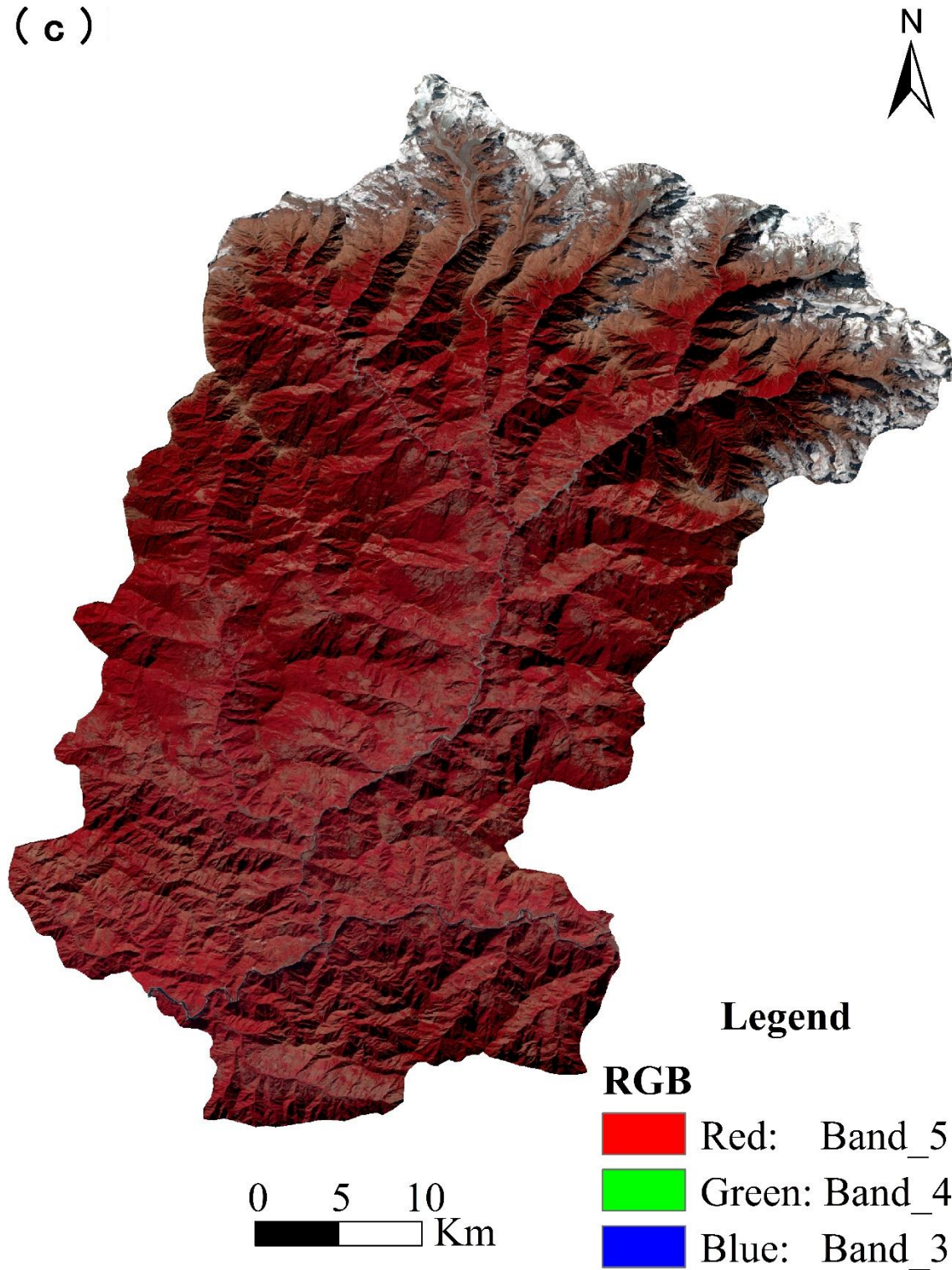
Figure 2.1 (continued). Temporal satellite image of study area: **(c)** Landsat 8 OLI of 2014.

2.2 Data preparation for forest fragmentation probability mapping

2.2.1 Patch forest

To obtain a final forest fragmentation probability map, patch forest that are completely degraded forests were considered as an evidence to apply weight-of-evidence (WOE) method. Patch forests were extracted from forest fragmentation map using analyst tools in ArcGIS.

2.2.2 Forest fragmentation causative factors

Despite the fact that anthropogenic activities are responsible for forest fragmentation, it is assumed that both natural and human drivers are responsible for forest fragmentation in this highly vulnerable region. Therefore, factors of topographic and human activities were considered to obtain final forest fragmentation probability map. Based on previous studies and data availability, causative factors such as slope angle, slope aspect, distance to streams, distance to roads, distance to agriculture land, distance to built-up area, and altitude zones were considered. On the other hand, other factors (such as temperature, landslides and floods) could not be used due to the lack of complete and reliable data, even though their potential influence may be important. Map layers depicting altitude zone, slope angle, slope aspect, and distance to streams, were derived from 10-m resolution stereoscopic Cartosat-1 data digital elevation model (DEM) provided by Indian Space Research Organization (ISRO), and roads were extracted from BHUVAN open data web portal provided by ISRO, Landsat 8 OLI satellite data provided by USGS. The descriptions of the preparation procedure of each data layer are provided below.

The slope angle and slope aspect are derived from a 10-m digital elevation model (DEM) extracted from the stereoscopic Cartosat-1 data using the ArcGIS. Distance to streams produced from DEM by hydrology tools in ArcGIS. The layers of distance to streams, distance to built-up area, distance to agriculture land and distance to roads were calculated by Euclidean distance system in spatial analyst tools of ArcGIS. Landsat 8 OLI satellite image was used for producing agriculture land and built-up area. The altitude zone map was produced in accordance with the Indian Metrological Department (IMD). All data were converted to raster format with the same pixels and each raster was divided into several classes. Figure 2.2 shows the final outputs of causative factor maps.
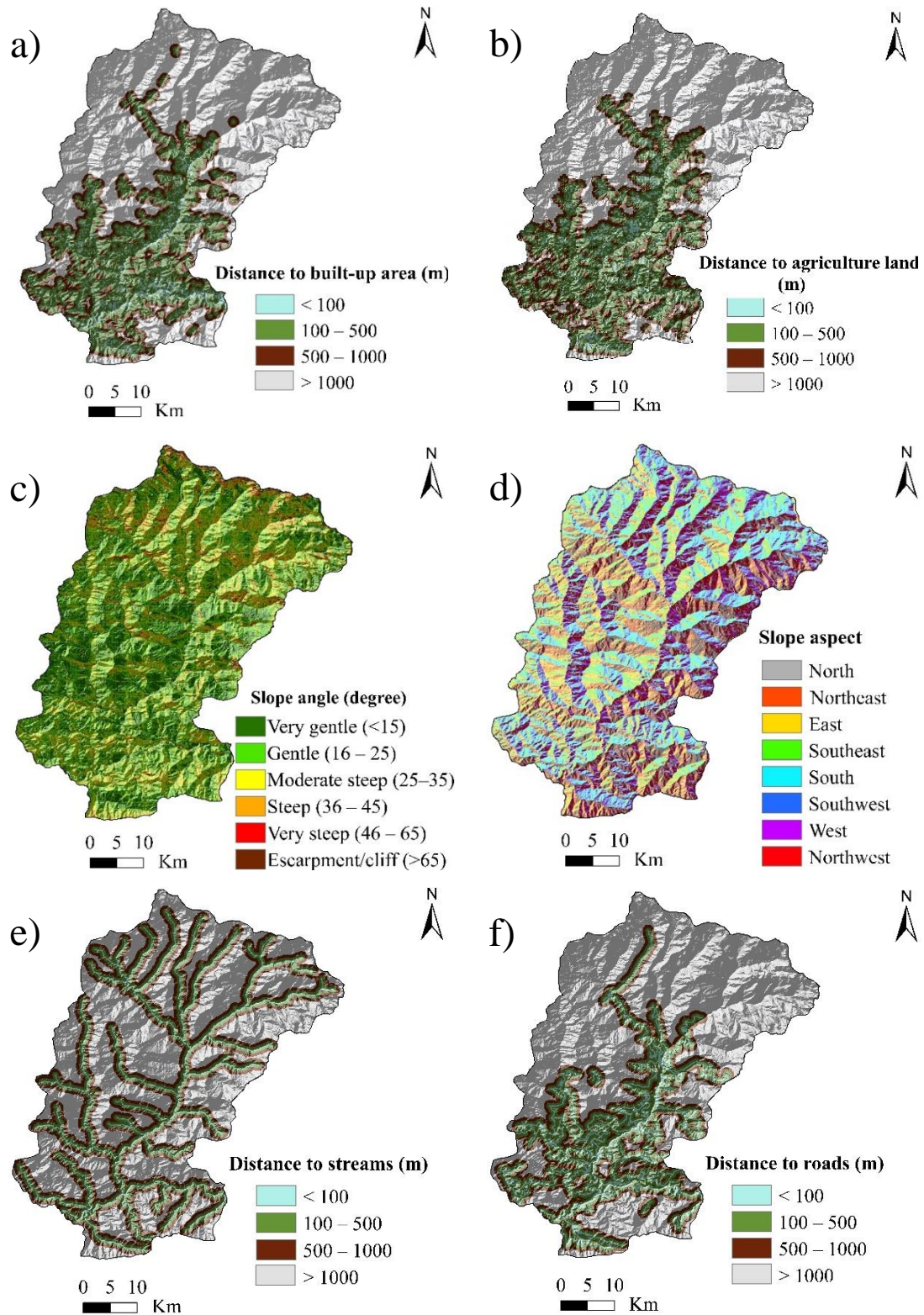
Figure 2.2. Maps of forest fragmentation causative factors for the study area: **(a)** distance to built-up area, **(b)** distance to agriculture land, **(c)** slope angle, **(d)** slope aspect, **(e)** distance to streams, and **(f)** distance to roads.

19
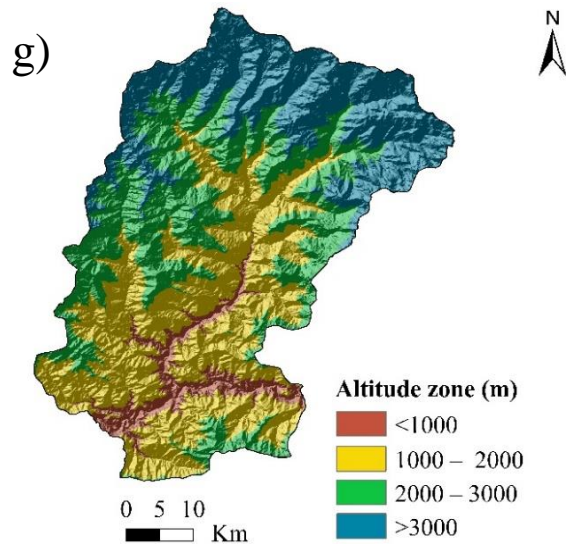
Figure 2.2 (continued). Map of forest fragmentation factors for the study area: **(g)** altitude zone based on rainfall.

2.3 Data preparation for landslide susceptibility mapping

2.3.1 Landslide inventory

In order to apply the weight-of-evidence (WOE) method, which is based on the assumption that past is key for future, the historical landslide data are necessary (Van Westen et al., 2008). The landslide distribution map was prepared through combination of multiple sources, i.e., BHUVAN open data web portal and Google Earth® archive from 2011 to 2013 with the help of field survey (Sato and Harp, 2009, Vakhshoori and Zare, 2016). Point locations of landslides could ignore the size or magnitudes of the existing landslides and might yield a biased result (Regmi et al., 2010). Therefore, to reduce these uncertainties, landslide polygons were used in this study and then transformed to grid cells with the same pixel size. Figure 2.3 shows an example of the landslides detected by Google Earth® in the study area.

GeoEye-1 images	BHUVAN (ISRO)	Google Earth® images
Pre-landslide images	2012/03/30	2011/11/09
Post-landslide images	2012/09/19	2013/06/17 2012/09/19
		2013/06/17	2013/11/19
Sources	National Remote Sensing Centre (NRSC), Report, 2012	BHUVAN open web data portal, (http://bhuvan.nrsc.gov.in)	Google Earth® archives
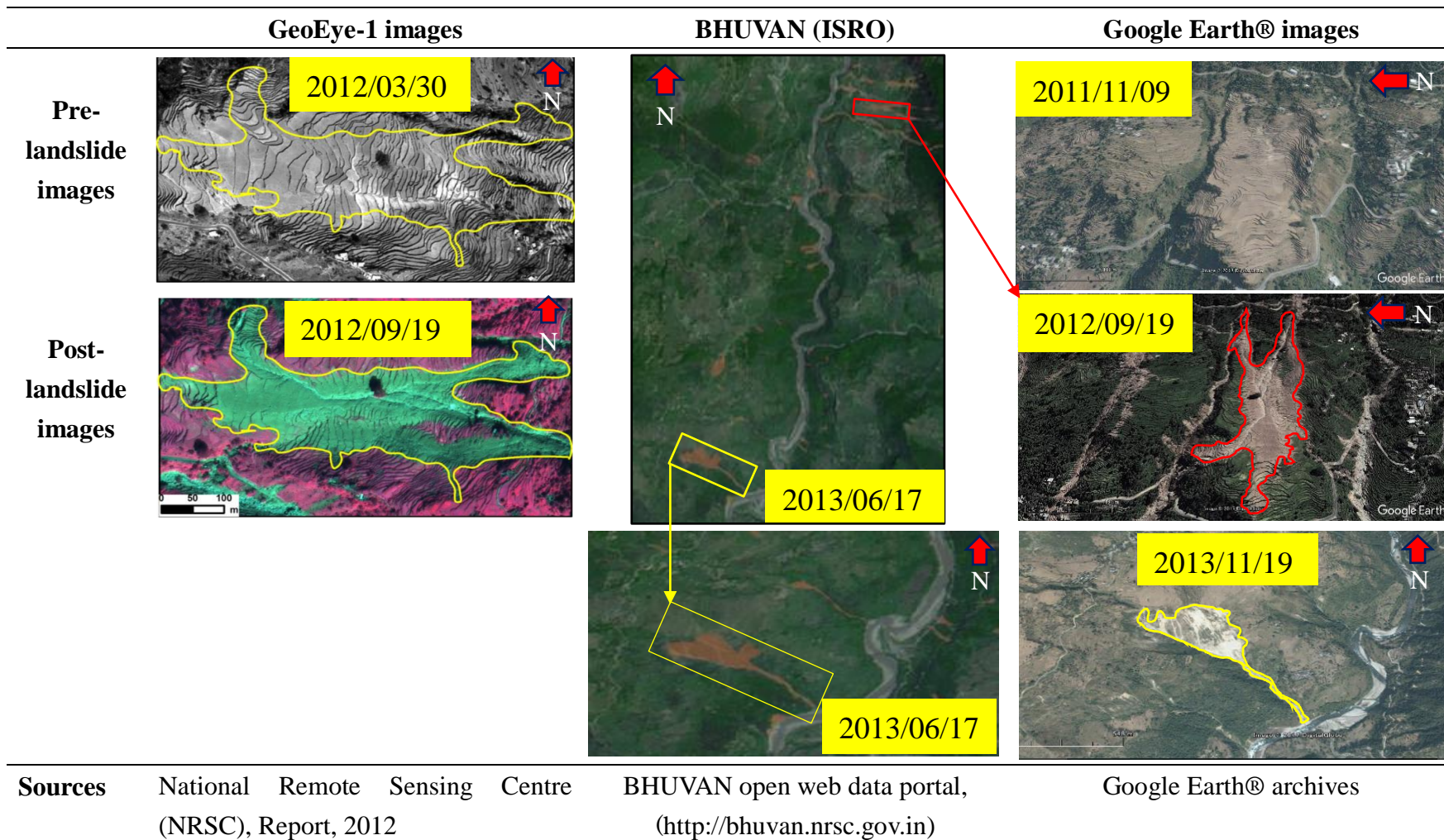
Figure 2.3. An example of the landslides detected by Google Earth® in the study area.

2.3.2 Landslide causative factors

For the landslide susceptibility mapping, there are no universal guidelines for selecting the parameters that influence landslides in susceptibility mapping (Ayalew et al., 2005; Yalcin, 2008). Therefore, based on previous research and data availability (Magliulo et al., 2008) the landslide-related spatial and attribute data, such as geology, geomorphology, soil type, soil depth, slope angle, slope aspect, relative relief, distance to faults, distance to thrusts, distance to lineaments, distance to streams, distance to roads, land use/cover, and altitude zones were collected. Map layers depicting geology, geomorphology and major structures (thrust, fault, and lineament) were derived from the geological maps prepared by Disaster Mitigation Management Centre (DMMC), 10-m resolution stereoscopic Cartosat-1 DEM from ISRO, Landsat 8 OLI satellite data provided by USGC, soil data from Uttrakhand Soil Information and altitude zone produced in accordance with the IMD. Brief description of the preparation procedure of each data layer is provided below.

The slope angle and slope aspect derived from a 10-m DEM extracted from the stereoscopic Cartosat-1 data. Relative relief was derived from the DEM using the zonal statistics tool of ArcGIS, wherein DEM were used as zones. Distance to streams were produced from DEM by hydrology tools in ArcGIS. The layers of distance to streams, faults, thrusts, lineaments and roads were calculated by Euclidean distance system in spatial analyst tools of ArcGIS. Landsat 8 OLI satellite image was used for producing the land use/cover. The land use/cover map was produced by supervised classification of satellite data and was generalized to nine classes. The altitude zone produced in accordance with the IMD. All data were converted to raster format with the same pixels and each raster was divided into several classes. Figure 2.4 shown the final outputs of causative factor maps for landslides occurrence.
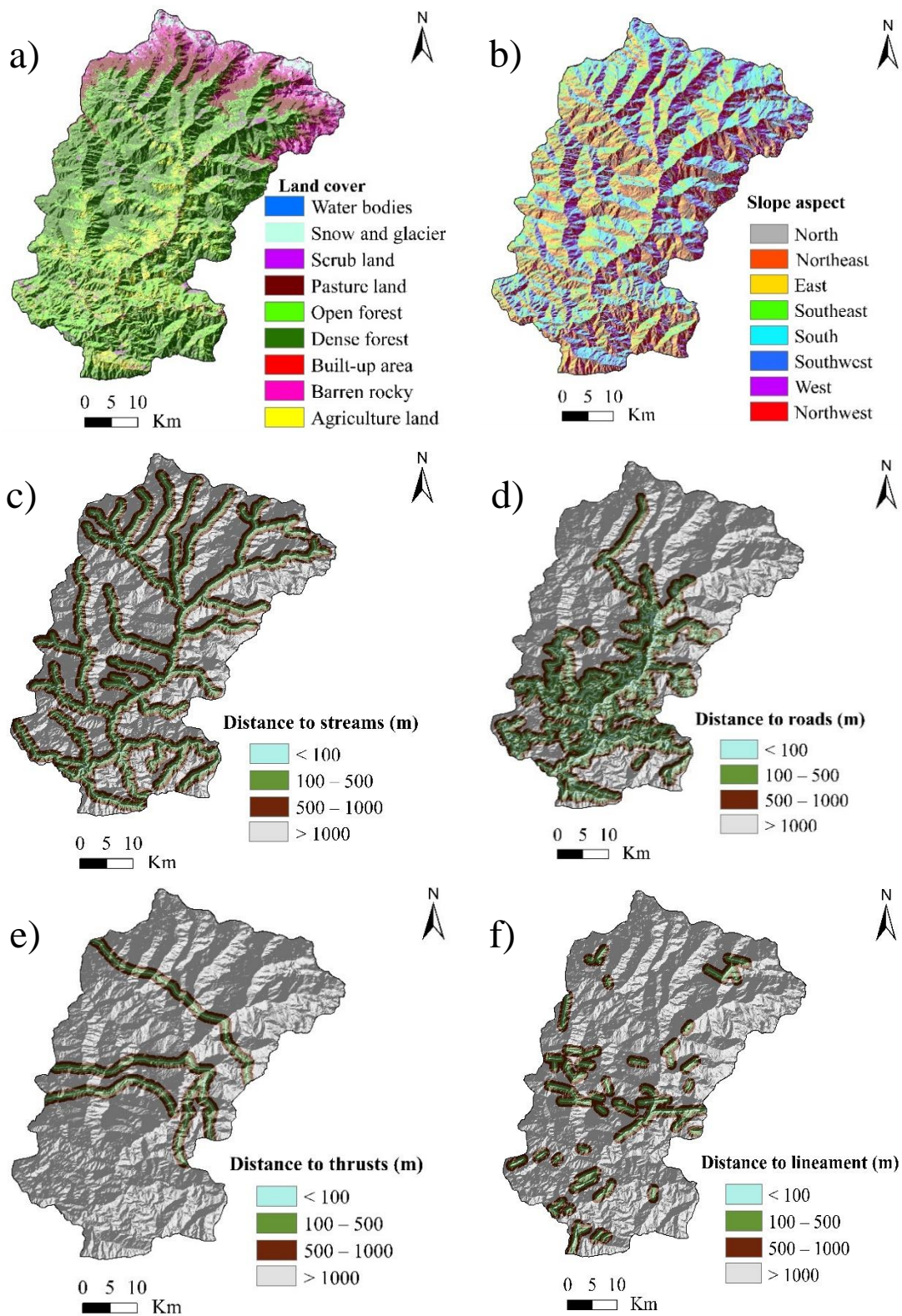
Figure 2.4. Landslide causative factors for the study area: **(a)** land-cover, **(b)** slope aspect, **(c)** distance to streams, **(d)** distance to roads, **(e)** distance to thrusts, and **(f)** distance to lineaments.
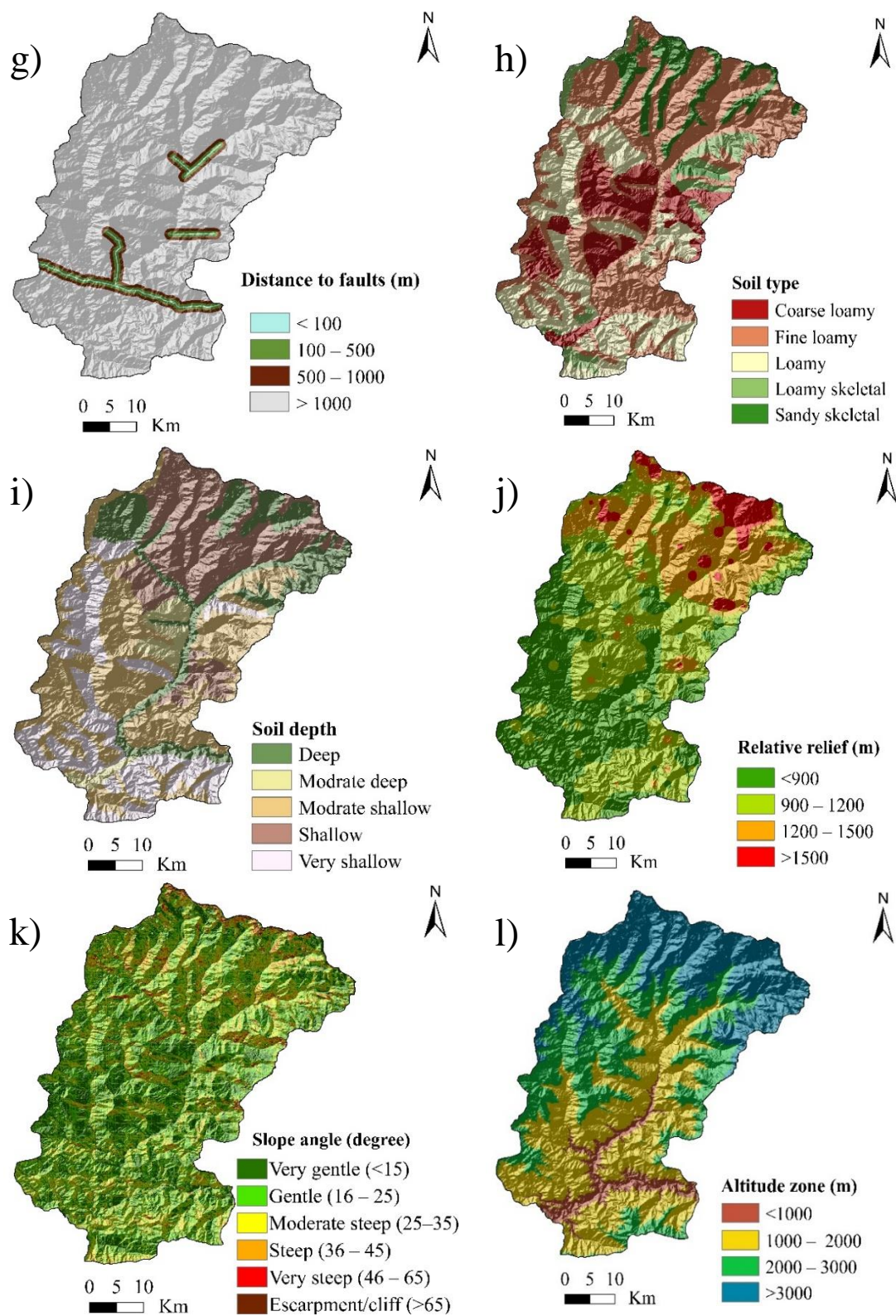
Figure 2.4 (continued). Landslide causative factors for the study area: **(g)** distance to faults, **(h)** soil type, **(i)** soil depth, **(j)** relative relief, **(k)** slope angle, and **(l)** altitude zone based on rainfall.
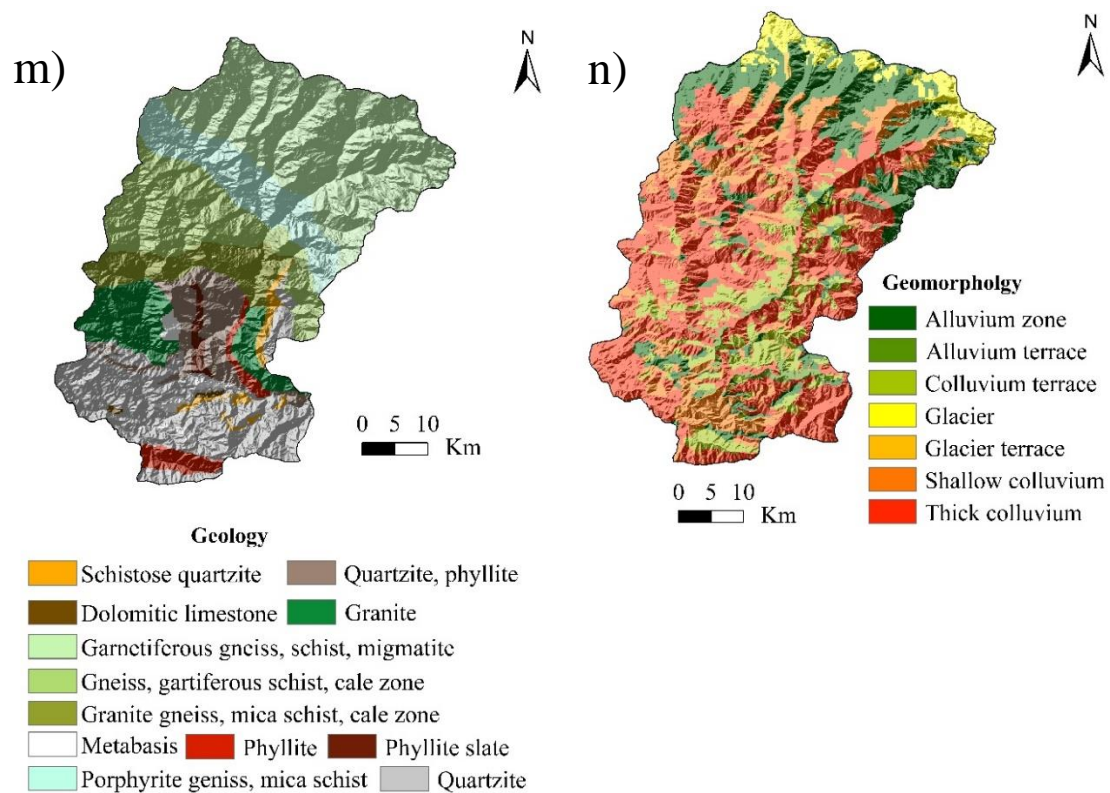
Figure 2.4 (continued). Landslide causative factors for the study area: **(m)** geology, and **(n)** geomorphology.

2.4 Methods

Figure 2.5 shows the overall methodological framework. Land-cover maps were derived based on Landsat images of the years 1976, 1998, and 2014, using supervised classification with the maximum likelihood method. Then, land-cover maps were analysed to understand the changes in LULC, using the cross-tabulation module detection method in Arc GIS and annual rate of change for each class of LULC. Regarding forest fragmentation mapping, all land-cover maps were converted to forest and non-forest areas to detect forest fragmentation areas, using the landscape fragmentation tool (LFT v2.0). Using the WOE model, forest fragmentation probability and landslide susceptibility maps were derived. Finally, to identify the potential change of area, forest fragmentation probability in zone of landslide susceptibility were analysed using the reclassify method, raster calculator and zonal statistics in ArcGIS. The details of the procedure are given in the following sections (Figure 2.5).

Step: 1 Land cover mapping

- -

```
Data Base          Image pre-          Image          Land cover
(Satellite Data)  →  processing  →    processing  →     maps
```

Step: 2 Analysis of land use and land cover

- -

```
Annual rate of      Gain and        Change          A cross-tabulation
    change      ←      loss    ←    trajectories  ←       module
```

Step: 3 Forest fragmentation mapping

- -

```
Forest fragmentation     Forest          Forest and       Land cover
        map          ←  fragmentation  ←  non-forest  ←   reclassification
                          tool
```

Step: 4 Analysis of forest fragmentation change

- -

```
Change rates  →  Annual rate of change
```

Step: 5 Forest fragmentation probability mapping

- -

```
Patch forest  →       Forest        →  Weight-of-  →       Forest
                   fragmentation        evidence        fragmentation
                  causative factor                     probability map
```

Step: 6 Landslide susceptibility mapping

```
Landslides   →    Landslides     →  Weight-of-  →    Landslide
 inventory       causative factor     evidence      susceptibility
                                                         map
```

- -

Step: 7 Observed potential change of forest fragmentation and landslide susceptibility

```
Final Result  ←  Raster calculator and zonal statistics
```

Figure 2.5. Overall flow chart for study area

26

2.4.1 Land-cover mapping

2.4.1.1 Land-cover classification scheme

Due to the mountainous topography of the study area, image preprocessing of the satellite images was necessary to reduce or eliminate differences between the two dates due to atmospheric or sensor variations (Jensen, 1996; Paolini et al., 2006). Therefore, Fast Line-of-sight Atmospheric Analysis of Spectral Hypercube (FLAASH®) model was applied to improve radiometric and atmospheric correction in this study using the software ENVI 5.1. FLAASH model technique was applied for handling particularly to stress such as the presence of clouds and surface reflectance. For geometric registration, the 2014 image was geo-referenced using ground control points by GPS and Google Earth®. Then, the images of 1976 and 1998 were matched with the geometrically corrected OLI images from 2014 by means of an image-to-image matching method, provided by ERDAS Imagine software. Afterwards, all images were re-sampled using the nearest neighbor technique with a root mean square error of less than ± 0.5 pixel per image to a 30-m resolution with the common Universal Traverse Mercator (UTM) 44N zone.

A classification scheme was developed based on ancillary information (Table 2.2), fieldwork, local knowledge, and visual interpretation of each class of land-cover (Table 2.3). The visual interpretation was completed using ArcGIS. To obtain a training set for each class was completed based on field observation and Google Earth. In addition, unsupervised classification and NDVI (Normalized Difference Vegetation Index) determination were also applied before the supervised classification to aid in identification of dominant land-cover types and to improve classification accuracy. Then, supervised classification using the maximum likelihood method was performed in ERDAS IMAGINE for the 1976, 1998, and 2014 Landsat images. For each class, 20 ground-truth polygons were digitized based on a visual analysis of locations on Google Earth and on the image itself. To improve classification, training polygons with confusing spectral signatures were discarded, and new ones were created based on a visual analysis of the locations on Google Earth and on the image itself. Afterwards, the maximum likelihood algorithm was run again (Fonji and Taff, 2014). The land-covers were classified into nine: dense forest, open forest, pasture land, agriculture land, built-up area, scrub land, barren land, water bodies, and snow/glaciers.

Table 2.2. Land-cover classification scheme in this study. For comparison, available classification scheme by Forest Survey of India (FSI) is also shown.
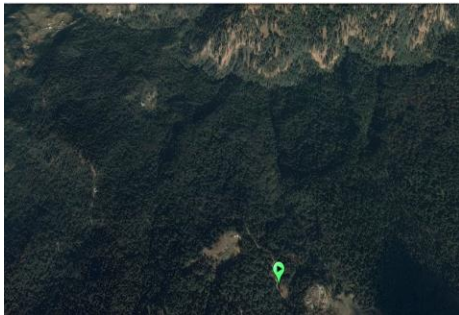
Forest Survey of India, 2011		Present study		
Land-cover classes	Description	Land-cover classes	Google Earth®	Field photos
Very dense forest	All land cover tree canopy density of 70% and above	Dense forest		
Moderate dense forest	All lands with tree canopy density of 40% and more but less than 70%			

Table 2.2 (continued). Land-cover classification scheme in this study. For comparison, available classification scheme by Forest Survey of India (FSI) is also shown.
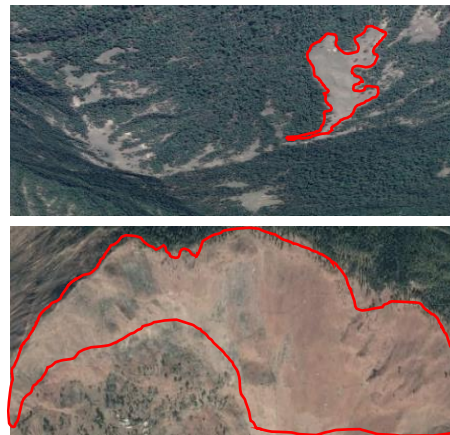
Land-cover classes	Description	Land-cover classes	Google Earth®	Field photos
Open forest	All lands with tree canopy density of 10% and more but less than 40%	Open forest		
Scrub	Degraded forest lands with canopy density less than 10%	Scrub land		

Table 2.2 (continued). Land-cover classification scheme in this study. For comparison, available classification scheme by Forest Survey of India (FSI) is also shown.

Land-cover classes	Description	Land-cover classes	Google Earth®	Field photos
Non-forest	Lands not included in any of the above classes	Pasture land		
		Barren land		

Table 2.2 (continued). Land-cover classification scheme in this study. For comparison, available classification scheme by Forest Survey of India (FSI) is also shown.

Land-cover classes	Description	Land-cover classes	Google Earth®	Field photos
		Water bodies		
		Snow and glaciers		

31

Table 2.2 (continued). Land-cover classification scheme in this study. For comparison, available classification scheme by Forest Survey of India (FSI) is also shown.
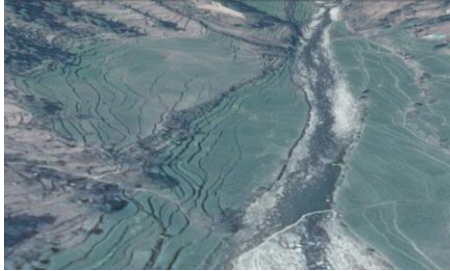
Land-cover classes	Description	Land-cover classes	Google Earth®	Field photos
		Agriculture land		
		Built-up area		

Table 2.3. Visual image interpretation

Land-cover Classes	Tone	Pattern	Association	Description
Dense forest	Dark red to tan red	Contiguous	On the ridge valleys of mountain at high elevation	A forest that has a large area of land covered with tree and canopies form a continuous closed cover.
Open forest	Light red to pinkish	Contiguous	On the ridge valleys of mountain at lower elevation	Light forest are mixtures of tress and canopies that do not form a continuous closed cover.
Scrub land	Red to pinkish	Contiguous	Associated with light forest, settlement and agriculture	Land areas of exposed soil surface as influenced by human impacts and/or natural causes. It contains-sparse vegetation with very low plant cover.
Barren land	Cyan to bullish	Scattered	At the high altitude between the snow cover area	Land that has not been used or that would be prohibitively difficult to use (e.g., bare rock and extremely steep slopes).
Pasture land	Light brown	Contiguous	At the high altitude near the snow cover area	Pasture land is generally distributed at high elevation with short vegetation.
Built-up area	Bluish grey	Linear	In valley portion along drainage/river course and near the agriculture area	Areas that have been populated with residential, commercial, industrial, transportation and facilities.

Table 2.3 (continued). Visual image interpretation

Land-cover Classes	Tone	Pattern	Association	Description
Agriculture land	Greenish blue	Contiguous	In valley portion along drainage/river course and the gentle slopes	Areas cultivated with crops, including old arable land, newly cultivated land, fallow land, and land undergoing crop rotation, as well as fruit crops and agro-forestry land mainly used to cultivate crops.
Snow and glaciers	Bright white	Contiguous	At the high altitude	Area at the high altitude, with glaciers.
Water bodies	Dark blue to black	Scattered	With drainage system	Areas covered with water such as rivers, ponds and lakes.

2.4.1.2 Accuracy assessment

Accuracy assessment is important for validating the digitally classified images. It is the procedure, used to compare the classification results to geographical reference data that are assumed to be true (Richards, 2006). Due to the mountainous topography of the study area, ground reference data were collected from Google Earth with limited ground GPS points. To assess the accuracy of classification, field visits were made to obtain ground control point in the area below 3000 m in elevation (as the elevations above this were not accessible due to difficult terrain), using a handheld Garmin Global Positioning System (GPS; 12-channel Garmin eTrex 30–Summit mode). The accuracy assessment of the 1976 and 1998 images were not possible due to lack of data availability and a clear Google Earth image archive. Therefore, an accuracy assessment was performed for the 2014 image only. For the 2014 image, a total of 270 testing pixels (30 pixels from each class) were generated at random throughout the study area. The testing pixels were compared with the classified map. To evaluate the user's and the producer's accuracy, an error matrix was applied, to compare the relationship between the classified map and reference data (Congalton, 1991). As a result, the producer's accuracy, user's accuracy, overall accuracy, and kappa coefficient were computed for the final land-cover maps produced. Kappa coefficient for 2014 Landsat 8 OLI classified image was calculated following Kappa formula below (Congalton, 1991):

$$K = \frac{N \sum_{i=1}^{r} x_{ii} - \sum_{i=1}^{r}(x_{i+} \times x_{+i})}{N^2 - \sum_{i=1}^{r}(x_{i+} \times x_{+i})} \dots \dots \dots \dots \dots \dots \dots . (\ Equation\ 1)$$

where N is the total number of sites in the matrix, r is the number of rows in the matrix, x_{ii} is the number in row i and column i, x_{+i} is the total for row i and x_{i+} is the total for column i (Jensen, 1996).

2.4.1.3 Land-use and land-cover (LULC) change analysis

A cross-tabulation module detection method was used to detect land-use and land-cover (LULC) change in ArcGIS (Perez et al., 2005), through which a LULC change matrix was produced. This matrix provides essential information about the nature and spatial distribution of LULC (Shalaby and Tateishi, 2007). A change matrix enables the main types of changes or directions in the study area. Then, the change in LULC was analysed to depict gains and losses over the two time periods. The change matrices of the 1st period

(1976–1998) and the 2nd period (1998–2014) were also used to drive the gains and losses for land-cover categories. The gains for each class were derived from subtracting the persistence from the respective columns, and the losses were computed by subtracting the persistence from the respective rows.

2.4.2 Forest fragmentation mapping

2.4.2.1 Landscape Fragmentation Analysis (LFA) tool

The ArcGIS Landscape Fragmentation Analysis tool (LFT v2.0) was used to create forest fragmentation maps (Vogt et al., 2007). The input data of this tool, i.e., forest and non-forest data, were derived from land cover maps. The land cover maps for the years 1976, 1998, and 2014 were reclassified into forest and non-forest classes using the ArcGIS spatial analyst. Scrub land was not included in forest class (Table 2.2). Based on the forest and non-forest classes, the LFT v2.0 tool classifies a forest pattern into four main categories: patch, edge, perforated, and core (Vogt et al., 2007). Edge-width is the distance over which non-forest land covers can degrade forest land covers, although the edge-width varies by species and can range from 50 m to several 100 m. However, 100 m is often used as a general edge-width (Vogt et al., 2007). Therefore, using a specified edge width of 100 m, the forest fragmented areas were classified into five categories: (i) 'core' forest—the inner part of forest region and relatively distant from the non-forest boundary; (ii) 'patch' forest—small forest area surrounded by non-forested land cover, which does not contain any core pixel forests; (iii) 'perforated' forest—transition zone boundaries between core forest and relatively small perforations; (iv) 'edge' forest— transition zone boundaries between core forest and large non-forest land cover region; and (v) 'non-forest'—not pertaining to forest (Vogt et al., 2007; Uddin et al., 2015). Figure 2.6 shows diagrammatic representation of forest fragmentation classes.

Figure 2.6. Illustration of four types of spatial patterns of forest fragmentation on an artificial map (Vogt et al., 2007)

2.4.3 Annual rate of change of LULC and forest fragmentation

The annual rate of change for each class of LULC and an annual fragment creation rate were calculated using the following formula proposed by Puyravaud, (2003):

$$r = \left(\frac{1}{t_2 - t_1}\right) \times \ln\left(\frac{A_2}{A_1}\right) \dots \dots \dots \dots \dots \dots \dots \dots \dots \dots \dots \dots \text{(Equation 2)}$$

where r is change for each class per year, A_2 and A_1 are the class areas at the end and the beginning, respectively, for the period being evaluated, and t is the number of years spanning that period.

2.4.4 Forest fragmentation probability and landslide susceptibility

2.4.4.1 Patch forest (1976–2014)

In order to apply WOE method, past patch forests were considered as an evidence. Patch forests were extracted from forest fragmentation map from 1976 to 2014 using analyst tools in ArcGIS. Afterward, patch forests were re-sampled in the same pixel with the common UTM 44N zone.

2.4.4.2 Landslide inventory (2011–2013)

Landslide polygon inventory data were derived from two sources. First, landslide point locations were extracted as a reference based on ancillary information, i.e., open data sources from BHUVAN (Indian earth observation visualization) developed by ISRO, which provides location and distribution of landslides. Second, we used Google Earth® archive to extract landslide polygons. Thus, taking the advantage of all these free access open data sources with ground truth investigation, we prepared landslide inventory from 2011 to 2013. Later, this vector map, i.e., landslide polygons were converted to raster by using vector to raster conversion tool in ArcGIS for further computations. Afterward, all landslide polygons were re-sample in the same pixel with the common UTM 44N zone.

2.4.4.3 Weight-of-evidence (WOE) method

To obtain forest fragmentation probability map and landslide susceptibility map, WOE method was applied. The analysis was executed using the WOE modeling technique, a very well-documented technique that is widely applied in many scientific fields (van Westen et al., 2003; Duke and Steele 2010; Sterlacchini et al., 2011, Malek et al, 2015). WOE is a quantitative, data-driven Bayesian modeling method that can be applied to spatial data for producing maps of expected probability of occurrence. The method is based on the calculation of positive and negative weights (W^+ and W^-), by which the degree of spatial association among training points and each explanatory variable class may be modeled (Sterlacchini et al., 2011). In this study, the WOE modeling was used for the forest fragmentation probability and landslide susceptibility mapping, which is data-driven method and, which avoids the subjectivity of weight to choose the causative factor. WOE method was originally developed for the identification and exploration of mineral deposits (e.g., Bonham-Carter et al., 1989). Recently, this method has been widely applied

for landslide susceptibility, forest fire occurrence, and forest cover change mapping (Harris et al., 2000; Bonham-Carter, 2002; Lee and Choi, 2004; Mathew et al., 2007; Dahal et al., 2008a; Gosh et al., 2009; Pradhan, 2010; Regmi et al., 2010, Armas, 2012; Kayastha et al., 2012; Malek et al, 2015; Thomas et al., 2015). A detailed description of the mathematical formulation of this model is provided by Bonham-Carter, (2002) and described in detail by Dahal et al. (2008a); Regmi et al. (2010), Xu et al. (2012).

The method is based on the assumption that "past is the key for future" as already mentioned. Thus, it is believed that future landslides/forest fragmentation will occur under conditions similar to those contributing to previous landslides/forest fragmentation (Dai and Lee, 2001). The combination of causative factors assumes that the factors are conditionally independent with one another with respect to the landslides/forest fragmentation (Bonham-Carter, 2002; Lee and Choi, 2004; Dahal et al., 2008b). It is also further presumed that the combination of causative factors might have resulted into triggering of past landslides/forest fragmentation in the present study area. Therefore, the landslides/patch forest that occurred in the past were used in weighting factors that mainly contribute to or cause landslides/forest fragmentation. The WOE method calculates weight for each causative factor of a landslides/patch forest based on the presence (W^+) or absence (W^-) of landslides/patch forest within the area (Bonham-Carter 1989). This method is a correlation between positive weight (W^+), when the event occurs, and a negative weight (W^-), when the event does not occur of the factor maps, which are defined as:

$$W^+ = \log_e \frac{P\{B|D\}}{P\{B|\bar{D}\}} \dots\dots\dots\dots\dots\dots\dots\dots\dots\dots\dots\dots. \text{(Equation 3)}$$

$$W^- = \log_e \frac{P\{\bar{B}|D\}}{P\{\bar{B}|\bar{D}\}} \dots\dots\dots\dots\dots\dots\dots\dots\dots\dots\dots \text{(Equation 4)}$$

where P is the probability, B is the presence of desired class of landslide/patch forest causative factor, $\bar{B}$ is the absence of a desired class of landslide/patch forest causative factor, D is the presence of landslides/patch forest and $\bar{D}$ is the absence of a landslides/patch forest. Since the results are in log form, final weights can be used to produce a contrast value (C) for the particular susceptibility variable. The final weight or weight contrast (C) is the difference between two weights ($C = W^+ - W^-$) and its magnitude reflects the spatial association between the causative factor and the landslides/patch forest

(Pradhan et al., 2010; Regmi et al., 2010; Xu et al., 2012).

If the weight contrast is positive, the factor is favorable for the landslides/forest fragmentation, and if it is negative, it is unfavorable for the landslides/forest fragmentation. If the weight contrast is close to zero, this indicates that the factor shows little relation to the landslides/forest fragmentation. The forest fragmentation probability and landslide susceptibility index (LSI) map was constructed by summing the contrasts of each causative factor, as follows: LSI = ΣFc (where Fc = contrast of each factor). Higher positive LSI means that the susceptibility of landslides/forest fragmentation is high, and if LSI value is low or negative, it means that the susceptibility of landslides/forest fragmentation is low.

2.4.4.4 Validation of the forest fragmentation probability and landslide susceptibility

The accuracy of the forest fragmentation probability and landslide susceptibility maps were evaluated by calculating the relative operative characteristic (ROC) and the percentage of observed landslide points/patch forest in various susceptibility categories (Nandi and Shakoor, 2009). The area under curve (AUC) of the ROC represents the quality of the probabilistic model (its ability to predict the occurrence or non-occurrence of an event) (Yesilnacar and Topal, 2005). An AUC value close to 1 indicates high accuracy, and an AUC value close to 0.5 indicates inaccuracy (Fawcett, 2006). In this study, the success-rate curves were obtained using the IDRISI SELVA17.0 software package. The AUC values obtained from the susceptibility maps show that the model gave the highest success rate.

Chapter 3

Assessment of land-use and land-cover (LULC) change in the Garhwal Himalaya

3.1 Land-cover maps and status

The land-cover maps for the years 1976, 1998, and 2014 based on Landsat 2 (MSS), Landsat 5 (TM), and Landsat 8 (OLI) satellite data were prepared with nine land-cover types, namely, dense forest, open forest, pasture land, snow/glacier, barren land, scrub land, agriculture land, water bodies, and built-up area. Figure 3.1 shows the final output of the supervised classification, which consists of three classified maps and Figure 3.2 shows the comparison in terms of the total area for each land-cover category.

(a)

Land cover
- Dense forest
- Open forest
- Barren land
- Scrub land
- Pasture land
- Agriculture land
- Built-up area
- Snow/glaciers
- Water bodies

0 5 10 Km
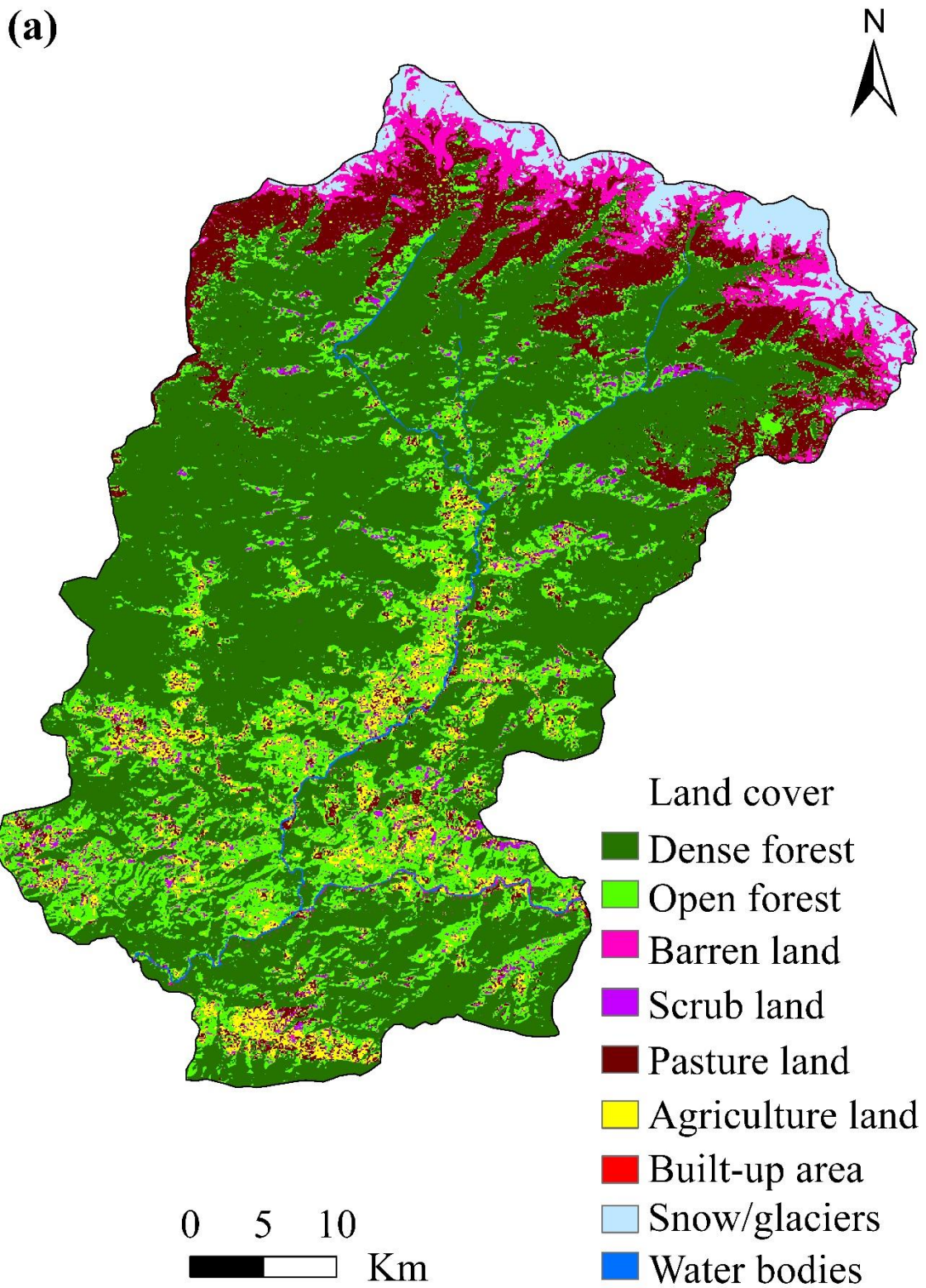
Figure 3.1a. Land-cover map for the year 1976

(b)

N

Land cover
- ■ Dense forest
- ■ Open forest
- ■ Barren land
- ■ Scrub land
- ■ Pasture land
- ■ Agriculture land
- ■ Built-up area
- ■ Snow/glaciers
- ■ Water bodies

0　5　10
Km
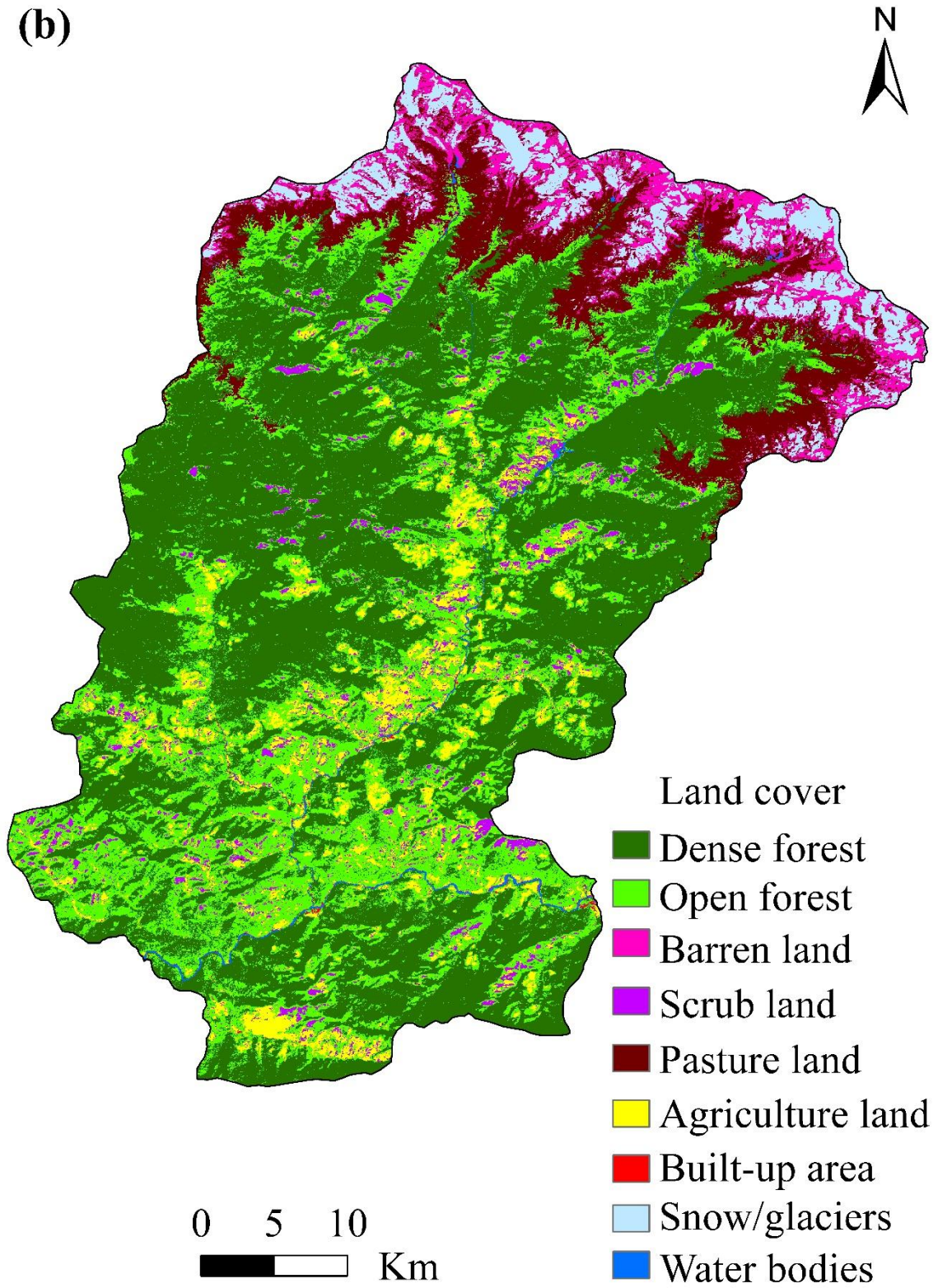
Figure 3.1b (continued). Land-cover map for the year 1998

(c)

Land cover
- Dense forest
- Open forest
- Barren land
- Scrub land
- Pasture land
- Agriculture land
- Built-up area
- Snow/glaciers
- Water bodies

0   5   10
Km
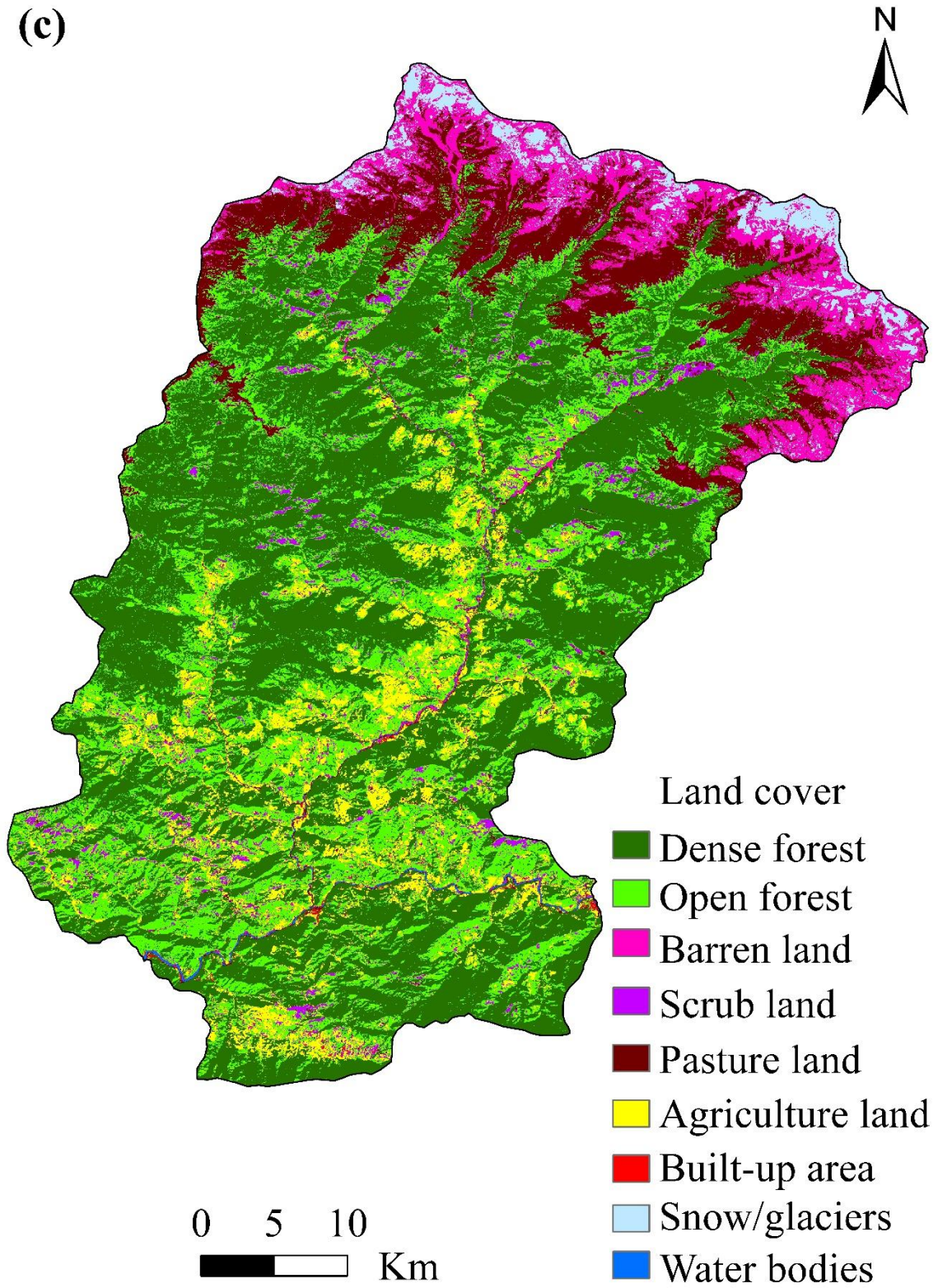
Figure 3.1c (continued). Land-cover map for the year 2014
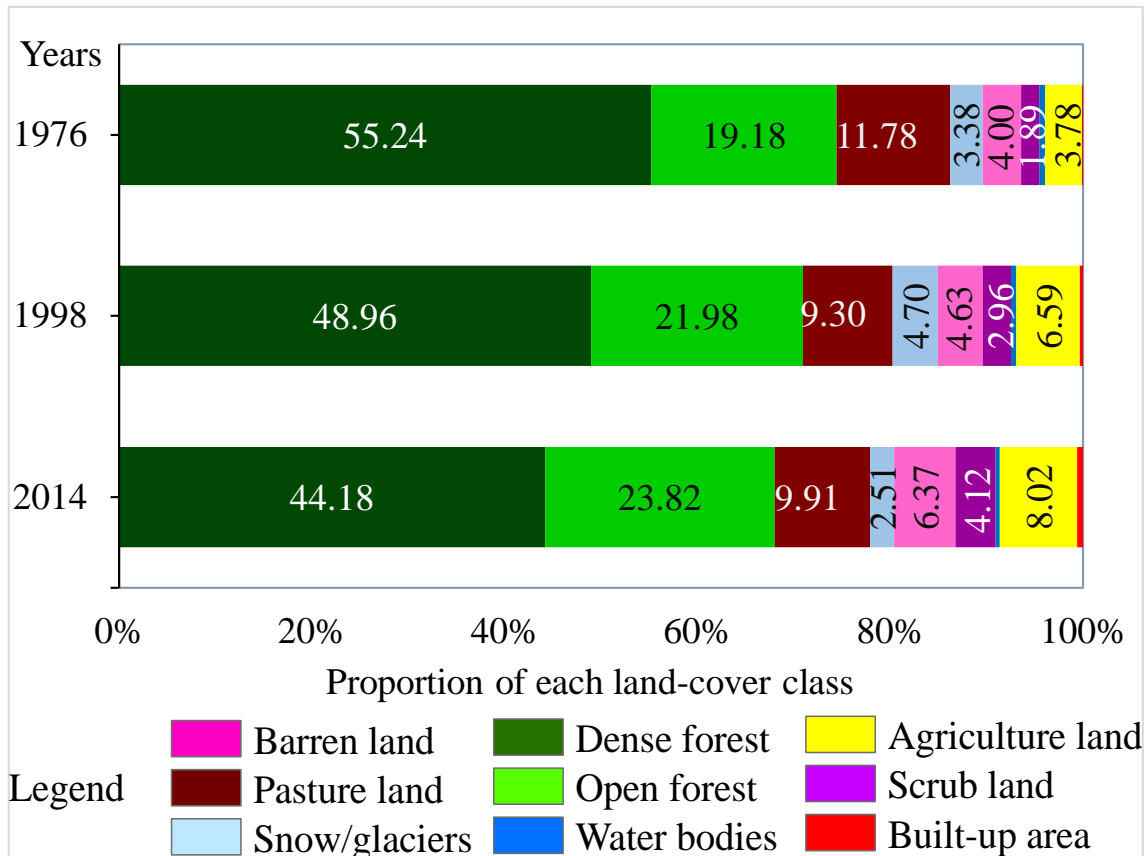
Figure 3.2. Comparison of land-use and land-cover (LULC) classes by percentage of the total area (study area = 1936.06 km^2)

3.2 Accuracy assessment

Table 3.1 shows the error matrix with the user's accuracy, procedure's accuracy and kappa coefficient. The overall accuracy was calculated from the error matrix (Table 3.1) by dividing the correctly classified pixel by the total number of the pixels, i.e., (240/267) × 100 = 89.88%. Therefore, the total accuracy was 89.88% for the 2014 classified map. Furthermore, the Kappa coefficient was calculated for the 2014 classified map at 0.8818 (88.18%).

Table 3.1. Cross-tabulation error matrix of classified vs. reference data for 2014

Classified Image	Reference Data									
	Dense forest	Open forest	Pasture land	Snow/ glaciers	Barren land	Scrub land	Water bodies	Agriculture land	Built-up area	Row totals
Dense forest	28	1								29
Open forest	1	25						1	1	28
Pasture land			26		1	2		1		30
Snow/glaciers				30	1					31
Barren land					27		1			28
Scrub land		1	3			26		1	1	33
Water bodies					1		29			30
Agriculture land	1	2	1			1		26	3	34
Built-up area		1						1	23	25
Column Totals	30	30	30	30	30	29	30	30	26	267
User's accuracy	96.55	89.29	86.67	96.77	87.10	81.25	96.67	76.47	92.00	
Producer's accuracy	93.33	83.33	86.67	100	90.00	89	96.67	86.67	82.14	
Total accuracy				90.00%						
Kappa statistics				88.18%						

3.3 Land-use and land-cover (LULC) changes

Table 3.2 summarized the results of land cover, change rate, and annual rate of change in area of each class of the Rudraprayag district. Forest area (dense forest and open forest) was main land cover in 1976 with 74.42% of the total area of the district, followed by pasture land (11.78%), barren land (4.00%), agriculture land (3.78%) and scrub land (1.89%). The area under dense forest decreased from 55.24% (1069.51 km^2) in 1976 to 44.18% (855.39 km^2) in 2014, showing a component change of 6.27%, 4.78% in the 1st period (1976–1998) and the 2nd period (1998–2014), respectively. Open forest has increased from 19.18% (371.30 km^2) in 1976 to 23.82% (461.08 km^2) in 2014, showing a component change of 2.80%, 1.83 % in the 1st period (1976–1998) and the 2nd period (1998–2014), respectively. The area under pasture has decreased from 11.78% (227.98 km^2) in 1976 to 9.91% (191.78 km^2) in 2014, showing a component change of 2.47%, 0.60 % in the 1st period (1976–1998) and the 2nd period, respectively. Agriculture and built-up area progressively increased from 3.78%, and 0.14% in 1976 to 8.02%, and 0.62% in 2014, respectively, showing a significant component change of 2.80 %, 0.19% in the 1st period (1976–1998) and 1.44 %, 0.28 % in the 2nd period (1998–2014),

respectively. Barren and scrub land area also progressively increased from 4.0 %, and 1.89% in 1976 to 6.37%, and 4.12% in 2014, respectively, showing a drastic component change of 0.63%, 1.07% in the 1st period (1976–1998) and 1.74%, 1.15% in the 2nd period (1998–2014), respectively. Due to climatic and/or seasonal variations, the area under snow and glaciers and water bodies decreased from 3.38% (65.5 km^2), and 0.61% (11.86 km^2) in 1976 to 2.51% (48.61 km^2), and 0.46 % (8.94 km^2) in 2014, respectively, showing a component change of 1.32%, 0.07% in the 1st period (1976–1998) and 2.19%, 0.08% in the 2nd period (1998–2014), respectively.

The overall annual rate of change in the declining phase of forest cover (dense and open forest) was observed at about 0.22% and 0.27% during the 1st period (1976–1998) and the 2nd period (1998–2014), respectively. Another declining annual rate of change was observed for pasture land and snow and glaciers during the 1st period (1976–1998), while water bodies and snow and glaciers were observed to be in decline during the 2nd period (1998–2014). Other land cover classes experienced an expansion at both time intervals.

Table 3.2. Land-cover area, percentage, change and annual rate of change of each class

Land cover type	1976		1998		2014		Change (1976–1998)	Change (1998–2014)	Annual rate of change (1976–1998)	Annual rate of change (1998–2014)
	km^2	%[a]	km^2	%[a]	km^2	%[a]	%[b]	%[b]	%[c]	%[c]
Dense forest	1069.51	55.24	947.96	48.96	855.39	44.18	-6.27	-4.78	-0.55	-0.64
Open forest	371.3	19.18	425.53	21.98	461.08	23.82	2.80	1.83	0.62	0.50
Pasture land	227.98	11.78	180.1	9.30	191.78	9.91	-2.47	0.60	-1.07	0.39
Snow/glaciers	65.50	3.38	91.09	4.70	48.61	2.51	1.32	-2.19	1.50	-3.93
Barren land	77.37	4.00	89.58	4.63	123.33	6.37	0.63	1.74	0.67	2.00
Scrub land	36.54	1.89	57.31	2.96	79.70	4.12	1.07	1.15	2.05	2.06
Water bodies	11.86	0.61	10.45	0.54	8.94	0.46	-0.07	-0.08	-0.58	-0.98
Agriculture land	73.22	3.78	127.51	6.59	155.34	8.02	2.80	1.44	2.52	1.23
Built-up area	2.78	0.14	6.53	0.34	11.91	0.62	0.19	0.28	3.88	3.75
Total area	1936.06	100	1936.06	100	1936.06	100				

[a] Percentage of each class out of the total area
[b] Percentage change in component
[c] Percentage of annual rate of change in each class

3.4 Land-use and land-cover (LULC) change trajectories

Tables 3.3 and 3.4 show the conversion of the land cover in the form of a change matrix for the 1st period (1976–1998) and the 2nd period (1998–2014). In the 1st period (1976–1998), there was a major conversion from forest cover (dense and open forest) to agriculture land (44.79 km^2), from forest to scrub land (25.33 km^2), from forest to barren land (5.86 km^2), and from forest to built-up area (2.18 km^2). In the same period, a change from snow and glaciers to barren land, from pasture to agriculture land, and from barren land to snow and glaciers were also observed. On the other hand, the 2nd period (1998–2014) showed the further major loss of forest cover (dense and open forest), being converted into agriculture land (39.8 km^2), scrub land (29.95 km^2), built-up area (4.13 km^2), barren land (3.51 km^2), and pasture land (5.13 km^2). During the same time period, another major change from snow and glacier to barren land was also observed. Small area was converted to forest area during both periods.

Table 3.3 Land-use and land-cover change matrix between 1976 and 1998

Land cover type (km^2)	Dense forest	Open forest	Pasture land	Snow/ glacier	Barren land	Scrub land	Water bodies	Agriculture land	Built-up area	Total (1998)
Dense forest	**928.26**	13.35	0.73	0.00	0.08	1.71	0.00	3.83	0.00	948.00
Open forest	130.43	**284.70**	1.62	0.00	0.4	3.09	0.00	5.28	0.00	425.50
Pasture land	0.48	4.85	**150.07**	0.00	19.61	2.45	0.18	2.46	0.00	180.10
Snow/ glaciers	0.02	0.55	32.85	**38.84**	18.83	0.00	0.00	0.00	0.00	91.09
Barren land	0.42	5.44	16.90	26.16	**36.94**	1.07	2.23	0.42	0.00	89.58
Scrub land	3.54	21.79	2.06	0.00	0.27	**21.41**	0.00	8.24	0.00	57.31
Water bodies	0.00	0.00	0.00	0.50	0.92	0.00	**8.93**	0.10	0.00	10.45
Agriculture land	6.01	38.78	23.56	0.00	0.32	6.64	0.45	**51.75**	0.00	127.50
Built-up area	0.35	1.83	0.19	0.00	0.00	0.17	0.07	1.14	**2.78**	6.53
Total (1976)	1069.51	371.00	227.98	65.50	77.37	36.50	11.86	73.22	2.78	1936.06

Note: The bold letters indicate that there is no change in LULC over the time period

Table 3.4. Land-use and land-cover change matrix between 1998 and 2014

Land cover type (km^2)	Dense forest	Open forest	Pasture land	Snow/ glaciers	Barren land	Scrub land	Water bodies	Agriculture land	Built-up area	Total (2014)
Dense forest	**832.30**	17.69	0.52	0.00	0.35	0.36	0.00	4.21	0.00	855.40
Open forest	104.90	**336.10**	1.15	0.00	2.16	8.33	0.00	8.42	0.00	461.10
Pasture land	0.82	4.31	**157.00**	0.00	23.60	2.72	0.39	3.32	0.00	191.80
Snow/ glaciers	0.00	0.00	0.93	**38.84**	8.85	0.00	0.00	0.00	0.00	48.61
Barren land	0.50	3.01	11.20	52.00	**53.80**	0.62	1.68	0.41	0.12	123.30
Scrub land	3.95	26.00	3.78	0.03	0.03	**41.20**	0.00	4.73	0.00	79.70
Water bodies	0.00	0.00	0.00	0.19	0.49	0.21	**7.35**	0.20	0.49	8.93
Agriculture land	4.63	35.17	5.75	0.00	0.32	3.70	0.82	**104.42**	0.53	155.30
Built-up area	0.92	3.21	0.18	0.00	0.00	0.19	0.21	1.80	**5.39**	11.90
Total (1998)	948.00	426.00	180.00	91.09	90.00	57.31	10.45	127.50	6.53	1936.06

Note: The bold letters indicate that there is no change in LULC over the time period

3.5 Gain and loss of land-use and land-cover (LULC)

The net change in the form of gain and loss for each LULC class during the 1st period (1976–1998) and the 2nd period (1998–2014) is shown in Figure 3.3. The highest loss was in the dense forest (121.55 km^2) during the 1st period, followed by pasture land (47.88 km^2), and water bodies (1.94 km^2), while a significant gain was observed in agriculture land (54.29 km^2), open forest (54.23 km^2), snow and glaciers (25.59 km^2), scrub land (20.77 km^2), barren land (12.21 km^2), built-up area (3.75 km^2), and water bodies (1.41 km^2). An overall loss of 67.32 km^2 of forest area (dense and open forest) was observed during the 1st period. On the other hand, the highest loss was observed in dense forest (92.57 km^2) and snow and glaciers (42.48 km^2), while the significant gain was observed in open forest (35.55 km^2), barren land (33.75 km^2), agriculture land (27.83 km^2), scrub land (22.39 km^2), pasture land (11.68 km^2), and built-up area (5.37 km^2) during the 2nd period. An overall loss of 57.03 km^2 of forest area (dense and open forest) was observed during the 2nd period. However, the overall net change was the highest during the 1st period.

49

	Net change (Gain - Loss) Period 1st (1976 - 1998)	Net change (Gain - Loss) Period 2nd (1998 - 2014)
■ Dense forest	-121.55	-92.57
■ Open forest	54.23	35.55
■ Pasture land	-47.88	11.68
■ Snow and glaciers	25.59	-42.48
■ Barren land	12.21	33.75
■ Scrub land	20.77	22.39
■ Water bodies	-1.41	-1.52
■ Agriculture land	54.29	27.83
■ Built-up area	3.75	5.37
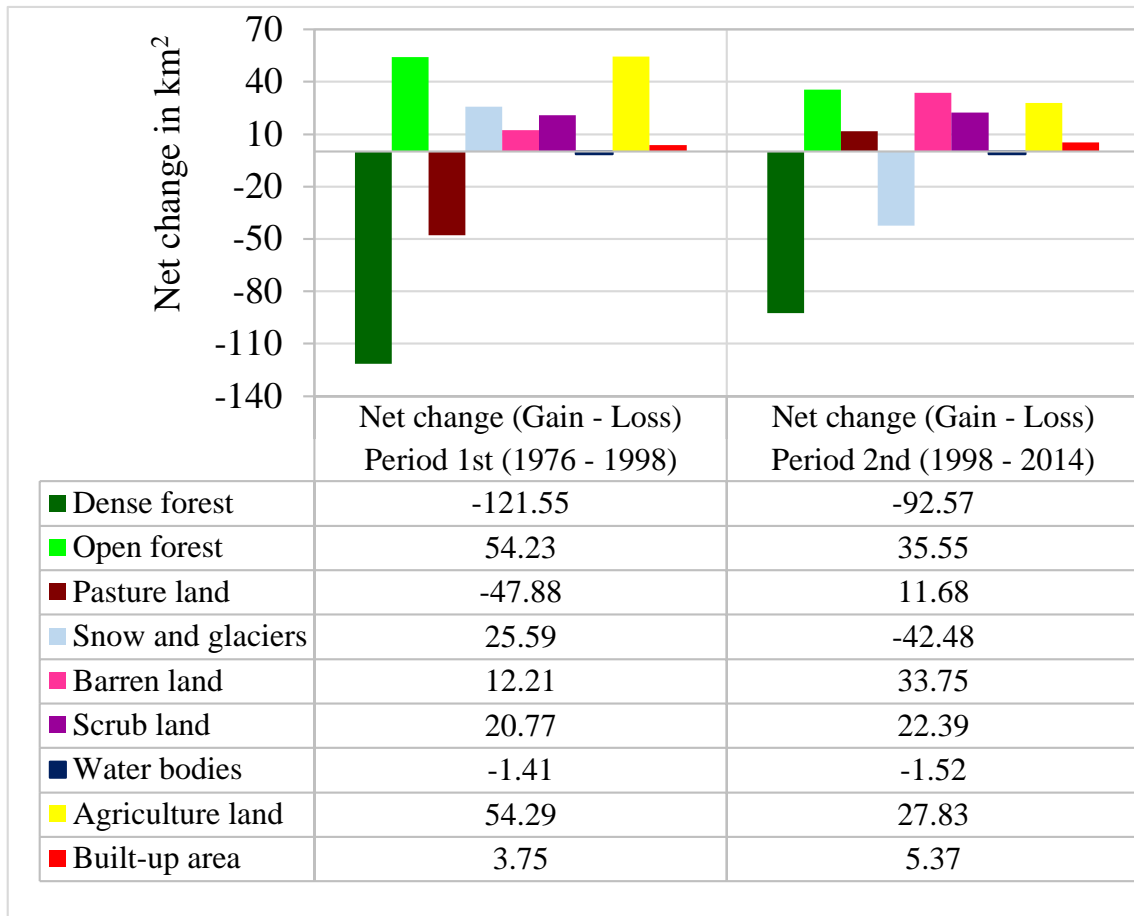
Figure 3.3. Net change (i.e. gains minus losses) for each land-cover class of the study area for the 1st period (1976–1998), and the 2nd period (1998–2014).

Chapter 4

Assessment of forest fragmentation based on land-use and land-cover (LULC) change in the Garhwal Himalaya

4.1 Forest and non-forest maps

To investigate forest fragmentation change due to LULC change, we reclassified land-cover types into two: forest and non-forest. The forest and non-forest cover map for the years 1976, 1998, and 2014 based on the Landsat 2 (MSS), Landsat 5 (TM) and Landsat 8 (OLI) satellite data were extracted using analyst tool in ArcGIS, having two land covers type namely, forest and non-forest area. Figure 4.1 shows the final outputs of forest and non-forest area, which consists of three forest and non-forest maps of the Rudraprayag district in 1976, 1998 and 2014.

4.2 Forest and non-forest changes

Table 4.1 summarizes the results of forest and non-forest areas in the district from 1976 to 2014. The area under forest has decreased from 74.42% (1440.81 km^2) in 1976 to 68% (1316.45 km^2) in 2014, showing a component change of 3.47 %, 2.95 % in the 1st period (1976–1998) and the 2nd period (1998–2014), respectively. Non-forest area progressively increased from 25.58 % (495.25 km^2) in 1976 to 32% (619.61 km^2) in 2014, showing a drastic component change of 3.47%, 2.95 % in the 1st period (1976–1998) and the 2nd period (1998–2014), respectively.

The overall annual rate of change in the decline form of forest cover (dense and open forest) was observed about 0.22% and 0.27% the 1st period (1976–1998) and the 2nd period (1998– 2014), respectively. As a result, the overall annual rate of change in increased form of non-forest was observed about 0.58% and 0.60% the 1st period (1976–1998) and the 2nd period (1998– 2014), respectively.

（a）

N

Legend

Non-forest area

Forest area

0   5   10
Km
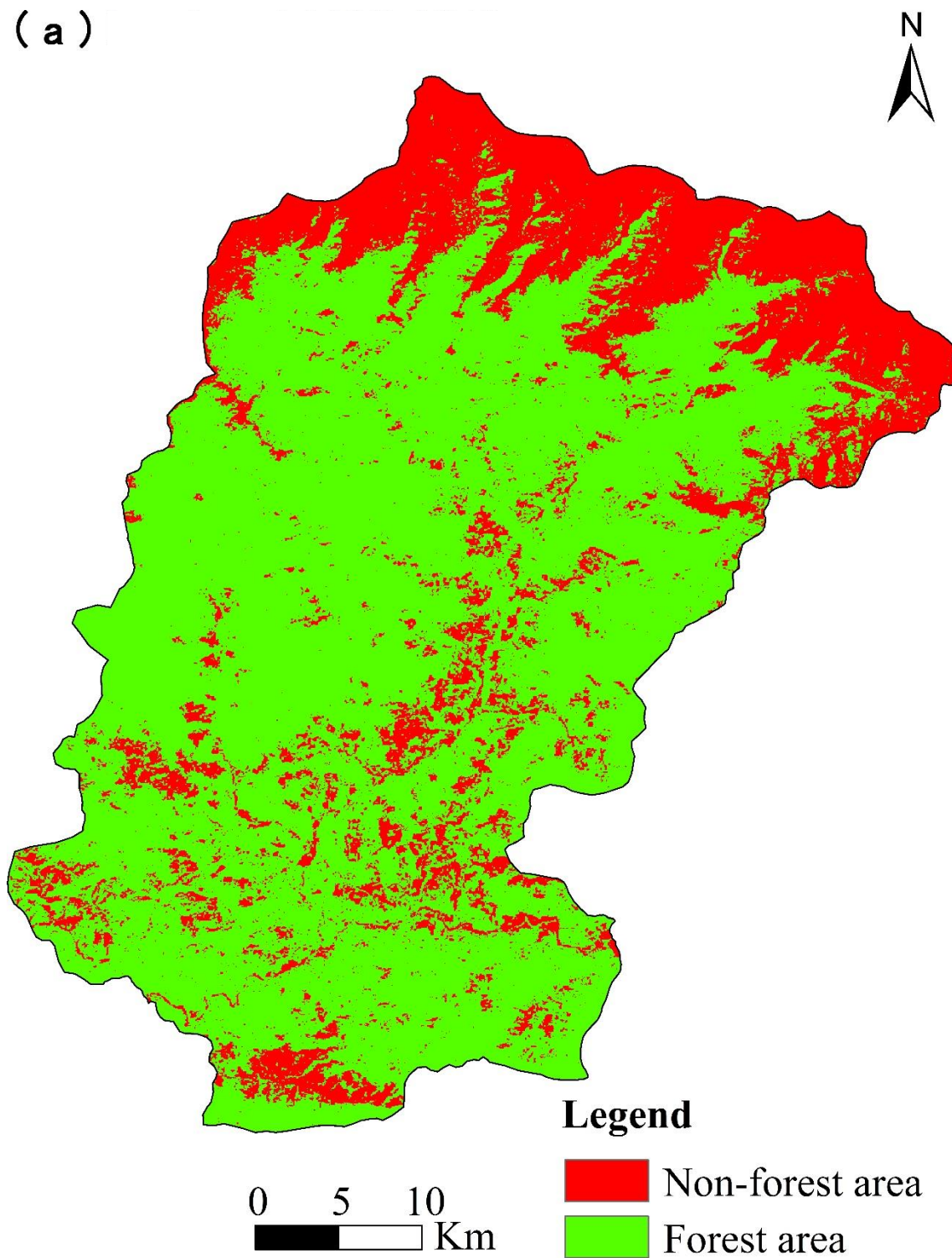
Figure 4.1a. Forest and non-forest map for the year 1976

52

（b）
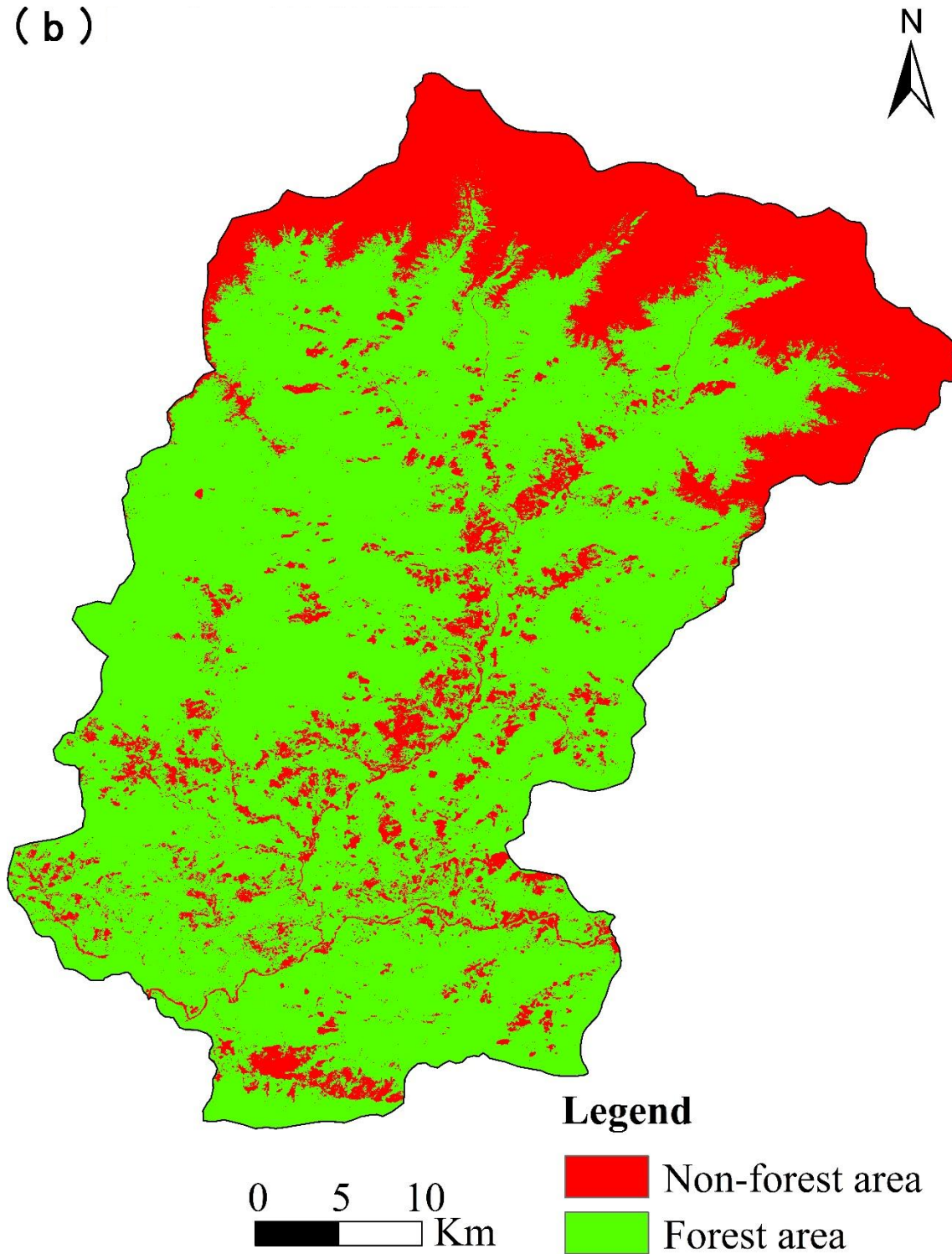
Figure 4.1b (continued). Forest and non-forest map for the year 1998

（c）
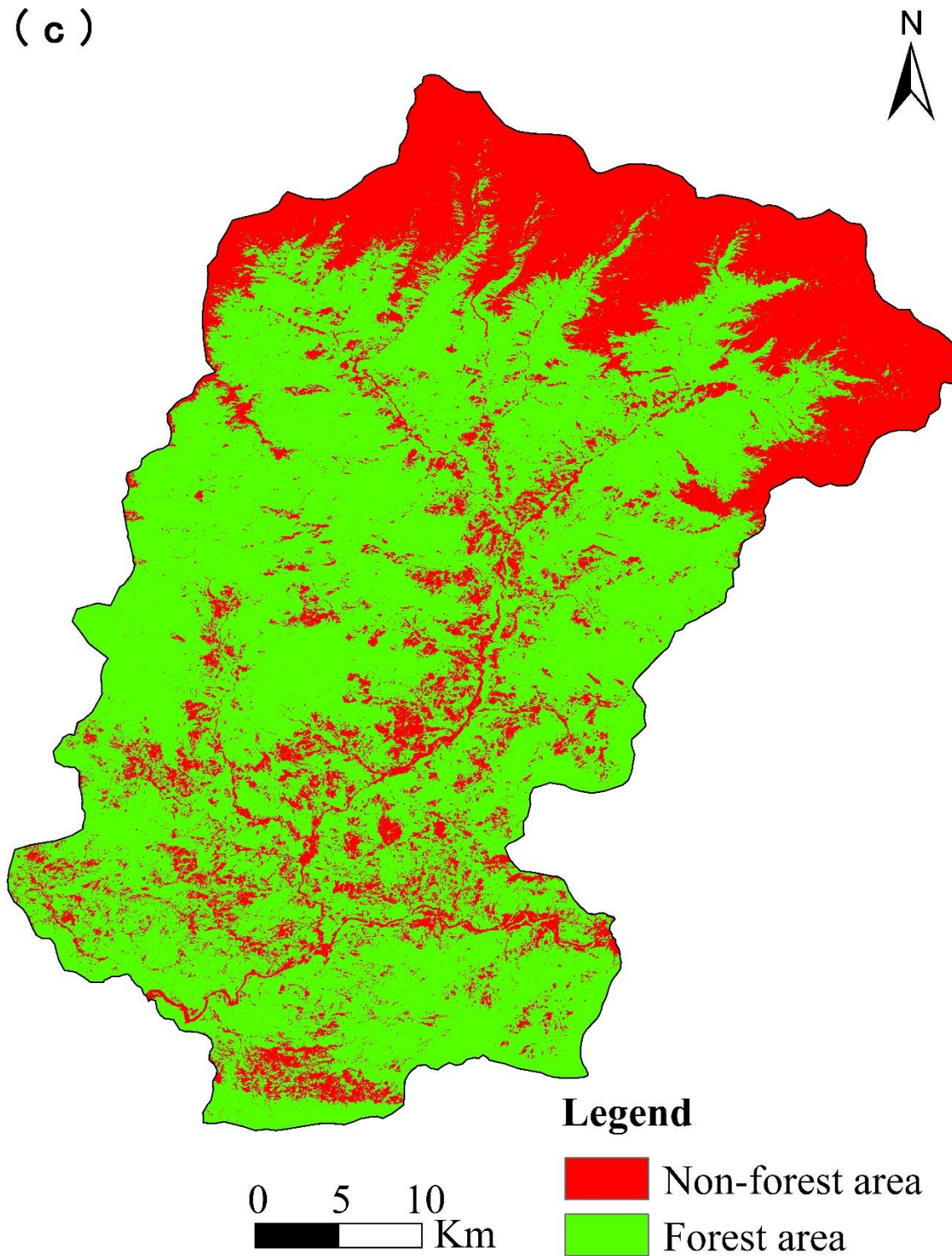
Figure 4.1c (continued). Forest and non-forest map for the year 2014

Table 4.1. Area, percentage, change, annual rate of change of the forest and non-forest classes.

Class type	1976		1998		2014		Change (1976–1998)	Change (1998–2014)	Annual rate of change (1976–1998)	Annual rate of change (1998–2014)
	Km^2	%[a]	Km^2	%[a]	Km^2	%[a]	%[b]	%[b]	%[c]	%[c]
Total forest	1440.81	74.42	1373.49	70.94	1316.45	68.00	-3.47	-2.95	-0.22	-0.27
Total non-forest	495.25	25.58	562.57	29.06	619.61	32.00	3.47	2.95	0.58	0.60
Total	1936.06	100	1936.06	100	1936.06	100				

[a] Percentage of each class out of the total area (study area=1936.06 km^2)
[b] Percentage change in component
[c] Percentage of annual rate of change in each class

4.3 Forest fragmentation pattern maps and status

The forest fragmentation pattern maps for the years 1976, 1998, and 2014 based on forest and non-forest areas were generated using the landscape fragmentation tool (LFT v2.0). A forest fragmentation pattern maps for the year 1976, 1998 and 2014 with categories of patch, edge, perforated, core small, core medium, and core large are shown in Figures 4.2 and 4.3 for the comparison in terms of the total area of each fragment classes.

（a）

Fragment classes
- ■ Patch (red)
- ■ Edge (blue)
- ■ Perforated (yellow)
- ■ Core small (bright green)
- ■ Core medium (olive green)
- ■ Core large (dark green)
- □ Non-forest area

0   5   10
         Km
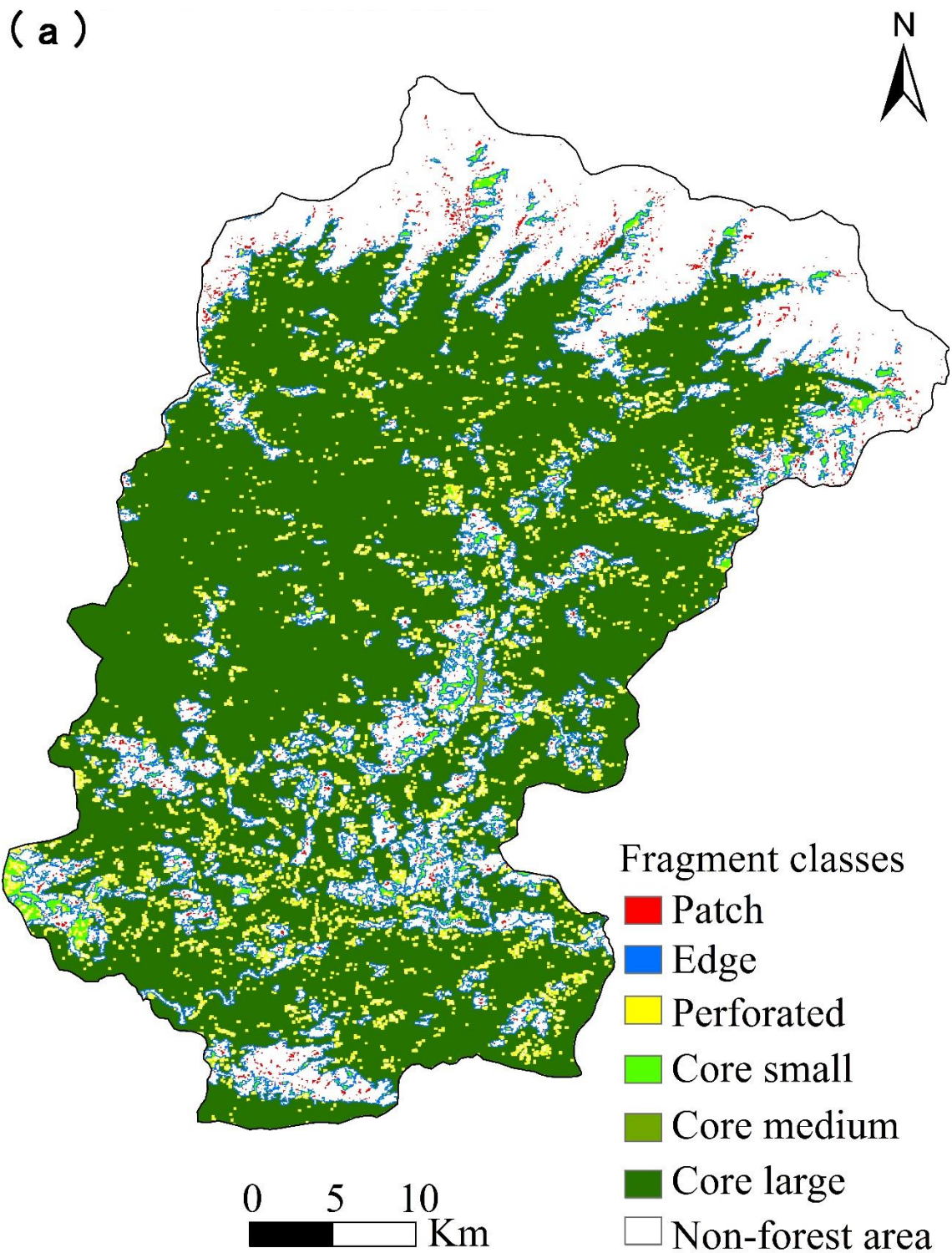
Figure 4.2a. Forest fragmentation map for the year 1976

（b）

Fragment classes
- ■ Patch
- ■ Edge
- ■ Perforated
- ■ Core small
- ■ Core medium
- ■ Core large
- □ Non-forest area

0   5   10
▬▬▬▬▬ Km
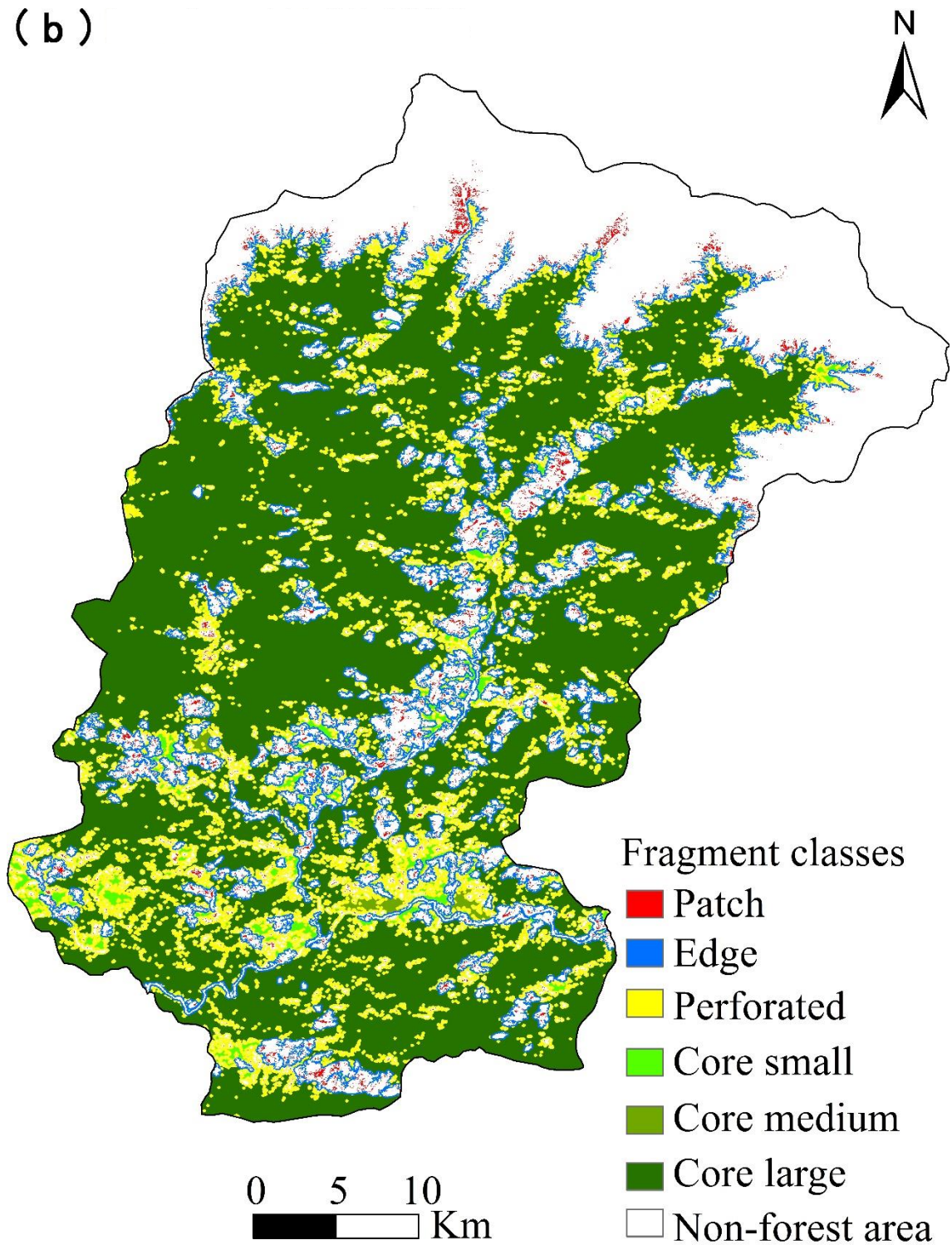
Figure 4.2b (continued). Forest fragmentation map for the year 1998

（c）

N

Fragment classes
- ⬛ Patch
- ⬛ Edge
- ⬛ Perforated
- ⬛ Core small
- ⬛ Core medium
- ⬛ Core large
- ⬜ Non-forest area

0   5   10
▬▬▬▬▬▭ Km
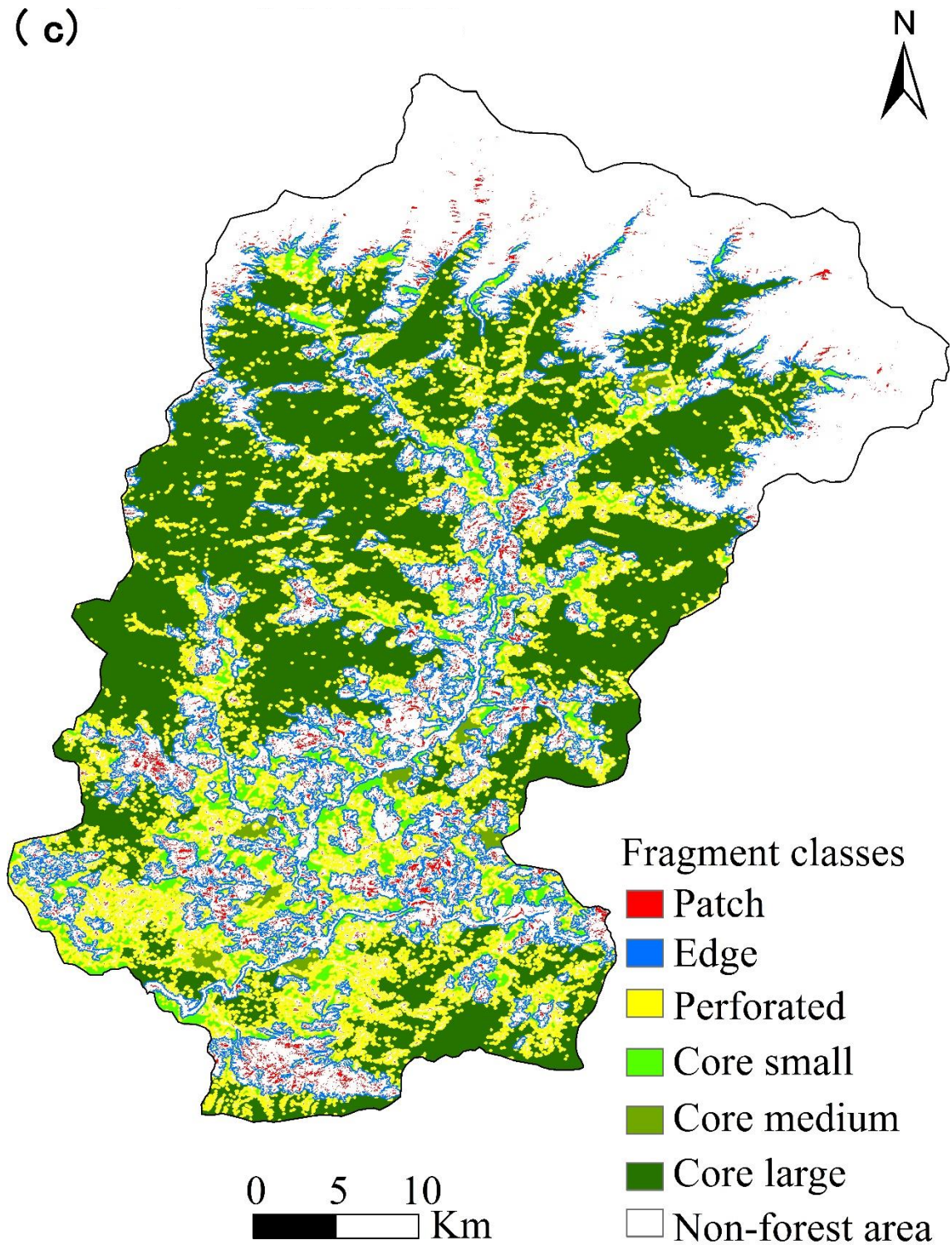
Figure 4.2c (continued). Forest fragmentation maps for the year 2014
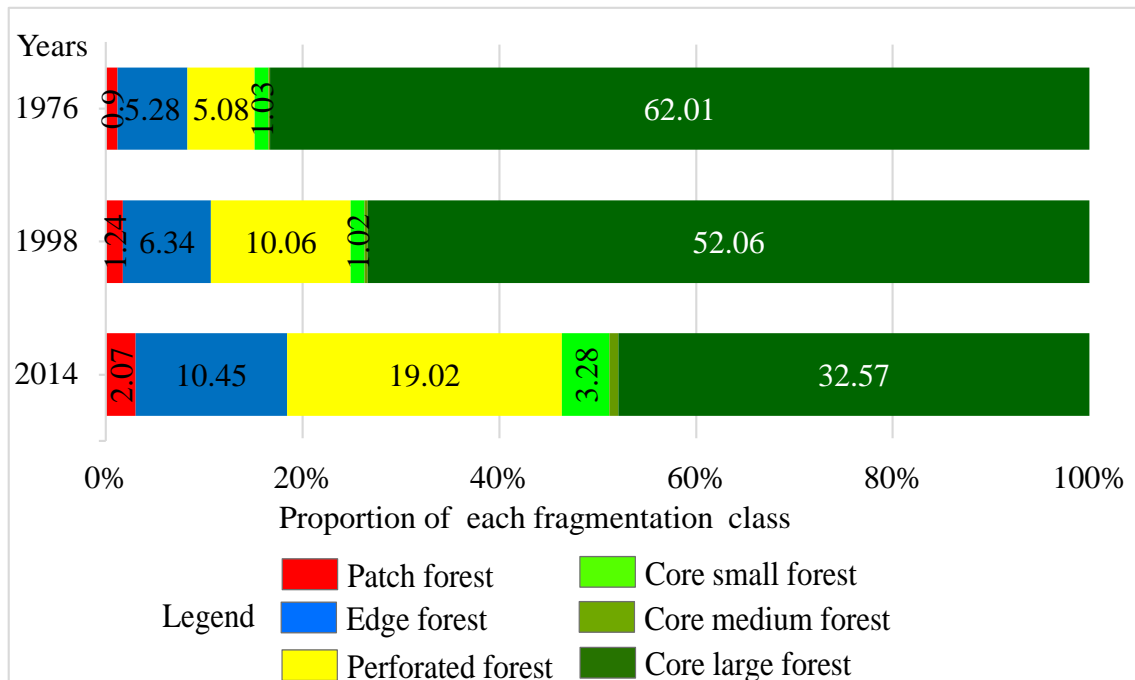
Figure 4.3. Comparison of forest fragmentation pattern classes by percentage of the total forest area (study area $= 1936.06 \ \text{km}^2$)

4.4 Forest fragmentation changes

Table 4.2 summarizes the result of forest fragmentation change from 1976 to 2014. Forest fragmentation analysis showed a significant decrease in the compact forest area (large core forest) from 1976 to 2014. In 1976, the large core forest was dominant covering 62.01 % of the total study area, followed by edge forest (5.28 %), perforated forest (5.08 %), core small (1.03 %), patch forest (0.90 %), and medium core (0.12 %). Between 1998 and 2014, the large core forest further decreased, while medium core, small core, edge, and patch forest increased.

The area under large core forest has decreased from 62.01 % in 1976 to 32.57 % in 2014, showing a component change of 9.95 %, and 19.49 % in the 1st period (1976–1998) and the 2nd period (1998–2014), respectively. The area under patch, edge, perforated, and medium core forest progressively increased from 0.90%, 5.28 %, 5.08 %, and 0.12 % in 1976 to 2.07 %, 10.45%, 19.02%, and 0.61% in 2014, respectively, showing a component change of 0.34 %, 1.32 %, 4.97 %, and 0.10 % in the 1st period (1976–1998) and 0.83 %, 4.01 %, 8.96 % and 0.38 % in the 2nd period (1998–2014), respectively. Small core forest slightly decreased by 1.02% in 1998, and then drastically increased by 3.28% in 2014,

showing a decreased change of 0.01% in the 1st period and an increased change of 2.25% in the 2nd period. An overall decrease in forest area from 3.47% in the 1st period to 2.94% in the 2nd period was observed, while an overall increase in non-forest area from 3.47% in the 1st period to 2.94% in the 2nd period was observed.

A declining annual rate of change for large core forest was observed at about 0.79% and 2.93% in the 1st period (1976–1998) and the 2nd period (1998–2014), respectively. Other increasing annual rates of change were observed in patch, edge, perforated, and medium core forests in the 1st period and the 2nd period, although small core forest decreased in the 1st period, and then increased again in the 2nd period. A declining overall annual rate of change for the total forest cover was observed at 0.22% and 0.27% for the 1st period and the 2nd period, respectively. As a result, the overall annual rate of change in non-forest increased from 0.58% in the 1st period to 0.60% in the 2nd period.

Table 4.2. Forest fragmentation in area, percentage, change, annual rate of change of each class

Fragmentation classes	1976		1998		2014		Change (1976–1998)	Change (1998–2014)	Annual rate of change (1976–1998)	Annual rate of change (1998–2014)
	km^2	%[a]	km^2	%[a]	km^2	%[a]	%[b]	%[b]	%[c]	%[c]
Patch	17.46	0.90	23.97	1.24	40.13	2.07	0.34	0.83	1.44	3.22
Edge	102.13	5.28	122.76	6.34	202.24	10.45	1.32	4.10	0.83	3.12
Perforated	98.32	5.08	194.69	10.06	368.32	19.02	4.97	8.96	3.11	3.98
Core small	19.91	1.03	19.74	1.02	63.41	3.28	-0.01	2.25	-0.04	7.29
Core medium	2.39	0.12	4.37	0.23	11.76	0.61	0.10	0.38	2.73	6.17
Core large	1200.57	62.01	1007.93	52.06	630.57	32.57	-9.95	-19.49	-0.79	-2.93
Total forest	1440.81	74.41	1373.49	70.94	1316.45	68.00	-3.47	-2.94	-0.22	-0.27
Total non-forest	495.25	25.58	562.57	29.06	619.61	32.00	3.47	2.94	0.58	0.60

[a] Percentage of each class out of the total study area (study area=1936.06 km^2)
[b] Percentage change in component
[c] Percentage of annual rate of change in each class

Chapter 5
Assessment of the forest fragmentation probability in the Garhwal Himalaya

5.1 Patch forest

The patch forest map was extracted from forest fragmentation map for the year 1976, 1998, and 2014, using the analyst tool in ArcGIS, which resulted in total of 39621 grid cells. The total forest patch cover area is of about 81.56 km^2, which is 4.21% of the total study area. The Figure 5.1 shows the final output of patch forest map of the Rudraprayag district.

5.2 Forest fragmentation probability map

The forest fragmentation probability map was derived based on patch forest and causative factors using the WOE method. The final output of forest probability map of the district is shown in Figure 5.2. There are various mathematical methods available to classify predicative degrees (Ayalew et al., 2004). The forest fragmentation probability map was divided into four classes by the defined interval method using ArcGIS. On the forest fragmentation probability map, 62.16% of the area has very low susceptibility, while 11.49%, 16.66%, and 9.69% of the area has low, medium, and high susceptibility, respectively. The majority of the areas falls under the very low forest fragmentation probability classes.

5.3 Validation of forest fragmentation probability map

In this study, the success-rate curves were obtained using the IDRISI Selva 17.0 software package. The AUC value obtained from the susceptibility maps clearly shows that the model gave the highest success rate (AUC = 0.786). The resulting map of areas susceptible to forest fragmentation has a prediction accuracy of 78.6%. The ROC (AUC) curve for this study is shown in Figure 5.3.

5.4 Analysis of forest fragmentation probability

Figure 5.4 shows that the forest fragmentation causative factors for the study area indicate weight contract value: positive weight contrast and negative weight contrast. The result of the weighted contrast value shows that forest fragmentation probability was primarily observed near built-up area (less than 500 m), agriculture land (less than 500 m), roads

(less than 1000 m), and streams (less than 500 m) with very gentle and gentle slopes (less than 25 degree) at the lower to middle altitude zones (less than 2000 m). The probability map of forest fragmentation shows that medium to high probabilities are primarily concentrated near the roads and agriculture land area on very gentle to gentle slopes at the lower altitudes. The probability map of forest fragmentation also shows that the role of higher altitude zone (more than 2000 m) is less significant, and the factors such as distance to roads, distance to agriculture land, distance to built-up area and slopes are more important.
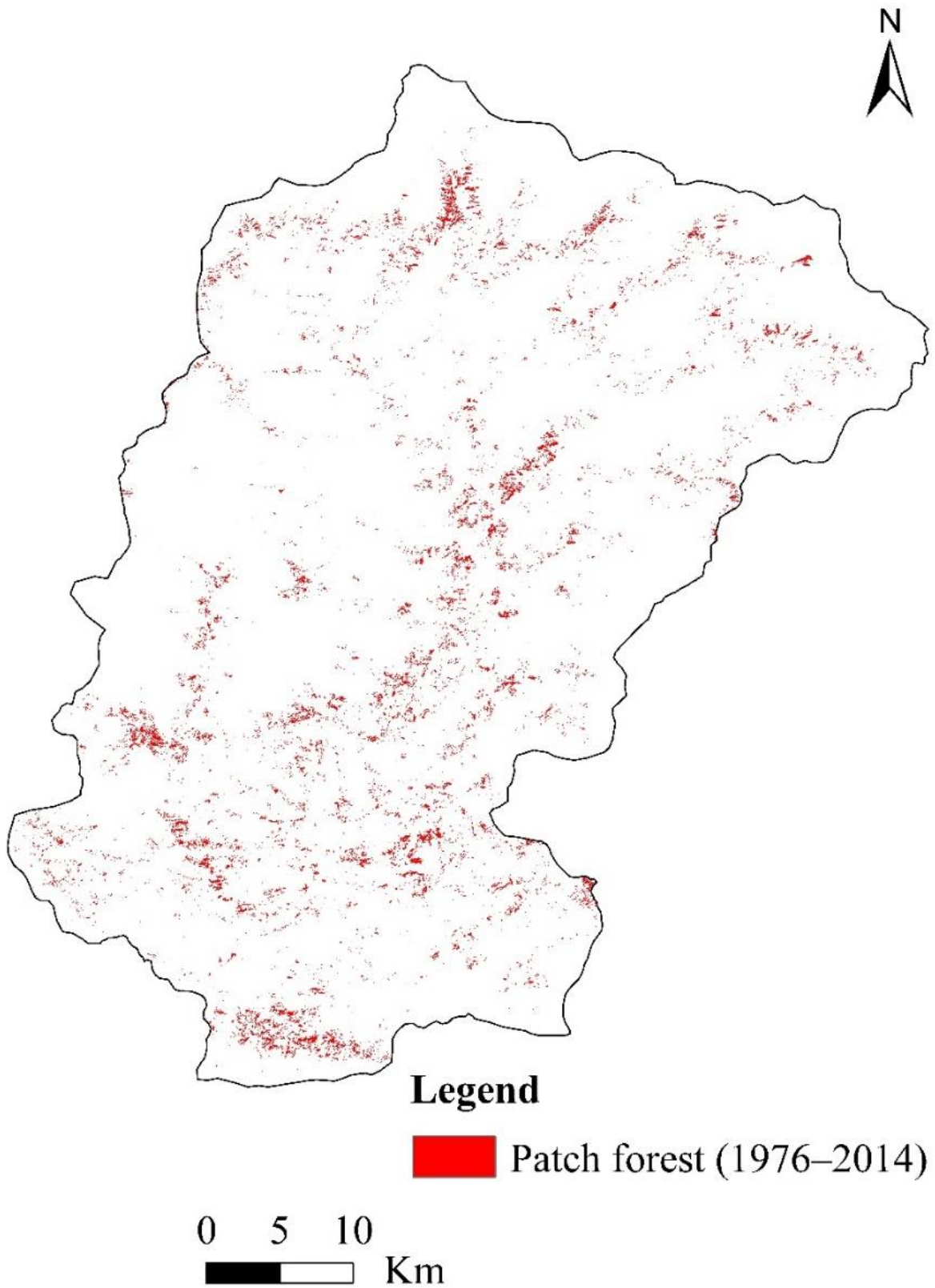
Figure 5.1. Distribution map of patch forest of the Rudraprayag district (1976–2014).
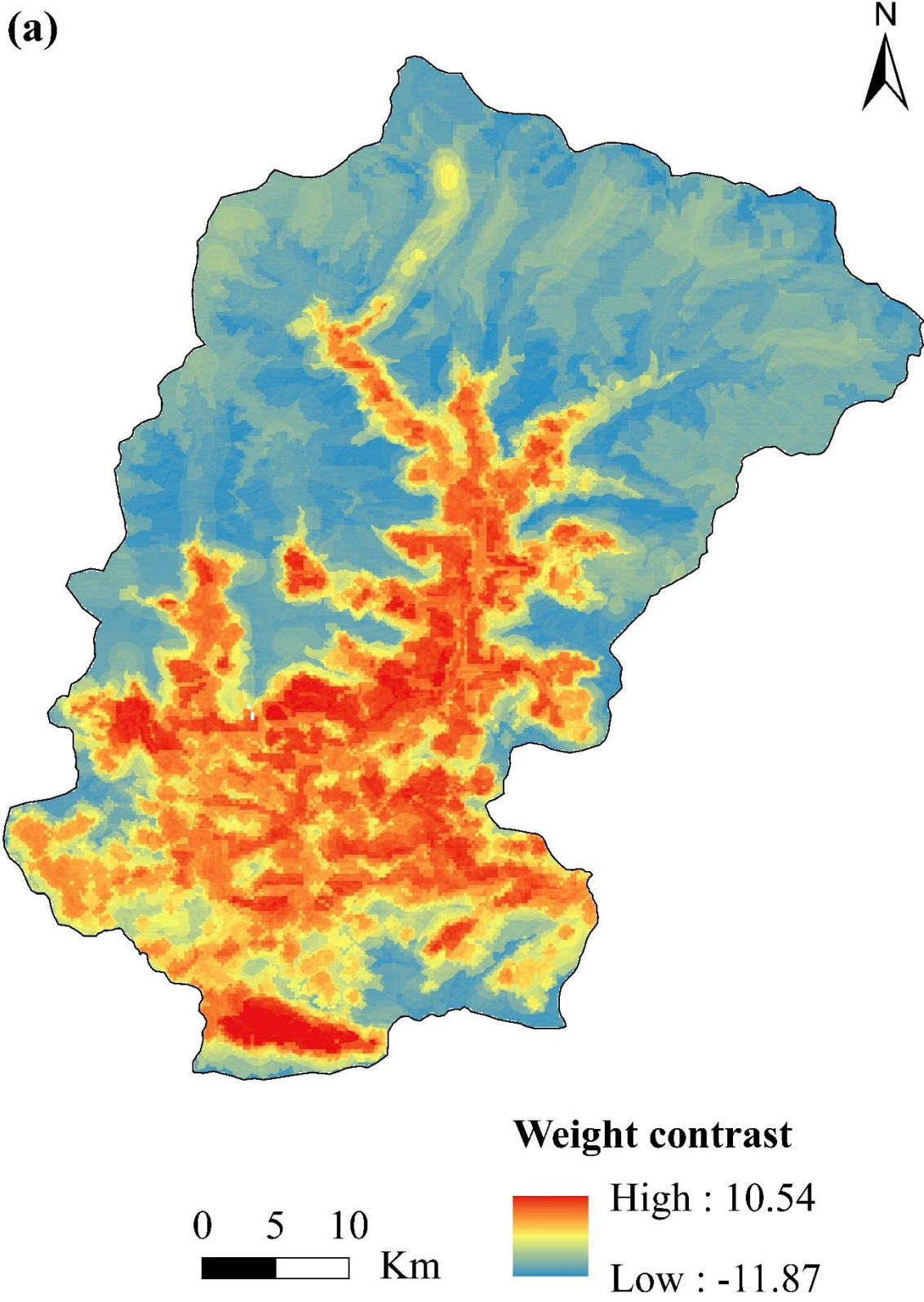
Figure 5.2(a). Forest fragmentation probability map showing the distribution of range of all weight contract values, i.e., negative and positive.

(b)

Probability classes

■ Very low (62.16%)

□ Low (11.49%)

■ Medium (16.66%)

■ High (9.69%)

0 5 10 Km
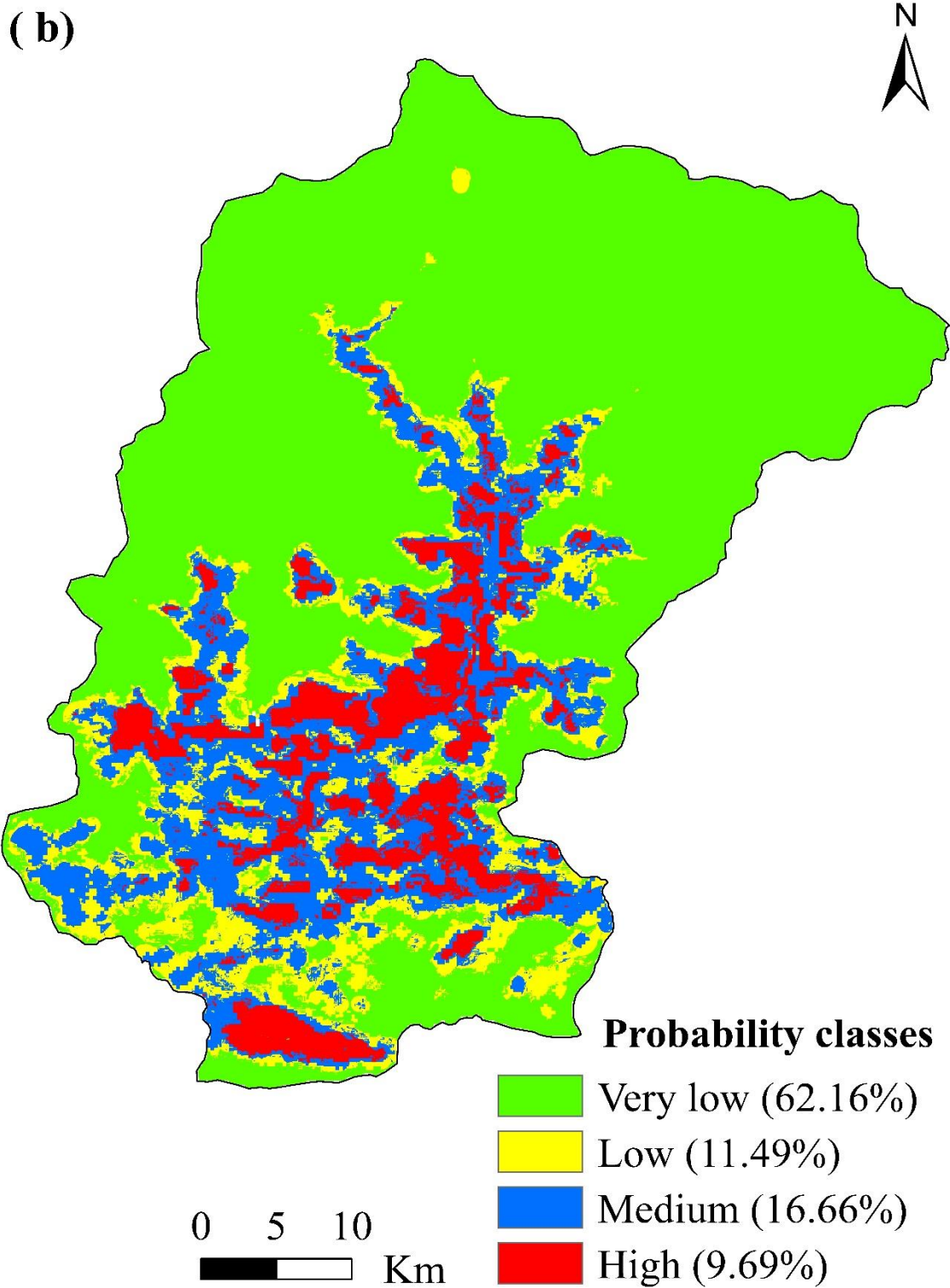
Figure 5.2(b) (continued). Forest fragmentation probability map showing the distribution of the different probability classes, i.e., very low to high forest fragmentation probability.
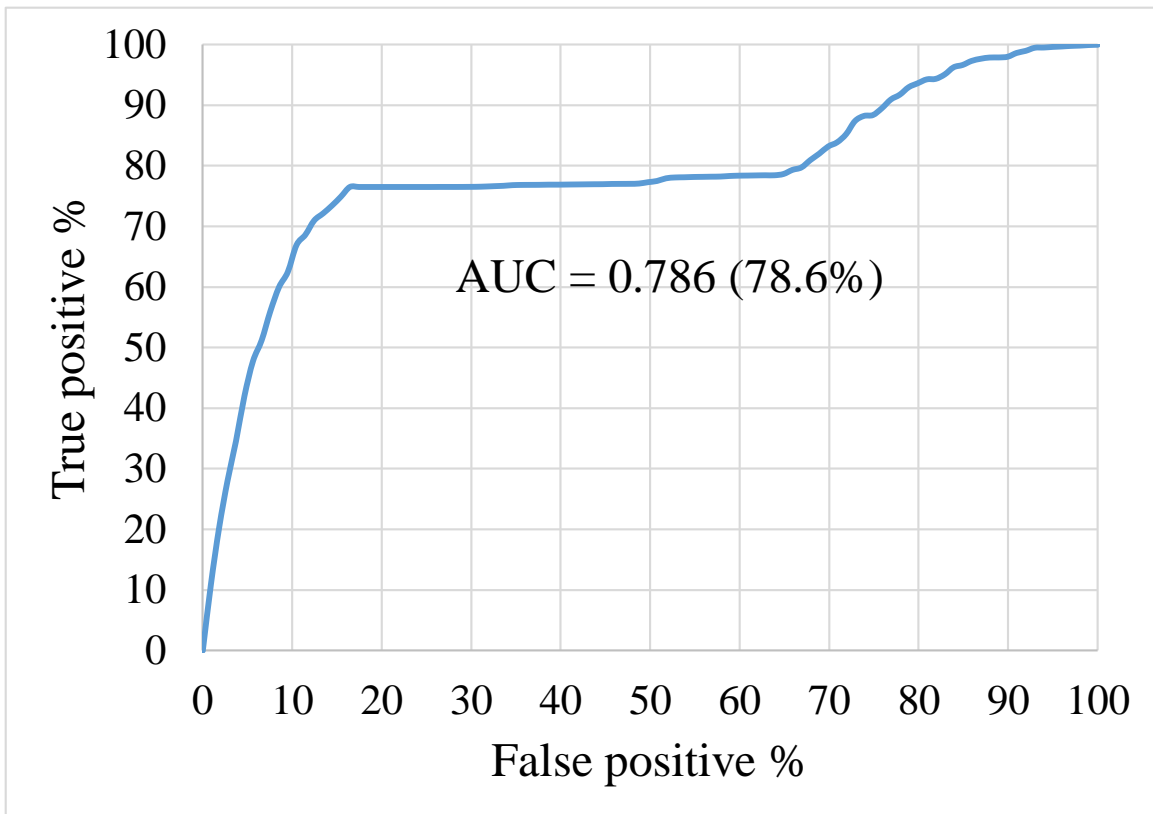
Figure 5.3. The graph showing validation of forest fragmentation probability map under ROC (AUC) curve using the IDRISI Selva.

a) Slope angle
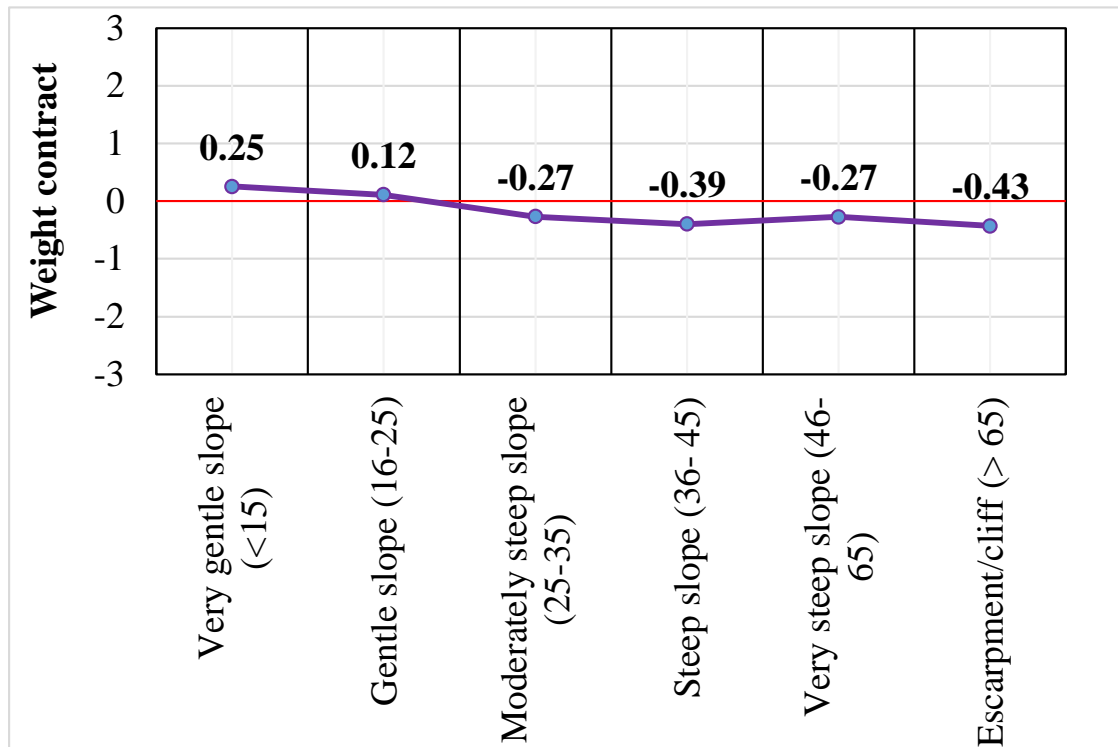
b) Slope aspect
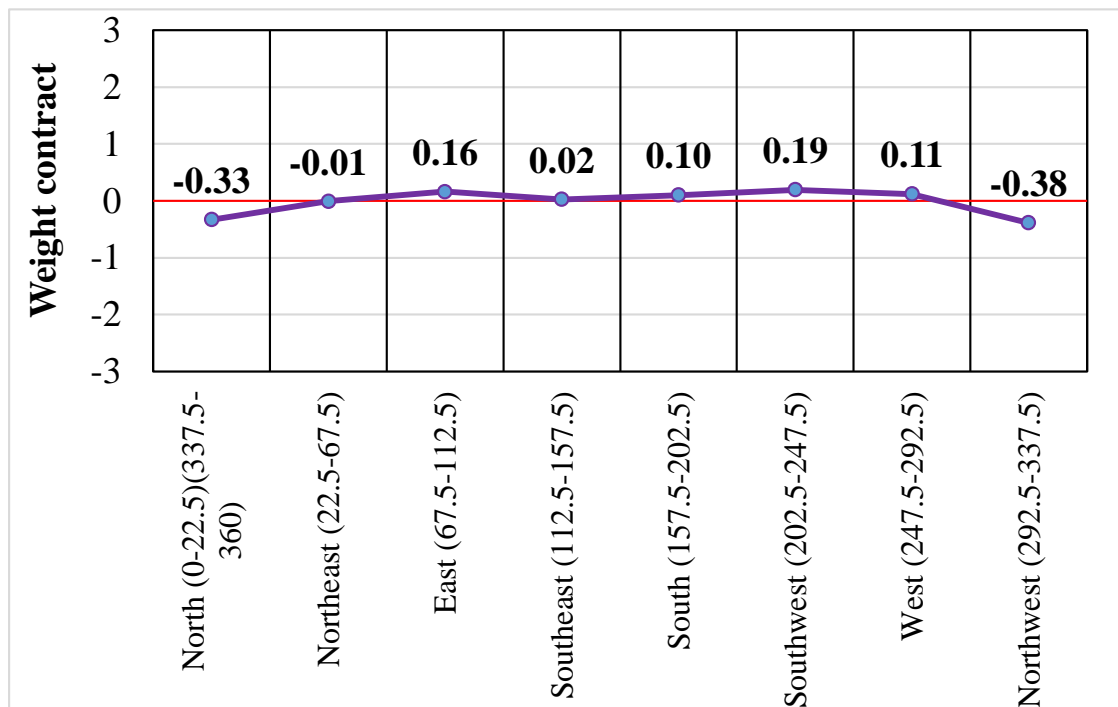
Figure 5.4. Forest fragmentation causative factors for the study area showing weight contract value, i.e., negative and positive: **(a)** slope angle, and **(b)** slope aspect.

c) Distance to streams
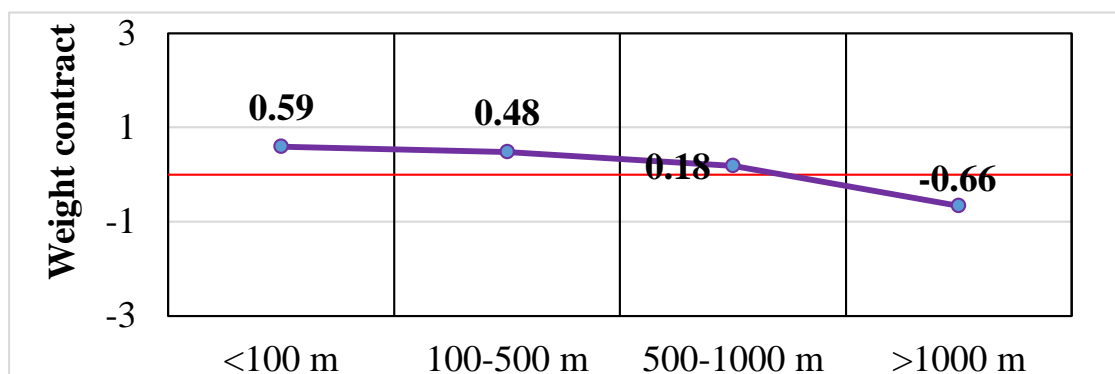
d) Altidude zone based on rainfall

e) Distance to roads
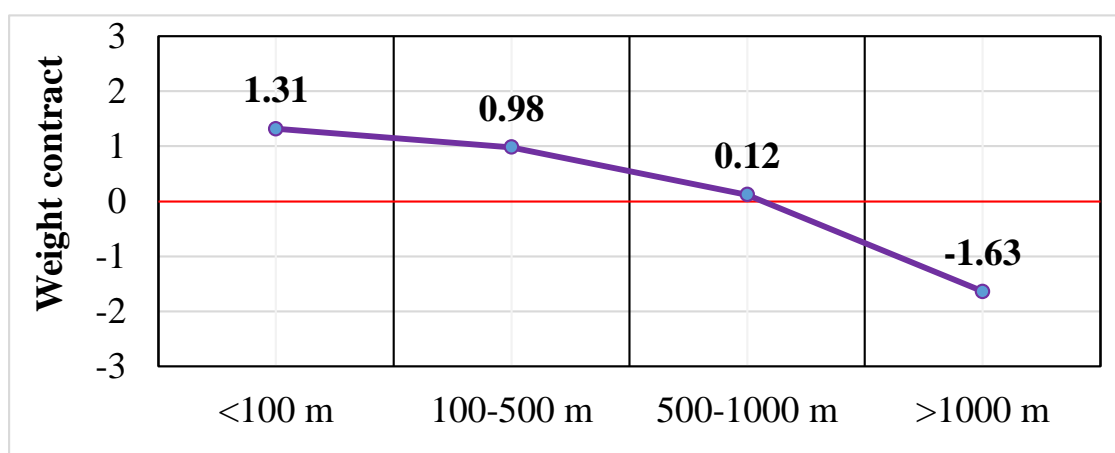
Figure 5.4 (continued). Forest fragmentation causative factors for the study area showing weight contract value, i.e., negative and positive: **(c)** distance to streams, **(d)** altitude zone, and **(e)** distance to roads.

f) Distance to agriculture land
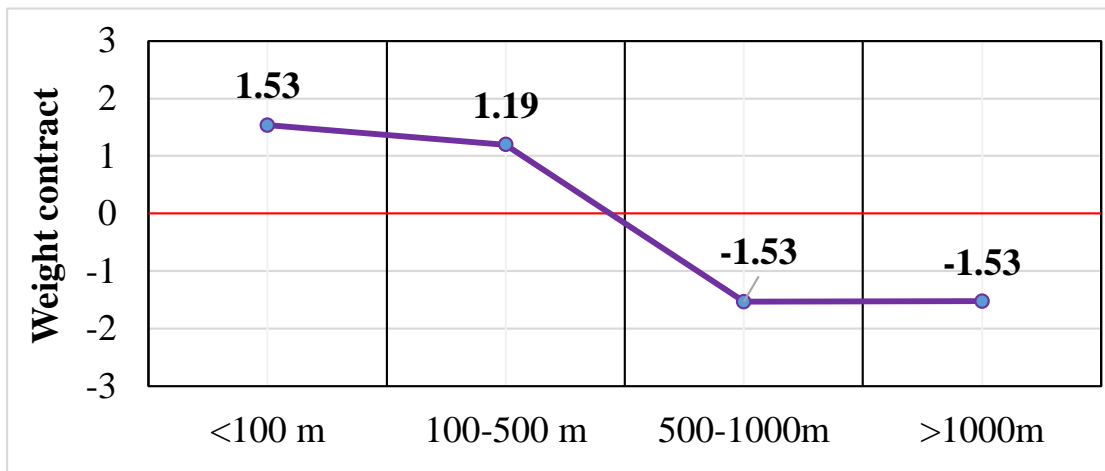
g) Distance to built-up area
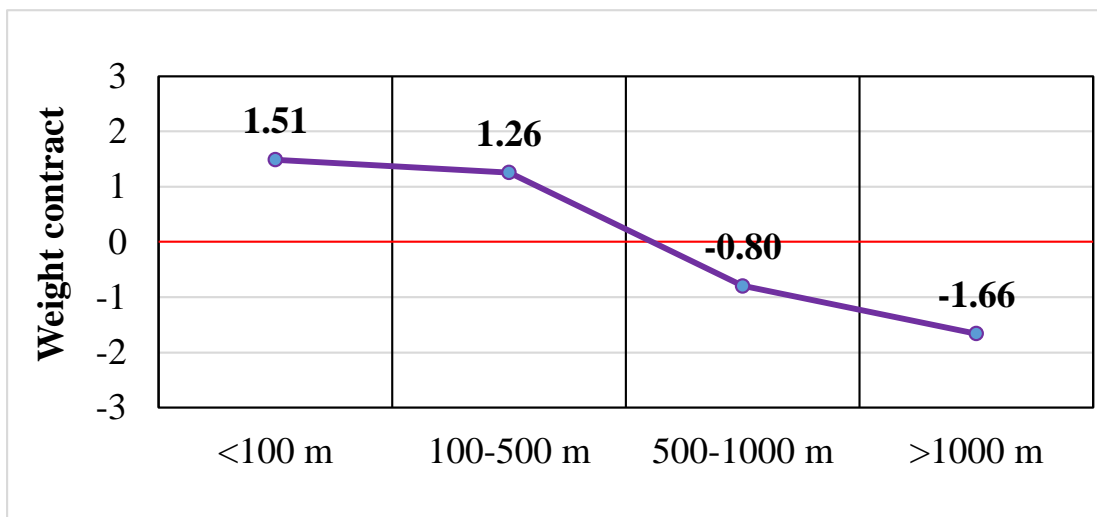
Figure 5.4 (continued). Forest fragmentation causative factors for the study area showing weight contract value, i.e., negative and positive: (**f**) distance to agriculture land, and (**g**) distance to built-up area.

Chapter 6
Assessment of the landslide susceptibility in the Garhwal Himalaya

6.1 Landslide inventory

In order to apply WOE method, 293 landslide polygons were extracted from the years 2011, 2012, 2013, which were based on open data sources and ground field work. Landslides cover an area of about 7.46 km^2 (total of 74704 grid cells), which is 0.38% of the total study area. The final output of the landslide inventory map of the district is shown in Figure 6.1.

6.2 Landslide susceptibility map

The landslide susceptibility map was derived based on landslide inventory and causative factor using the WOE method. Figure 6.2 shows the final output of the landslide susceptibility map of the district. The landslide susceptibility was divided into four classes by the defined interval method using ArcGIS. On the landslide susceptibility map, 61.57% of the area falls under very low susceptibility class, while 22.21%, 14.82%, and 1.40% of the area belong to low, medium and high susceptibility classes, respectively. The majority of the areas are belongs to very low landslide susceptibility class.

6.3 Validation of landslide susceptibility map

The AUC value obtained from the susceptibility maps shows that the model gave the highest success rate (AUC = 0.778), which implies that the resulting map of areas susceptible to landslides has a prediction accuracy of 77.8%. The ROC (AUC) curve for this study is shown in Figure 6.3.

6.4 Analysis of landslide susceptibility

Figure 6.4 show the graphs of landslide susceptibility causative factors for the study area, and their corresponding weight contract value: positive weight contrast and negative weight contrast. The most susceptible classes of the lithology factor, in the order of importance are: (1) garnetiferous gneiss, schist, and migmatite (2) porphyritic gneiss, and mica schist, and (3) granite gneiss, mica schist, cale zones. Regarding geomorphology, the most susceptible classes are alluvium zone, alluvium terrace, and glacier terrace. In

the case of soil types, the most susceptible classes are fine loamy, and loamy skeletal. The most susceptible classes of the soil depth are shallow, moderate deep, and deep. The weight contrast values of slope show that there is a strong correlation between the slope degree and the landslide occurrence, so that the weight contrast was increased with a greater degree of the slope apart from the slope above 65 degrees. In the case of slope aspect factor, the most susceptible classes were southeast and south directions. Regarding LULC factor, the susceptible classes were scrub land, built-up area, pasture land, barren land, and agriculture land showed that there is a strong correlation between the non-forest area and the landslide occurrence. The lack of vegetation at high altitude means that there is strong possibility of increasing slope exposure due to more rainfall. Regarding the altitude zone based on rainfall, one class with the precipitation (>100 to 200 m) higher than 3000 m is most susceptible to landslide occurrence. In the case of distance to roads and distance to streams, the susceptibility was reduced by moving away. This susceptible class indicates that there is a strong correlation between landslide occurrences and distance from roads and streams. However, for distance to faults, distance to thrusts, distance to lineaments, there is no clear evidence of susceptibility of the classes. In conclusion, the result clearly shows that medium to high landslide susceptibilities had occurred mainly in the non-forest area. The result of the weighted contrast value showed that most of the medium to high landslide susceptibilities are primarily concentrated in the areas adjacent to higher altitudes, steep slopes, and the non-forest area such as scrub land, barren land, built-up area, agriculture land, and pasture land.
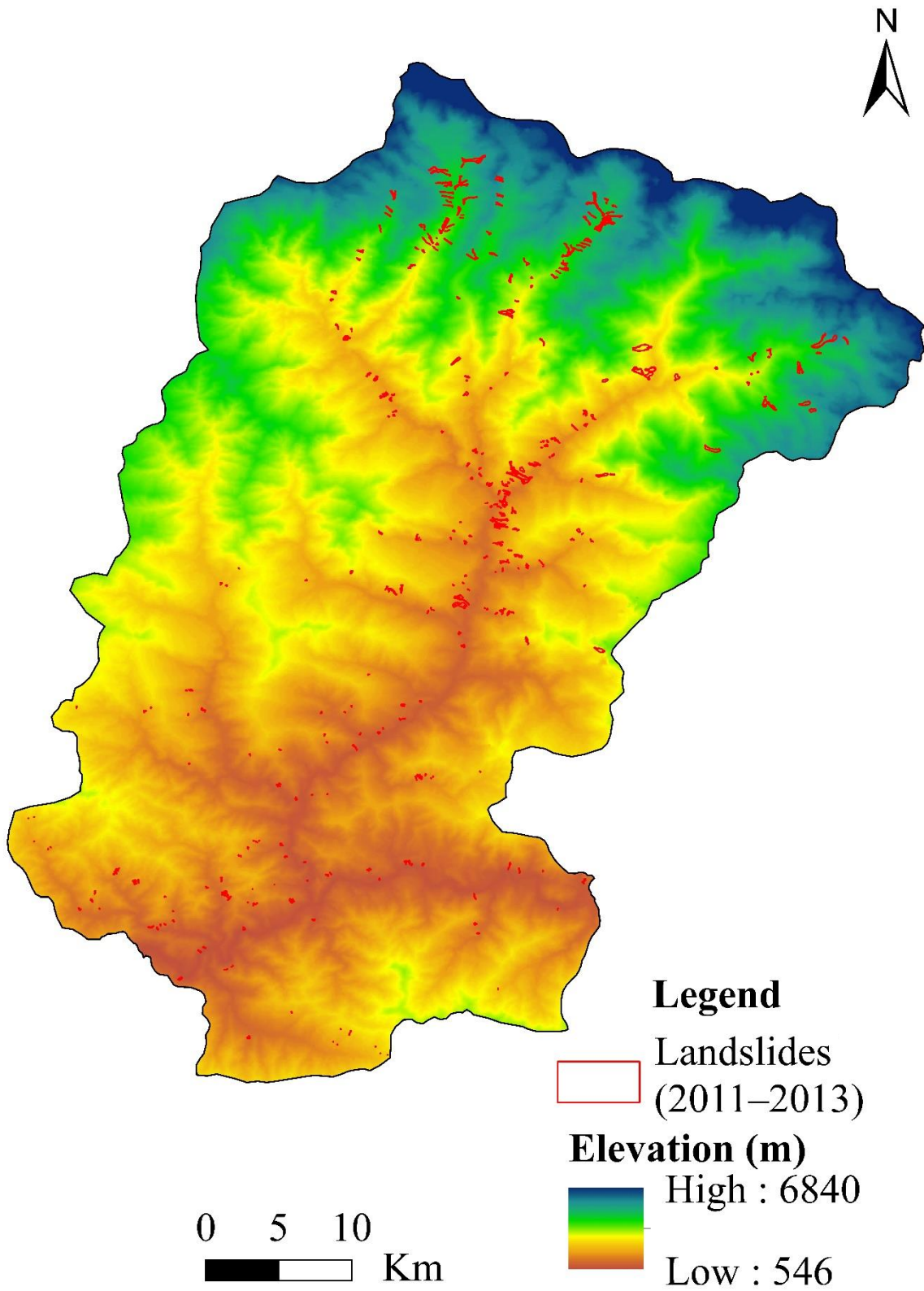
Figure 6.1. Distribution map of landslides in the Rudraprayag district (2011–2013).
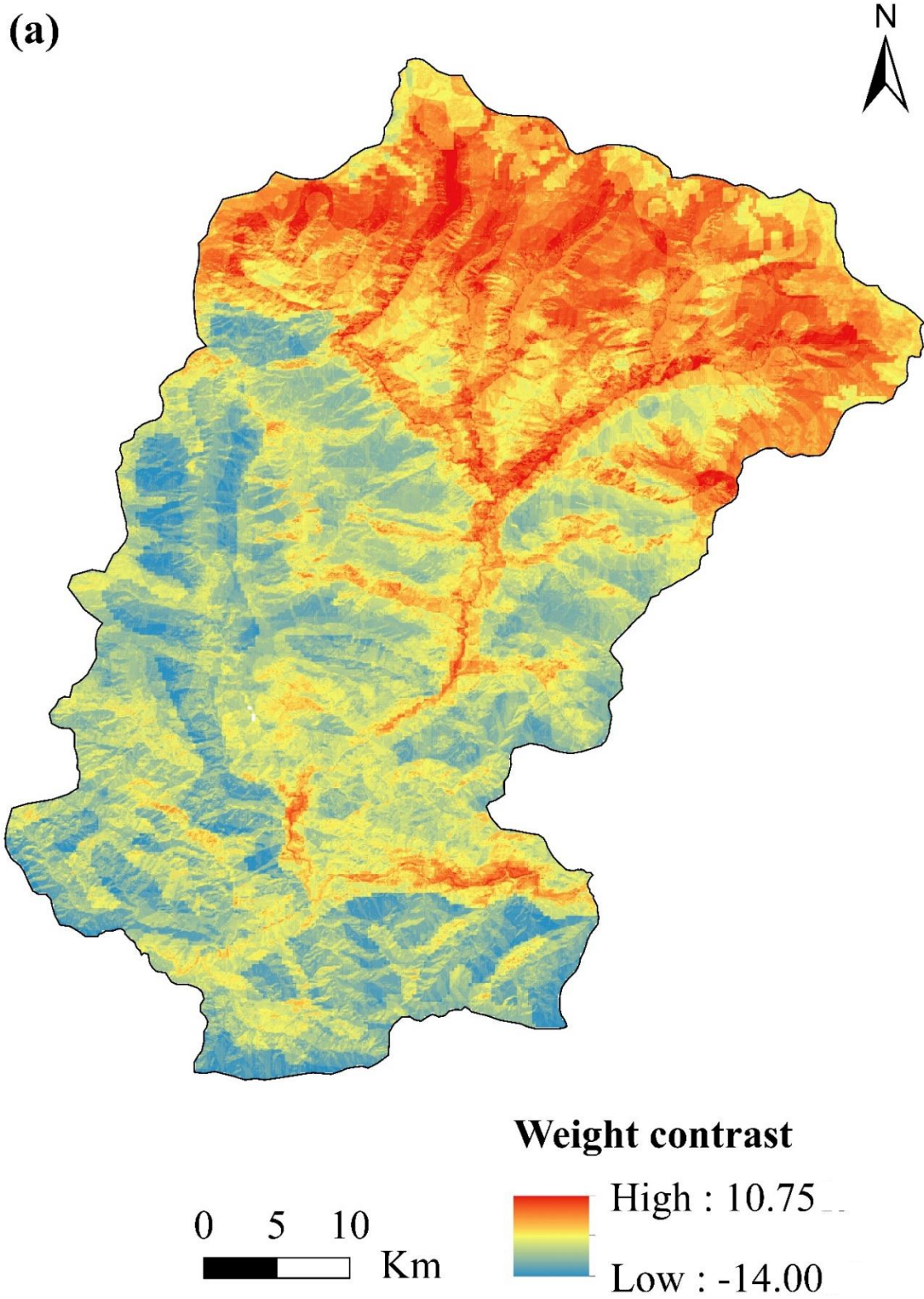
Figure 6.2a. Landslide susceptibility map showing the distribution of the range of all weight contract values, i.e., negative and positive.
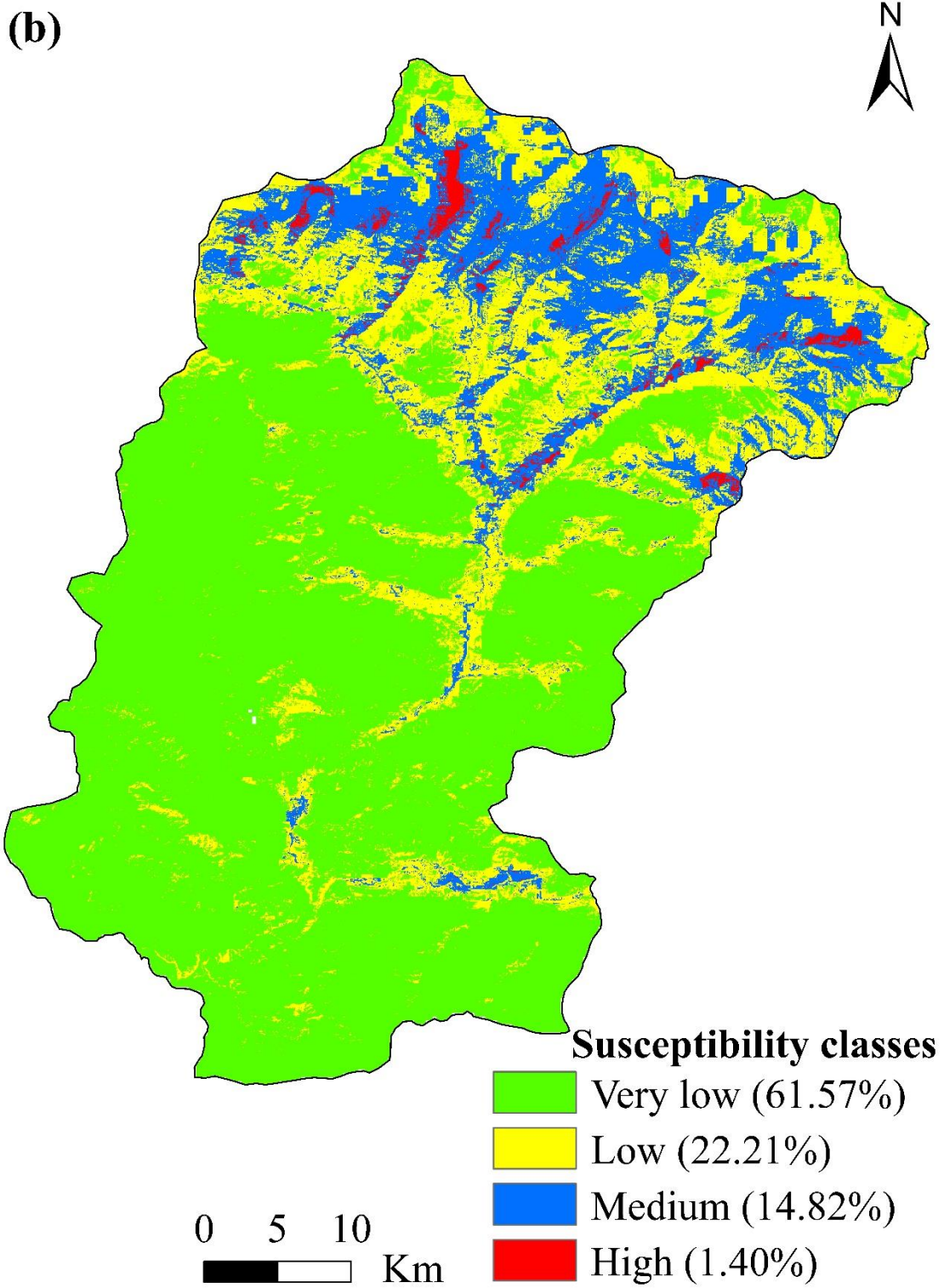
Figure 6.2b (continued). Landslide susceptibility map showing the distribution of the different probability classes, i.e., very low to high landslide susceptibility
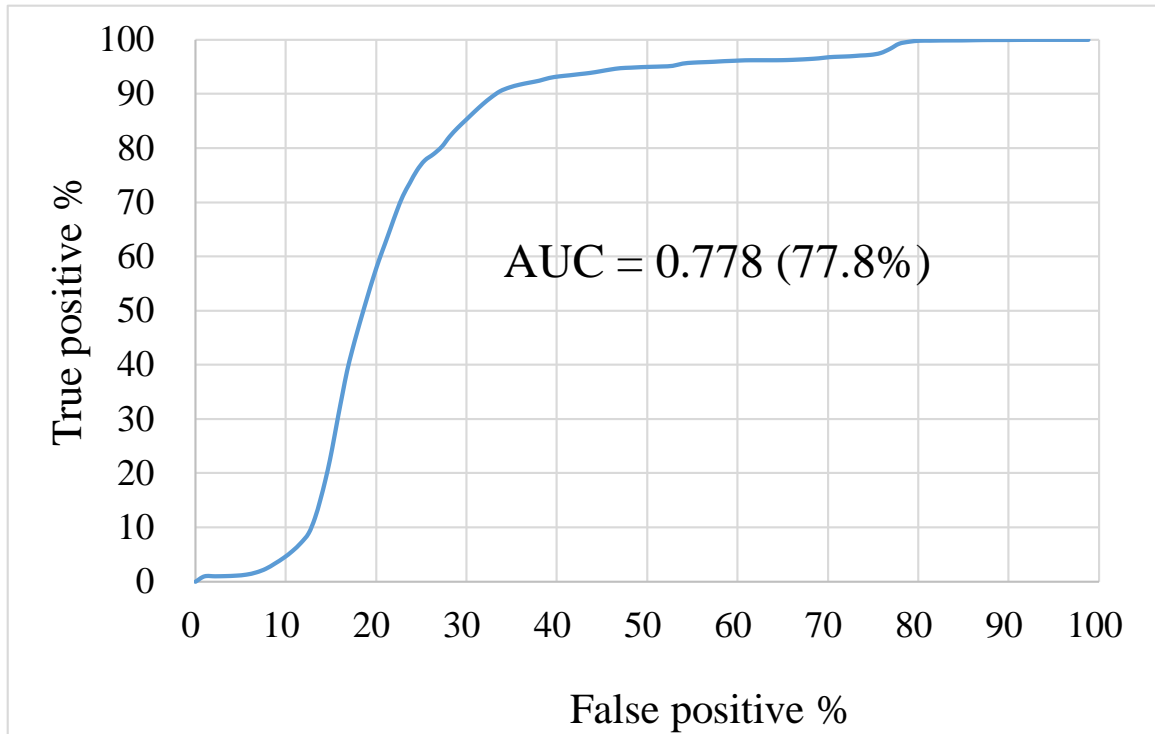
Figure 6.3. The graph showing validation of landslide susceptibility map under ROC (AUC) curve using the IDRISI Selva.

a) Geology
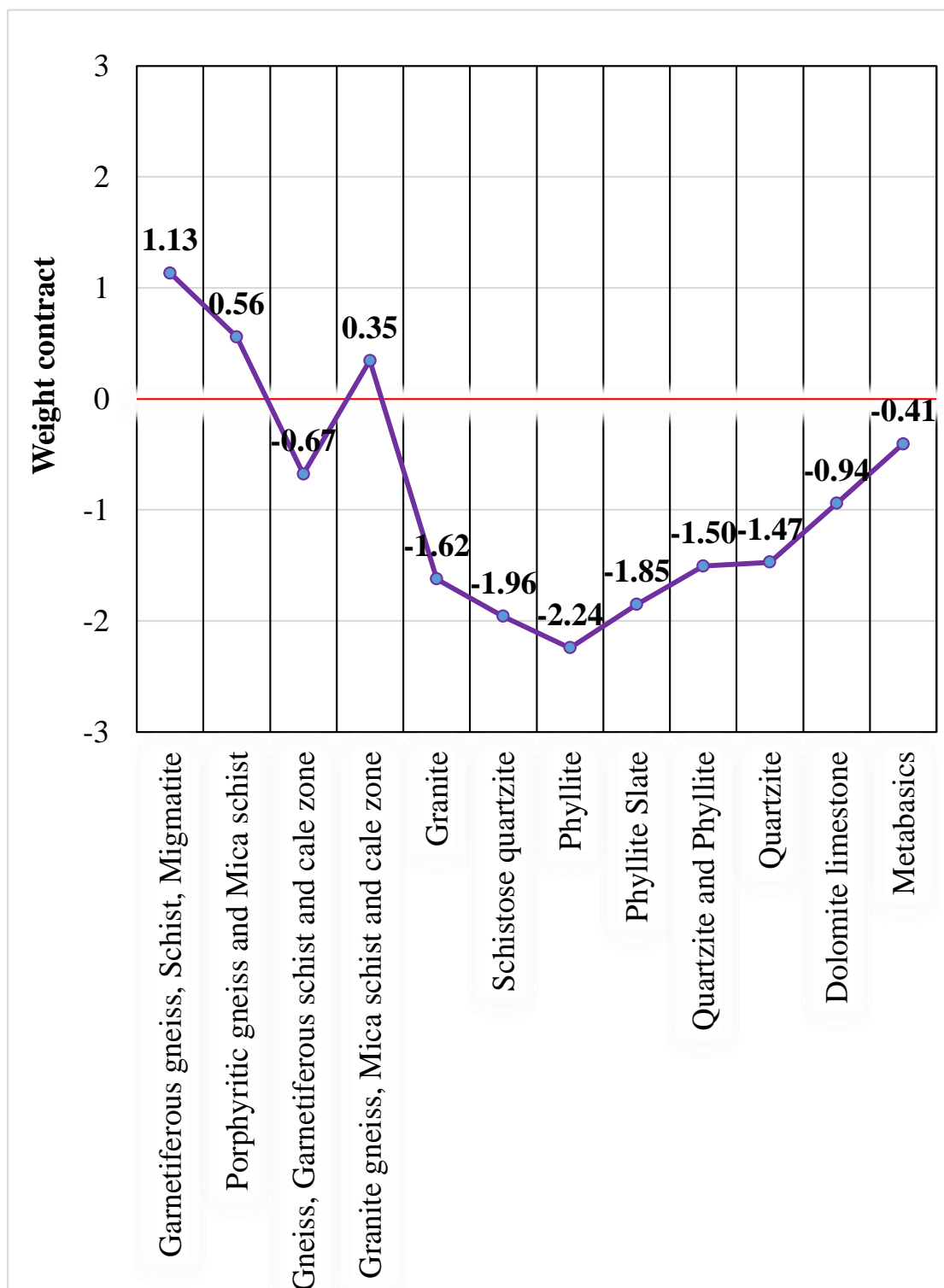
Figure 6.4a. Landslide susceptibility causative factors for the study area showing weight contract value, i.e., negative and positive: geology.

b) Geomorphology
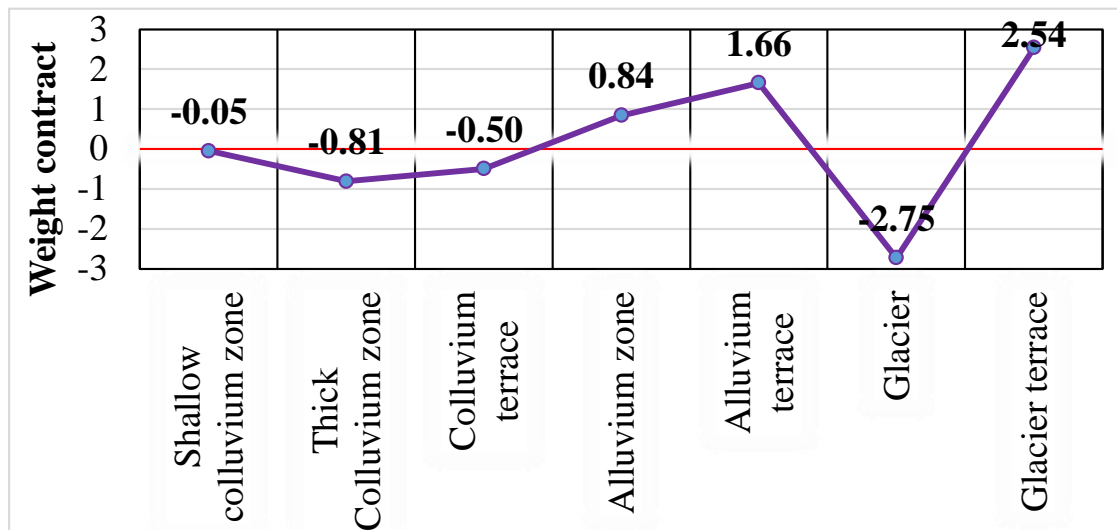
c) Soil type
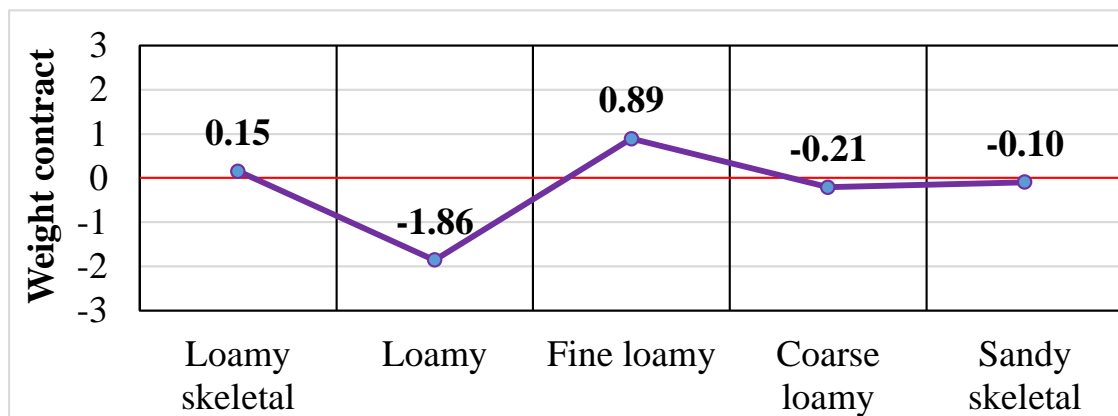
d) Soil depth
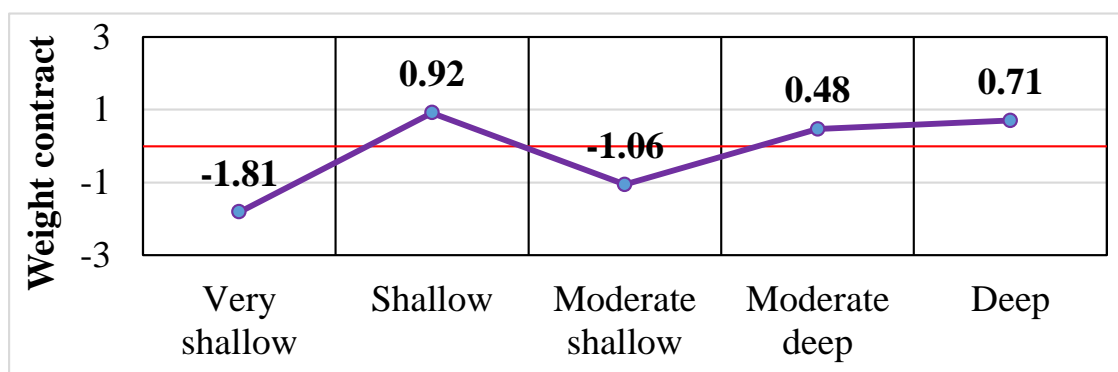
Figure 6.4b-d (continued). Landslide susceptibility causative factors for the study area showing weight contract value, i.e., negative and positive: **(b)** geomorphology, **(c)** slope type, and **(d)** soil depth.

e) Slope angle
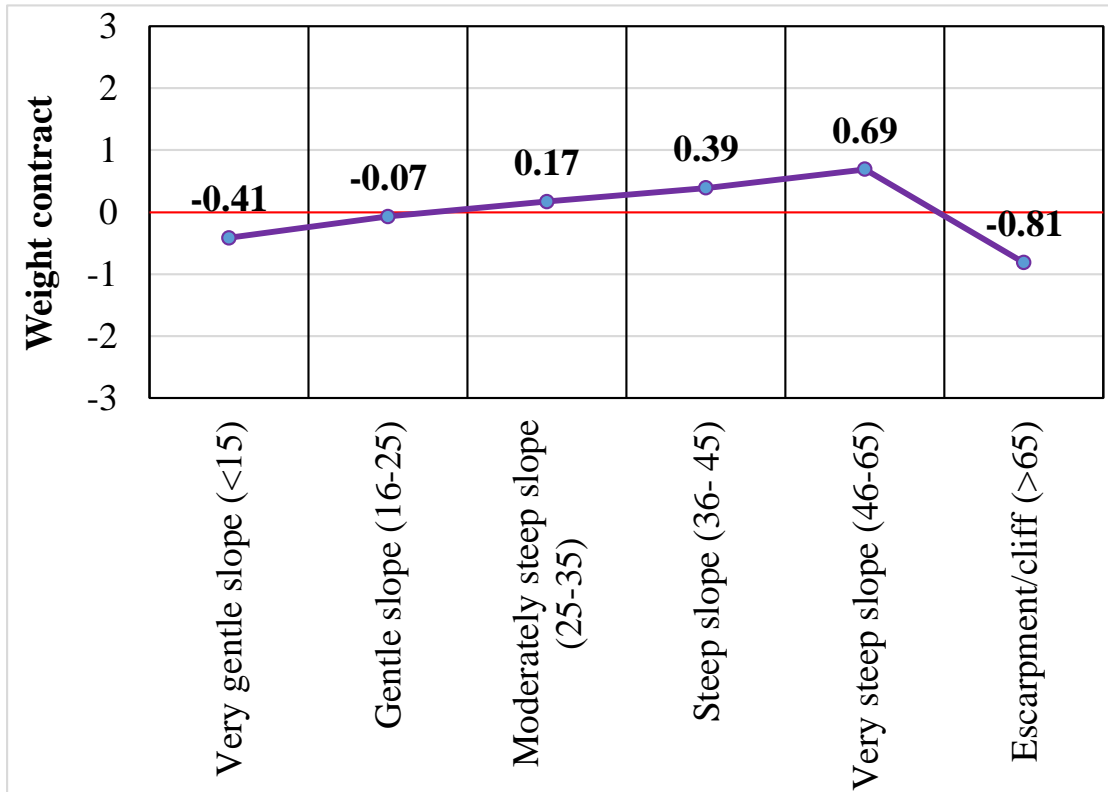
f) Slope aspect
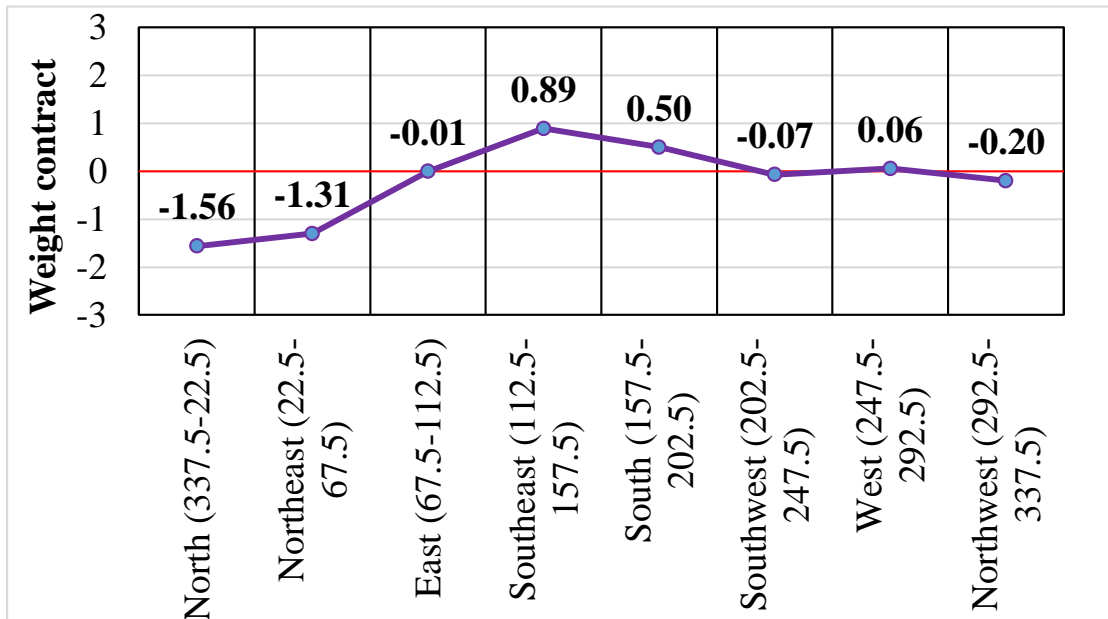
Figure 6.4e-f (continued). Landslide susceptibility causative factors for the study area showing weight contract value, i.e., negative and positive: (**e**) slope, and (**f**) slope aspect.

g) Distance to thrusts
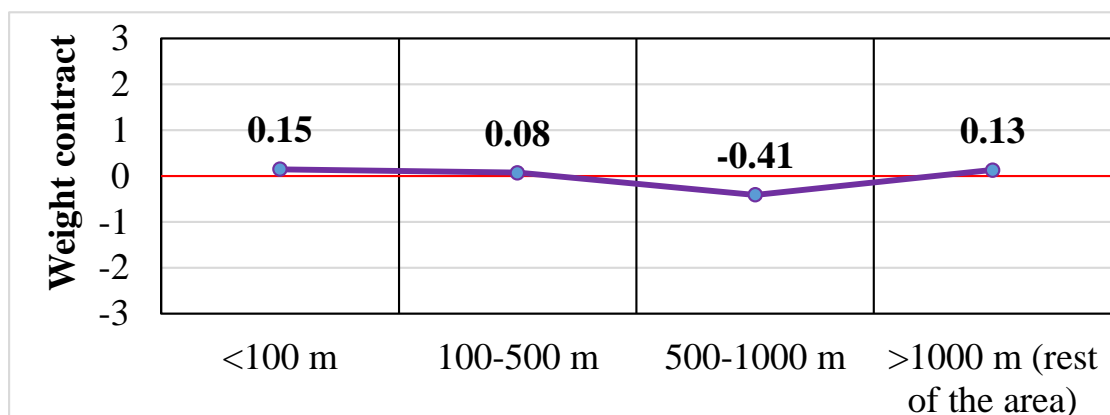
h) Distance to faults
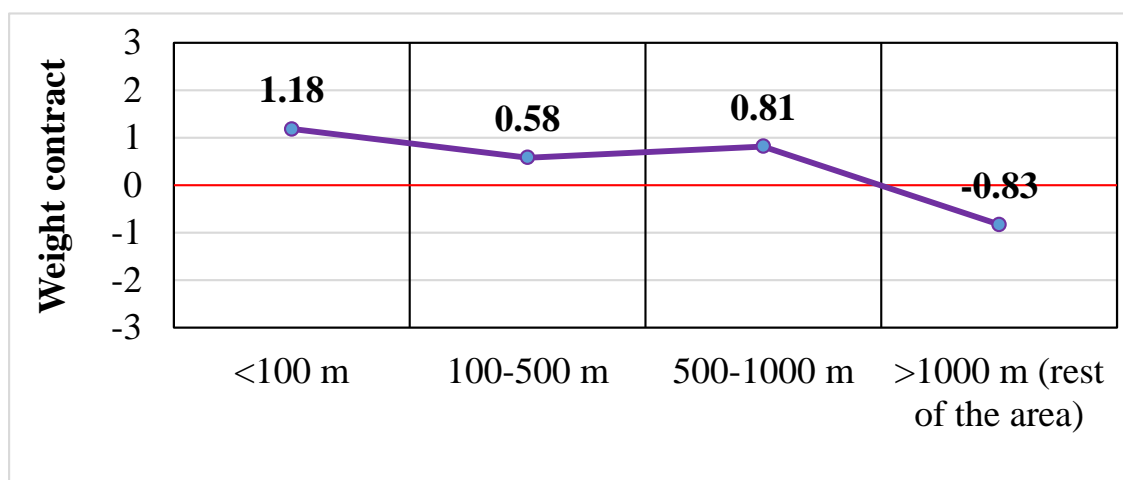
i) Distance to lineaments
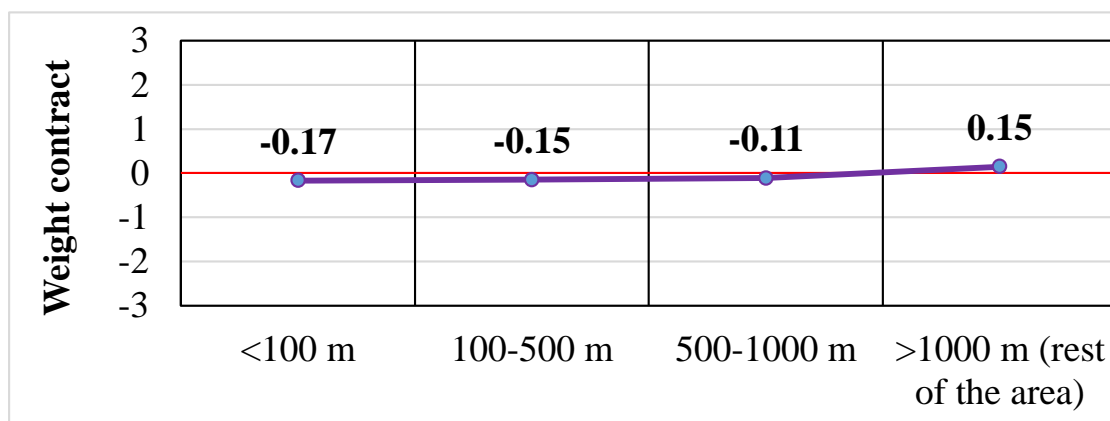
Figure 6.4g-i (continued). Landslide susceptibility causative factors for the study area showing weight contract value, i.e., negative and positive: **(g)** distance to thrusts, **(h)** distance to faults, and **(i)** distance to lineaments.

j) Land-cover
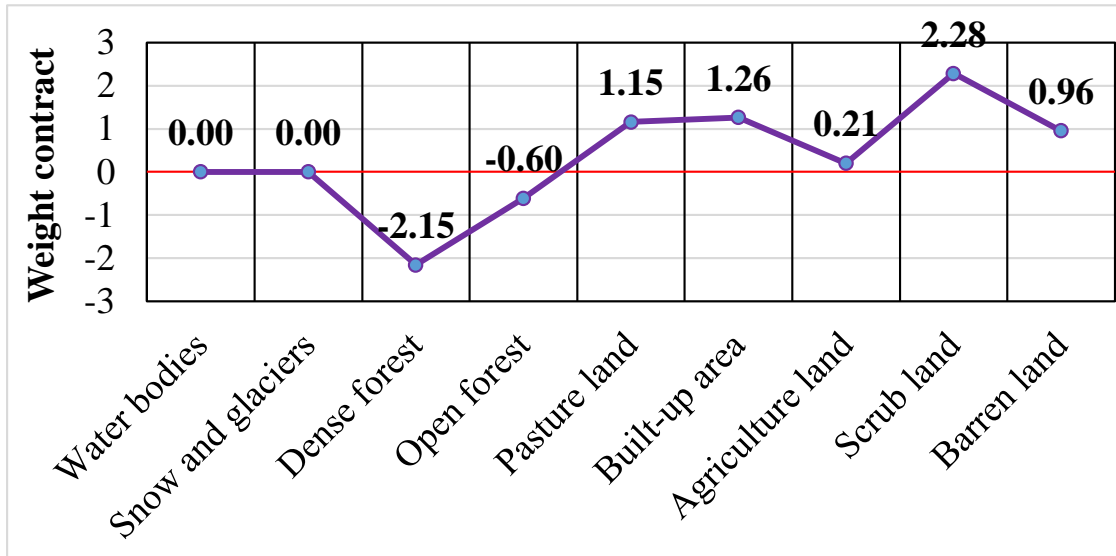
k) Distance to streams
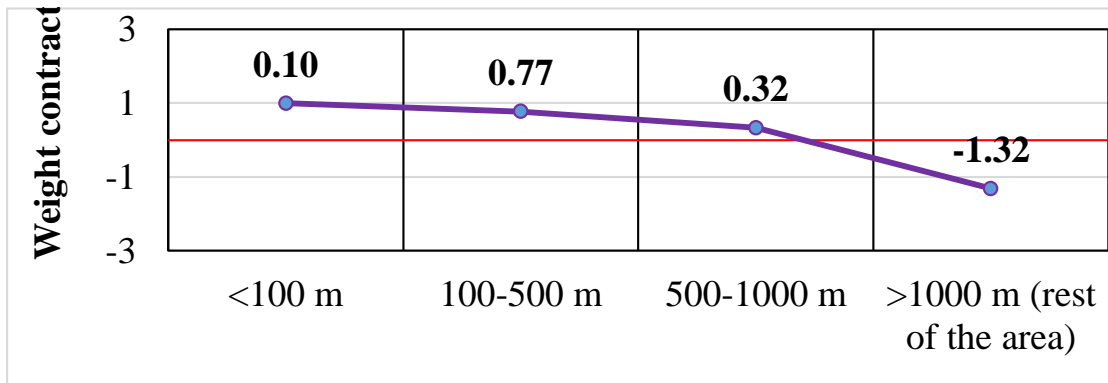
l) Relative relief
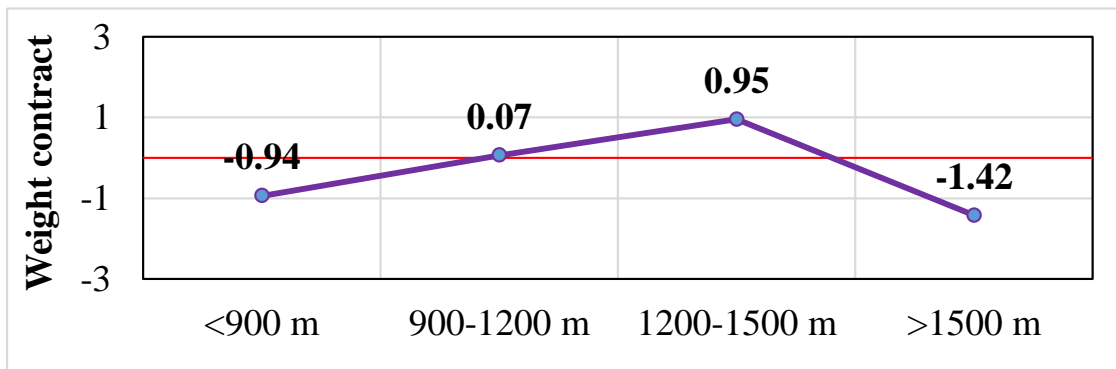
Figure 6.4j-l (continued). Landslide susceptibility causative factors for the study area showing weight contract value, i.e., negative and positive: **(j)** land-cover, **(k)** distance to streams, and **(l)** relative relief.

m) Distance to roads
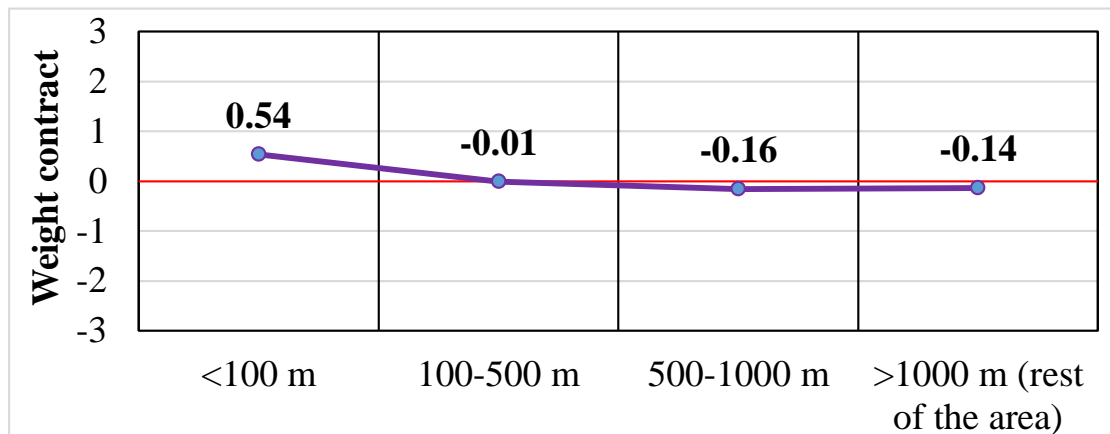
n) Altitude zone based on rainfall
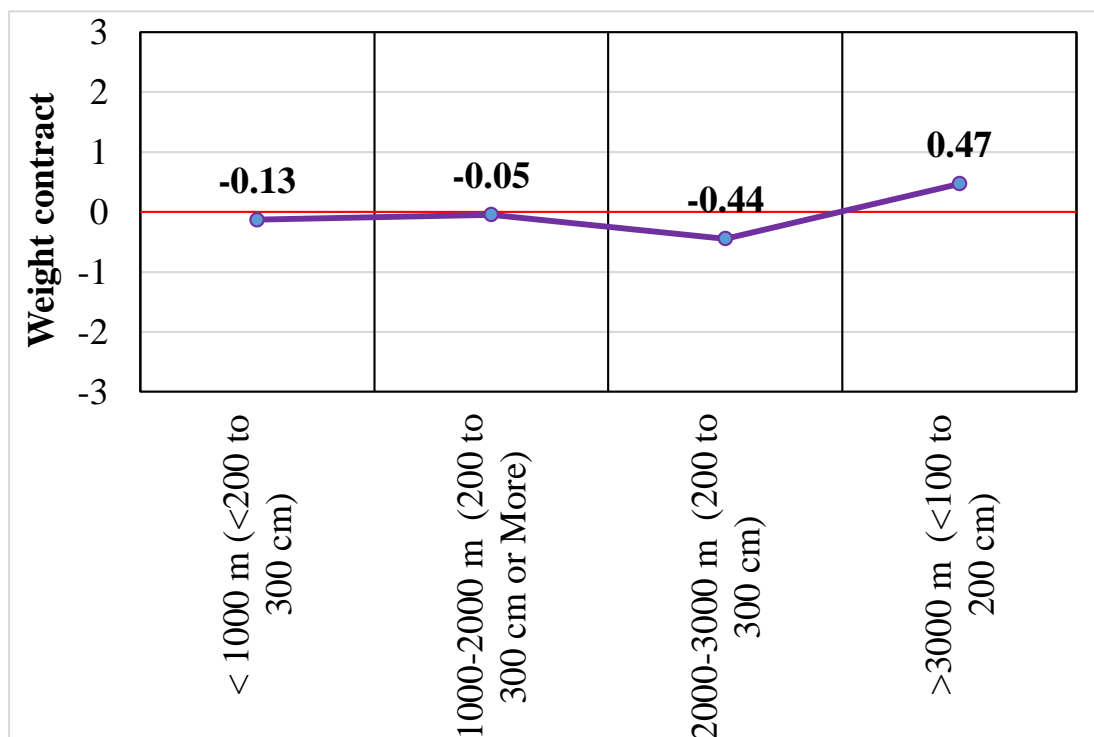
Figure 6.4m-n (continued). Landslide susceptibility causative factors for the study area showing weight contract value, i.e., negative and positive: **(m)** distance to roads, and **(n)** altitude zones based on rainfall.

Chapter 7

Discussion

7.1 Land-use and land-cover (LULC) change

Chapter 3 examined the significant change in land-use and land-cover occurred in the Rudraprayag district between 1976 and 2014. The result shows that the forest is the main land cover in the study area. The overall trend shows that the forest area has decreased and the non-forest area has increased in the district; the overall loss of the forest was 122.35 km^2 from 1976 to 2014. This result agrees with other studies conducted in the Himalayan region of India (Pandit et al., 2007; Sharma et al., 2016). The general trends of the change show an increase in agriculture land, barren land, built-up area, and scrub land. Mountain environments are sensitive to human activities, particularly to land-cover changes (Clawson and Stewart, 1965; Bosch and Hewlett, 1982). New land-cover patterns may occur not only by natural factors but also as a result of a number of anthropogenic activities (Promper, 2014). The local communities depend highly on agricultural activity, which would be further expected to cause a decline in forest cover. For example, Munsi et al., (2009) found that increased agriculture activities and human settlements are major drivers of land-use change in the Indian Himalayan state of Uttarakhand. Other studies also found similar causes of forest decline in the Hindu Kush Himalaya region (Tiwari, 2000; Rao and Pant, 2001; Rautela et al., 2002; Qasim et al., 2011; Uddin et al., 2015; Sharma et al., 2016). Although natural drivers could also play a role in land-use and land-cover change, the scope of this study focused mainly on anthropogenic activities. Loss of forest cover is particularly serious in mountain regions such as the Himalayas, where the landscape has a complex and fragile environment with rough terrain, unique topography, and vulnerability to numerous types of natural hazards. Figures 7.1 and 7.2 show an example of the damages of infrastructure and loss of the forest during the heavy flood disasters that took place on 16th and 17th June 2013. Therefore, the impact of natural drivers such as floods cause hazards on LULC changes should be analysed for further understanding.

The results displayed in Figure 3.1 clearly show that the majority of the agricultural activities and built-up areas are distributed along the roads and river channels at lower and middle altitudes. The significant increase in agriculture land and built-up areas contributed to the change in the forest cover, which indicates the possibility of decrease in the forest cover in the near future. Tourism is an important livelihood option for the

local people during the tourist season in the district. Figure 7.3 shows an example of re-development of infrastructure for tourism activities at Sonprayag in the district.

The continuous increase in the area of barren and scrub land contributed to wasteland land in the study area, which could lead to a huge loss in topsoil and further affect the health of the nearby forests. Significant changes in barren land at higher altitudes may also further contribute to an increase in mass movement and soil erosion (Singh, 1981; Yu et al., 2007; Qasim et al., 2011; Nandy et al., 2011) during heavy rainfall in the district. A drastic increase in barren land at higher altitudes might also result in high run-off during the rainfall season in the steep and narrow channels of the Mandakini valley, which indicates the possibility of increased flood activity in the downstream area (Rautela et al., 2014). A continued increase in scrub land showed that the forest land is degraded at a significant rate. Some of the forest, pasture, agriculture, and built-up areas were lost during the heavy floods that took place on 16th and 17th June 2013 (Gupta et al., 2013). The area under water bodies and snow/glaciers also shows a decreasing trend. This could be due to the temporal variations of snow over the time period.

Figure 7.1. An example of the damages of infrastructure and loss of the forest by the floods at Sonprayag, Rudraprayag district shown in white circle. **(a)**, **(b)**, **(c)**, and **(d)** field photos of different angle of damages of the settlements. **(e)** pre-post disaster and **(f)** post-disaster view shown in Google Earth® images indicate the loss of forest and infrastructure (Photo: Amit Kumar Batar).
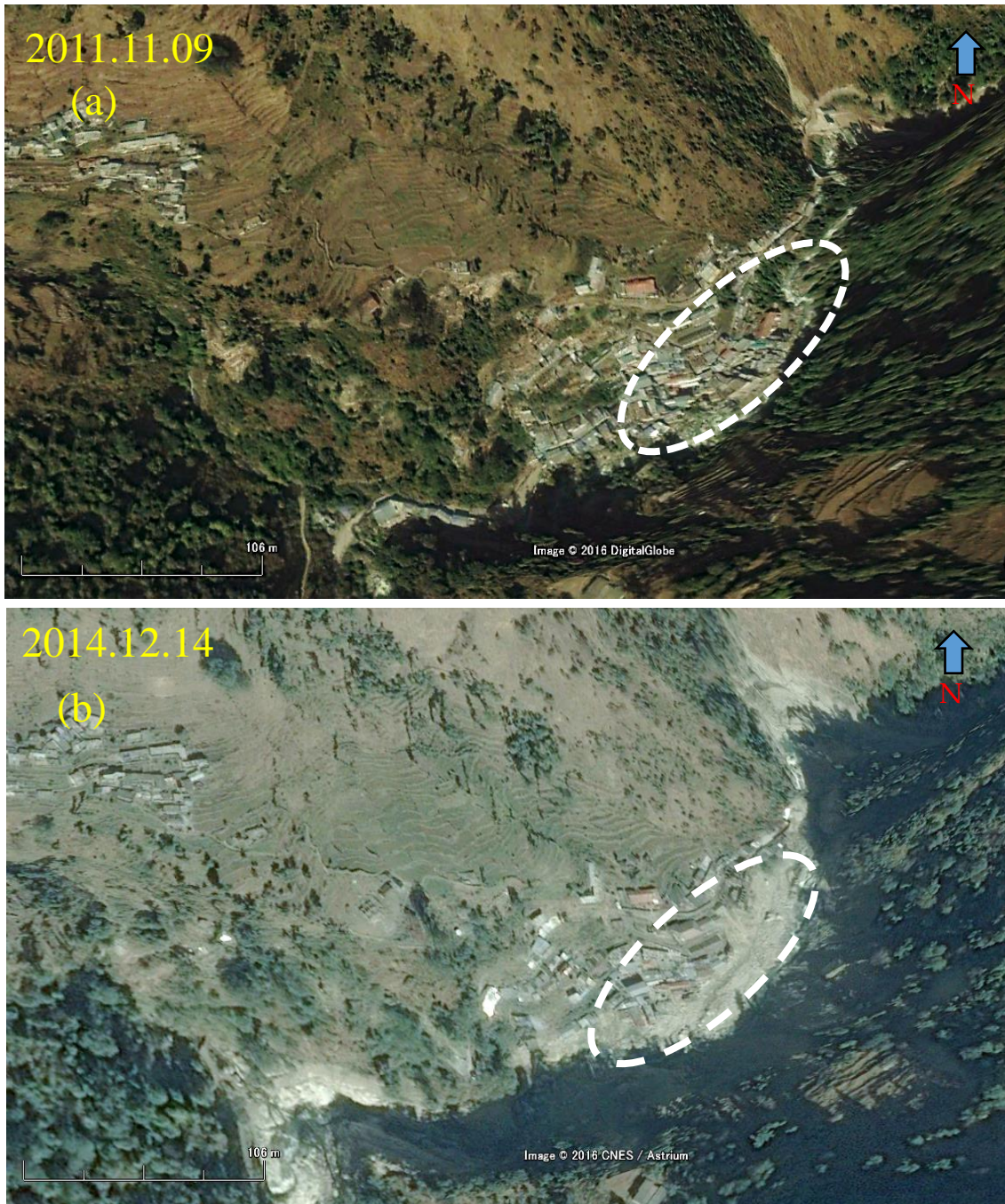
Figure 7.2. An example of damages of settlements by floods at Gurikund, Rudraprayag district in white dashed circle. **(a)** pre-disaster image, **(b)** post-disaster view shown in Google Earth® images
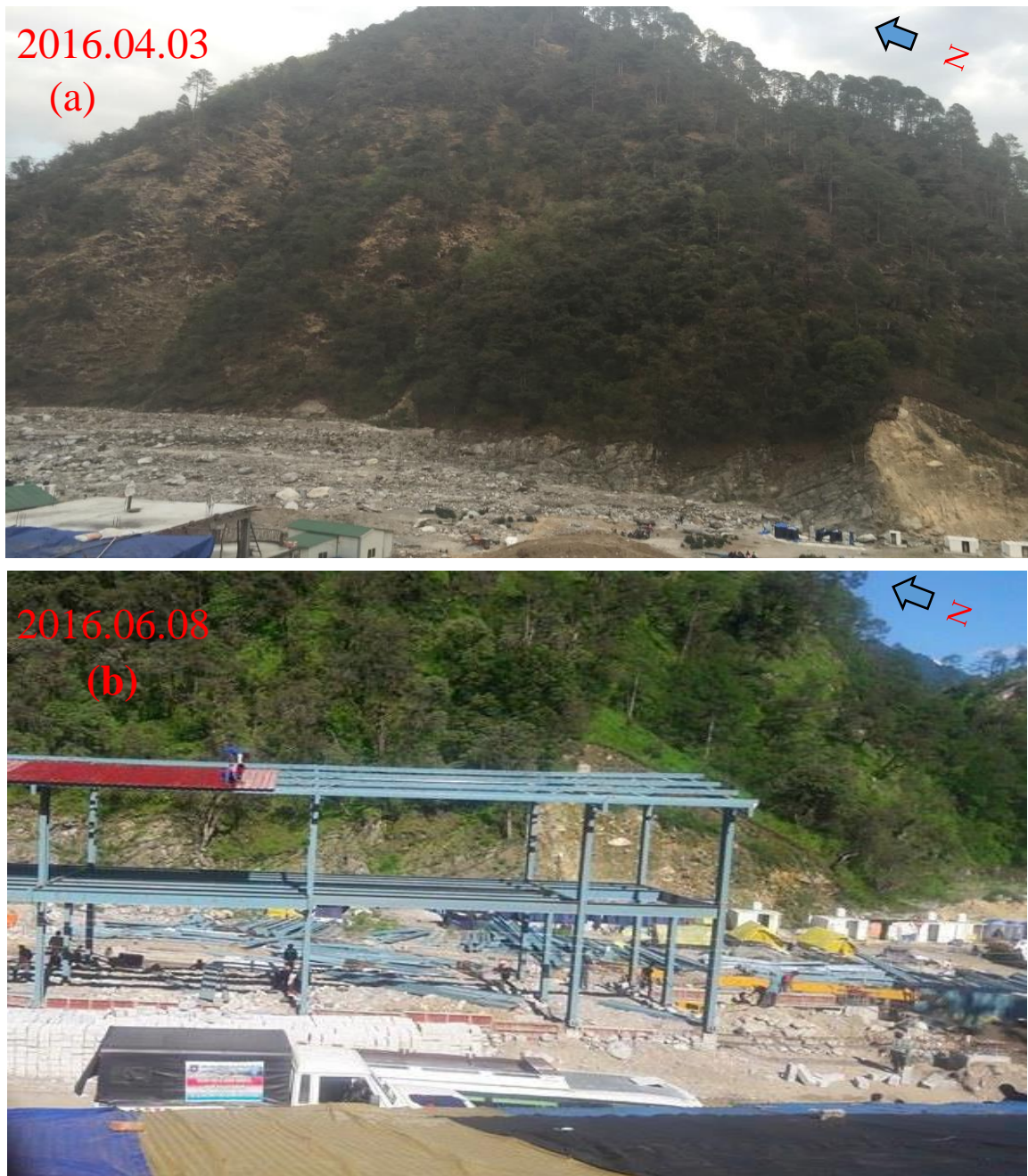
Figure 7.3. An example of re-development of infrastructure for tourism activities at Sonprayag, Rudraprayag district. **(a)** field photo after the damages of infrastructure, and **(b)** re-infrastructure for tourism activities (Photo: Amit Kumar Batar)

7.2 Forest fragmentation

Forest fragmentation has increased because the large core forest was diminished at a significant rate. A continued decrease in the large core forest and an increase in the perforated forest indicate an increase in forest fragmentation. The increase of patch, small core, and medium core forests are indicative of the continuing disconnection of the forests from the large core forest area. The patch forest has increased throughout the study period, completely degraded by the edge effect (Vogt et al., 2007). The result show that significant changes had occurred in the large core forest due to expansion of the non-forest area. The conversion of vegetation cover to non-forest area by human activities has increased forest fragmentation, posing a great threat to biodiversity (Sharma and Roy, 2007), although the increase in forest fragmentation is related to both natural and anthropogenic drivers (Geist and Lambin, 2001). The result of this study suggests that expansion in agriculture and built-up areas are the major drivers for forest fragmentation, where topography has played a significant role in the study area. At the same time the study area is highly vulnerable to natural hazards such as heavy floods, landslides. It is also vulnerable to modification of the forest cover and further increase in forest fragmentation, which would further deteriorate the overall forest landscape.

Fragmentation and the loss of forest by the conversion to agriculture and other land use indicate that the available wildlife habitat is shrinking (Munsi et al., 2009). Therefore, the overall change in forest fragmentation are likely to have a negative impact on the continuity and quantity of the forest land area (Zomar et al., 2016). The trends of forest fragmentation together with the land-cover change have serious impacts on biodiversity, habitat loss, and ecosystem services in the region. Moreover, the pattern of forest fragmentation may vary at a different scale and also depends on the spatial scale or resolution of the data.

In addition, the upper part of the study area is a protected area classified as a wildlife sanctuary. However, due to the disturbance of continuous human activities such as road development, the upward movement of people to higher elevations for agricultural activities, hydro-power projects, and the increase of the built-up area within the sanctuary, the wildlife sanctuary is seriously threatened (Misra et al, 2009), which may change the continuity, quantity, and connectivity of the sanctuary and may reduce the forest land area as a whole.

7.3 Forest fragmentation probability

Several studies have addressed the influence of forest fragmentation changes on forest landscape, either through identifying patch size (Collingham and Huntley, 2013) or through examining forest fragmentation process by a multiple landscape metrics analysis. (O'Neill et al., 1988, 1999; He et al., 2000; Jaeger, 2000). However, to our knowledge there is no study related to the forest fragmentation probability. Therefore, forest fragmentation probability map was prepared using the past evidence (patch forests are degraded forest) and causative factors in chapter 4. Seven causative factors were measured and weighted using the WOE method to create the map of areas susceptible to forest fragmentation. It should be understood that the model performance depends on the quality of the data collected, scale and size of the study area and uncertainties associated with the digitization of the data. The successes rate of the forest fragmentation probability map was checked against observed patch forest. The resulting map of area susceptible to forest fragmentation has a prediction accuracy of 78.6%.

The result of the weighted contrast value showed that the forest fragmentation probability was primarily observed near built-up area (less than 500 m), agriculture land (less than 500 m), roads (less than 1000 m), and streams (less than 500 m) with very gentle and gentle slopes (less than 25 degree) at the lower to middle altitude zone (less than 2000 m). The probability map of the forest fragmentation showed that the role of higher altitude zone (more than 2000 m) is less significant, and that factors such as distance to roads, distance to agriculture land, distance to built-up area and slopes are more important. The analysis of the forest fragmentation probability suggests that the area would experience more forest fragmentation in the future because of the increased areas of patch forest and perforated forest, meaning the increase in the forest degradation.

7.4 Landslide susceptibility

A quantitative model applied to observe landslides and their causative factors was created and illustrated in the susceptibility map (Chapter 5). Fourteen factors that cause landslides were measured and weighted using the WOE method to create the map of areas susceptible to landslides. The successes rate of the landslide susceptibility map was checked against observed landslides. The resulting map of areas susceptible to landslides has a prediction accuracy of 77.8%. It should be understood that model performance depends on the correct identification of the major factors of landslides, quality of the data

collected, number of landslides, scale and size of the study area and uncertainties associated with the digitization of the data. However, due to the difficulty in obtaining multi-temporal landslide inventories and high resolution dataset, the use of quantitative approach based on WOE method with validation has been always impeded in India and has not been widely attempted so far. Moreover, we were unable to evaluate the role of temperature, rainfall and snowmelt to influence landslides even though their potential influence may be important. We think that the result is satisfactory for a study at a regional-scale (1936.06 km^2) study.

The result of landslide susceptibility clearly showed that medium to high landslide susceptibilities had occurred mainly in the non-forest area. The result of the weighted contrast value showed that most of the medium to high landslide susceptibilities are primarily concentrated in the areas adjacent to higher altitudes, steep slopes, and the non-forest area such as scrub land, barren land, and pasture land.

In 1998, the Bureau of Indian Standards (BIS) formulated guidelines for landslide susceptibility zonation on macro scale (1:50,000) for the whole country (BIS, 1998). These guidelines proposed an indirect approach to landslide susceptibility mapping based on a generalized heuristic approach of fixed weighting or ranking of geo-factors without directly or indirectly considering the landslide inventory data (Anbalagan, 1992; Ghosh et al., 2009). This method might be difficult to carry out for landslide hazard mapping in data-scarce environments and without experts knowledge of causative factors. In the past and recent year, many statistical and GIS-based approaches also have been proposed and applied for landslide hazard zonation or landslide susceptibility in many parts of the Indian Himalayas (Gupta and Joshi, 1990; Pauchauri and Pant, 1992; Naithani, 2002; Saha et al., 2002; Sarkar and Kanungo, 2004; Sarkar et al., 2005; Mathew et al., 2007; Asthana and Sah,, 2007; Gupta and Ahmed, 2007; Pradhan and Pirasteh, 2010; Martha et al., 2013). However, only a few studies have attempted in detailing landslide hazard mapping and their validation (Sarkar and Kanungo, 2004; Mathew et al., 2007). A few more studies were also done in comparison to different techniques for better landslide hazard mapping in India (Kanungo et al., 2006). Recently, Gosh et al., (2009) has compared BIS and WOE methods to improve landslide susceptibility mapping in Indian mountains. The experience shows that WOE gives much better results compared to BIS method. Other studies were also conducted in the Western Ghats of India comparing BIS and Multi-criteria analysis (MCA), and Frequency ratio (FR) method. The results show that FR method is more predictable compared to BIS and MCA (Kannan, et al., 2015).

However, identification of the hazardous areas is important for promoting safe human occupation, infrastructure development and environmental protection in mountainous area such as the Himalayas. Therefore, this research will also fill the gap to assess the landslide susceptibility of a hilly area in a raster-based GIS environment, using a quantitative approach based on WOE model.

7.5 Observed potential change of forest fragmentation probability and landslide susceptibility

Several studies have addressed the influence of future land-cover changes on risk, either through identifying risk hotspots (Promper et al., 2014) or through overlaying the scenarios with a hazard map (Barredo and Engelen, 2010). Due to lack of data on landslide hazards, we used a landslide susceptibility map (Malek et al, 2015). Landslide susceptibility analysis has already been used to study the influence of past and current land-cover (Chitu et al., 2015; Reichenbach et al., 2015). Regarding potential changes in forest fragmentation probability and landslide susceptibility (Chapter 6), the results demonstrated that the forest fragmentation probability was observed in the areas where landslides are less likely to occur. These results are not surprising, as the upper part of the study area has less forest cover (Naithani, 2001). Figure 7.4 shows that the distribution of forest fragmentation potential change in zone of landslide susceptibility classes. The potential change of forest fragmentation in area with higher landslide susceptibility cannot be considered insignificant, as the upper and middle parts of the Rudraprayag district are considered as a tourist hotspot. This study also suggests that the probability of landslides would not give a major influence on forest fragmentation and vice versa.
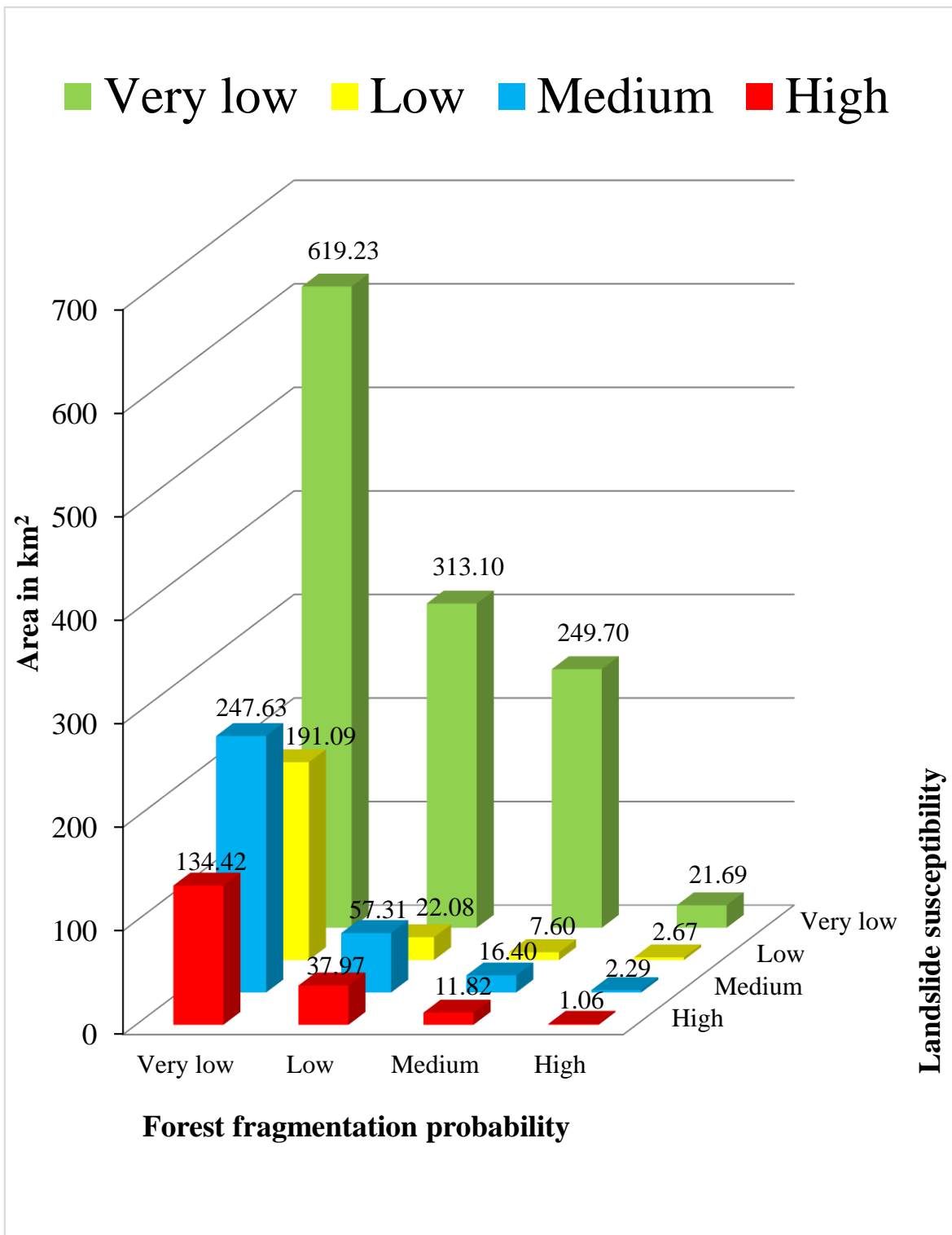
Figure 7.4. Distribution of forest fragmentation potential change in zone of landslide susceptibility classes

Chapter 8
Conclusions

This study focused on land-use and land-cover (LULC) change and forest fragmentation in the Rudraprayag district, a landslide prone district in the Garhwal Himalaya of India. Studies on LULC change and forest fragmentation in the Garhwal Himalaya provide the evidence of replacement of forest covers by agricultural activities and infrastructure development, leading to forest fragmentation. Past and current trends suggest that the area might expect a future increase in forest loss and forest fragmentation. The quantitative method, i.e., weight-of-evidence (WOE) method can be applied to spatial data for producing maps of expected probability of occurrence. In this study WOE was used to create maps of landslide susceptibility and forest fragmentation probability to identify potential changes of forest fragmentation in zone of landslide susceptibility. The resultant susceptibility maps were validated using the receiver operating characteristics (ROCs) based upon the area under curve (AUC) method. The present study showed that remote sensing techniques aided by GIS can provide a useful tool to study on LULC change and forest fragmentation, potential change of forest fragmentation area in zone of landslide susceptibility and vice versa.

The results show that significant change in LULC occurred in the Rudraprayag district between 1976 and 2014. The forest is the main land-cover in the study area. The overall trend shows that the forest area had decreased and the non-forest area had increased in the district. The overall loss of the forest was 122.35 km^2 from 1976 to 2014.

The current and potential forest fragmentation changes occur because of the expansion of agriculture land, built-up areas in the district. The result of the forest fragmentation probability suggested that the area would experience more forest fragmentation near agriculture land and built-up area at lower to middle altitudes in the future. However, it should be understood that forest fragmentation depends on the scale, resolution of the data, and uncertainties associated with the digitization of the data.

The results of the landslide susceptibility clearly showed that most landslide susceptibility area had occurred in the non-forest area at higher altitudes. However, the landslide mechanisms in the Indian Himalayas are very complicated and mainly controlled by geologic conditions. Therefore, additional and detailed geologic information or high-resolution datasets should be used to analyze landslide susceptibility in the future and

more landslide location data are needed.

The potential change of the forest fragmentation in zone of landslide susceptibility showed that probability of landslide would not give a major influence on forest fragmentation; however, forest fragmentation might increase due to an increase in the area of non-forest, perforated forests and patch forests. The forest fragmentation probability map showed that the role of landslide susceptibility on forest fragmentation is less significant, and factors such as distance to roads, distance to agriculture land, distance to built-up area and slopes are more important. The study also indicated that forest fragmentation probability would not give a major influence on landslide susceptibility; however, risk might increase at higher altitudes. Moreover, improved understanding of the drivers, i.e., anthropogenic and natural drivers can help to reveal the dynamics of LULC change and the forest fragmentation process of the Himalayan region at different scales.

This study contributes to the understanding of the spatio-temporal trends in LULC change, pattern of forest fragmentation, changes of the forest fragmentation pattern caused by LULC change as well as potential change of forest fragmentation in the zone of landslide susceptibility and vice versa. Finding the areas where changes have occurred will help to fill the gap necessary to lead to prioritization in forest management, conservation, and biodiversity policies. This study will also fill an information gap regarding area classification, which has been poorly researched with poor data availability heretofore and, will improve information at the regional and national levels.

References

Agarwal, C.; Green, G. M.; Grove, J. M.; Evan, T. P.; Schweik, C. M. (2002). *A review and assessment of land use change models: dynamics of space, time and human choice*.USDA (Forest Services), Technical Report NE–297, 1–67.

Anbalagan, R. (1992). Landslide hazard evaluation and zonation mapping in mountainous terrain. Eng. Geol., 32, 269–277.

Armas, I. (2012). Weights of evidence method for landslide susceptibility mapping, Prahova Sub-carpathians, Romania. Nat. Hazards, 60, 937–950.

Asthana, A. K. L.; Sah, M. P. (2007). Landslides and cloudbursts in the Mandakini Basin of Garhwal Himalaya. Himalayan Geology, 28 (2), 59–67.

Ayalew, L.; Yamagishi, H. (2005). The application of GIS-based logistic regression for landslide susceptibility mapping in the Kakuda-Yahiko Mountains, Central Japan. Geomorphology, 65, 15–31.

Barredo, J. I.; Engelen, G. (2010). Land use scenario modeling for flood risk mitigation. Sustainability, 2, 1327–1344.

Bawa, K. S.; Joseph, G.; Setty, S. (2007). Poverty, biodiversity and institutions in forest-agriculture ecotones in the Western Ghats and Eastern Himalaya ranges of India. Agric. Ecosyst. Environ., 121, 287–295.

Bazilian, M.; Rogner, H.; Howells, M.; Hermann, S.; Arent, D.; Gielen, D.; Steduto, P.; Mueller, A.; Komor, P.; Tol, S.; and Yumkella, K. (2011). Considering the energy, water and food nexus: towards an integrated modelling approach. Energy Policy, 39 (12), 7896–7906.

Beniston, M. (2003). Climate change in mountain regions: A review of possible impacts. Climate Change, 59, 5–31.

Bhat, J. A.; Kumar, M.; Negi, A. K.; Todaria, N. P. (2013). Informants consensus on ethnomedicinal plants in Kedarnath Wildlife Sanctuary of Indian Himalayas. J. Med. Plant Res, 7 (4), 148–154.

BIS. (1998). Preparation of landslide hazard zonation maps in mountainous terrains-Guidelines, Bureau of Indian Standards IS 14496 (Part–2).

Biswas, S.; Khan, D. K. (2013). Habitat fragmentation and nutrient dynamics in tropical dry deciduous forests of West Bengal, India. ARPN J. Sci. Technol., 3, 109–119.

Bonham-Carter, G. F. (2002). Geographic information systems for geoscientist: Modelling with GIS. In: Merriam, D.F. (Ed.), C*omputer Methods in the Geosciences,* Pergamon/Elsevier, New York, 13, 302–334.

Bonham-Carter, G. F.; Agterberg, F.P.; Wright, D.F. (1989). Weights of evidence modelling: a new approach to mapping mineral potential. Statistical Applications in Earth Sciences, 89 (9), 171–183.

Bosch, J. M.; Hewlett, J. D. (1982). A review of catchment experiments to determine the effect of vegetation changes on water yield and evapotranspiration. Journal of Hydrology, 55, 3–23.

Bruschi, V. M.; Bonachea, J.; Remondo, J.; Gómez-Arozamena, J.; Rivas, V.; Barbieri, M.; Capocchi, S.; Soldati, M.; Cendrero, A. (2013). Land management versus natural factors in land instability: some examples in northern Spain. Environ Manag., 52 (2), 398–416.

Cabral, A. I. R.; Vasconcelos, M. J.; Oom, D. and Sardinha, R. (2010). Spatial dynamics and quantification of deforestation in the central-plateau woodlands of Angola (1990-2009). Applied Geography, 31, 1185–1193.

Center for International Earth Science Information Network (CIESIN)-Columbia University, International Food Policy Research Institute (IFPRI), The World Bank, and Centro Internacional de Agricultura Tropical (CIAT). (2011). Global Rural-Urban Mapping Project, Version 1 (GRUMPv1): Population Density Grid. Palisades, NY: NASA Socioeconomic Data and Applications Center (SEDAC). http://dx.doi.org/10.7927/H4R20Z93 (accessed on 1 July 2017).

Center for International Earth Science Information Network (CIESIN)-Columbia University. (2016). Gridded Population of the World, Version 4 (GPWv4): Population density. Palisades, NY: NASA Socioeconomic Data and Applications Center (SEDAC), http://dx.doi.org/10.7927/H4NP22DQ (accessed on 1 July 2017).

Chandra, J.; Rawat, V. S.; Rawat, Y. S.; Ram, J. (2010). Vegetational diversity along an altitudinal range in Garhwal Himalaya. Int. J. of Biodiversity and Conservation, 2 (1), 14–18.

Chettri, N.; Sharma, E.; Deb, D. C.; Sundriyal, R. C. (2002). Impact of firewood extraction on tree structure, regeneration and woody biomass productivity in a trekking corridor of the Sikkim Himalaya. Mt. Res. Dev., 22, 150–158.

Chitu, Z.; Istrate, A.; Adler, M-J et al. (2015). Comparative study of the methods for assessing landslide susceptibility in Ialomita Subcarpathians, Romania. In: Lollino G, Giordan D, Crosta GB et al (eds) *Engineering Geology for Society Territory*, Springer International Publishing, 2, 1205–1209.

Clawson, and Stewart L., (1965). Land use information: A critical survey of U.S. statistics including possibilities for greater uniformity: Baltimore, Md., The Johns Hopkins Press for Resources for the Future, Inc., pp. 402.

Collingham, Y. C.; Huntley, B. (2013). Impacts of habitat fragmentation and patch size upon migration Rates. Ecol. Appl., 10, 131–144.

Congalton, R. G. (1991). A review of assessing the accuracy of classifications of remotely sensed data. Remote Sens. Environ., 37, 35–46.

Coops, N. C.; White, J. D.; Scott, N. A. (2004). Estimating fragmentation effects on simulated forest net primary productivity derived from satellite imagery. International Journal of Remote Sensing, 25, 819–838.

Dahal, R. K.; Hasegawa, S.; Masuda, T.; Yamanaka, M. (2006). Roadside slope failures in Nepal during torrential rainfall and their mitigation. Disaster Mitigation of Debris Flows, Slope Failures and Landslides, 503–514.

Dahal, R. K.; Hasegawa, S.; Nonomura, A.; Yamanaka, M.; Dhakal, S.; Paudyal, P. (2008a). Predictive modelling of rainfall-induced landslide hazard in the Lesser Himalaya of Nepal based on weights-of-evidence. Geomorphology, 102, 496–510.

Dahal, R.K.; Hasegawa, S.; Nonomura, A.; Yamanaka, M.; Masuda, T.; Nishino, K. (2008b). GIS based weights-of-evidence modelling of rainfall-induced landslides in small catchments for landslide susceptibility mapping. Environmental Geology, 54, 311–324.

Dai, F. C.; Lee, C. F. (2001). Frequency-volume relation and prediction of rainfall-induced landslides. Engineering Geology, 9, 253–266.

Dai, F. C.; Lee, C. F. (2002). Landslide characteristics and slope instability modeling using GIS, Lantau Island, Hong Kong. Geomorphology, 42, 213–228.

Duke, C.; Steele, J. (2010). Geology and lithic procurement in Upper Palaeolithic Europe: a weights-of-evidence based GIS model of lithic resource potential. J Archaeol Sci., 37 (4), 813–824.

Fahrig, L. (2003). Effects of habitat fragmentation on biodiversity. Annu Rev Ecol Evol Syst., 34, 487–515.

Fawcett, T. (2006). An introduction to ROC analysis. Pattern Recognition Letters, 27, 861–874.

Fischer, J.; Lindenmayer, D. B. (2007). Landscape modification and habitat fragmentation: a sunthesis. Glob. Ecol. Biogeogr., 16, 265–280.

Foley, J. A. (2005). Global Consequences of land use. Science., 309, 570–574.

Fonji, S. F.; Taff, G. N. (2014). Using satellite data to monitor land-use land-cover change in North-eastern Latvia. Springerplus, 3, 61.

Forest Survey of India (FSI). (2004). *Annual Report, Forest Survey of India, Dehradun, India.*

Forest Survey of India (FSI). (2011). *India State of Forest Report.* Dehradun, India.

Geist, H. J.; Lambin, E. F. (2001). *What Drives Tropical Deforestation; A meta-analysis of proximate and underlying causes of deforestation based on subnational case study evidence.* LUCC report series; 4. Land-Use and Land-Cover Change project. CIACO, Louvain-la-Neuve, Belgium; Vol. 1.

Ghimire, S.; Higaki, D.; Bhattarai, T. (2013). Estimation of soil erosion rates and eroded sediment in a degraded catchment of the Siwalik Hills, Nepal. Land, 2, 370–391.

Ghosh, S.; van Westen, C. J.; Carranza, E. J. M.; Ghoshal, T.; Sarkar, N.; Surendranath, M. (2009). A quantitative approach for improving the BIS (Indian) method of medium-scale landslide susceptibility. Journal of the Geological Society of India, 74, 625–638.

Glade, T. (2003). Landslide occurrence as a response to land use change: a review of evidence from New Zealand. Catena, 51, 297–314.

Gorsevski et al. (2006). Spatially and temporally distributed modeling for landslide susceptibility. Geomorphology, 80, 178–198.

Greenway, D. R. (1987). Vegetation and slope stability. In: M. Gerson, K.S. Richards (Eds.), *Slope stability.* John Wiley and Sons, Chichester, UK, 187–230.

Gupta, A. K; Dobhal, D. P.; Mehta, M.; Verma, A.; Pratap, B.; Kesarwani, K. (2013). *Kedarnath Devastation.* Dehradun, India.

Gupta, R. P.; Joshi, B. C. (1990). Landslide hazard zonation using the GIS approach - A case study from the Ramganga catchment, Himalayas. Engg. Geology, 28, 119–131.

Gupta, V.; Ahmed, I. (2007). Geotechnical characteristics of Surabhi Resort landslide in Mussoorie, Garhwal Himalaya, India. Himalayan Geology, 28 (2), 21–32.

Hansen, A. J.; Dale, R. P.; Flather, V. H.; Iverson, C.; Currie, L. (2001). Global change in forests: Responses of species, communities and biomass. Bioscience, 51, 765–779.

Harris, J. R.; Wilkinson, L.; Grunsky, E. C. (2000). Effective use and interpretation of lithogeochemical data in regional mineral exploration programs: application of Geographic Information Systems (GIS) technology. Ore Geology Reviews, 16 (3–4), 107–143.

He, H. S.; DeZonia, B. E., Mladenoff, D. J. (2000). An aggregation index (AI) to quantify spatial patterns of landscapes. Landsc. Ecol., 15, 591–601.

Huebner, C. D.; Randolph, J. C. (1995). Environmental factors affecting Understory diversity in second-growth deciduous forests. Am. Midl. Nat., 134, 155–165.

Ives, J. D. and Messerli, B. (1989). *The Himalayan dilemma: reconciling development and conservation.* London, Routledge.

Jaeger, J. A. G. (2000). Landscape division, splitting index, and effective mesh size: a new measures of landscape fragmentation. Landsc. Ecol., 15, 115–130.

Jasrotia, A. S.; Singh, R. (2006). Modeling runoff and soil erosion in a catchment area using the GIS in the Himalayan region, India. Environ. Geol., 51, 29–37.

Jensen, J. R. (1996). *Introductory digital image processing: a remote sensing perspective. Upper Saddle River*, New Jersey, Second edition.

Joshi, P. K., R. A.; Narula Sheen, S. V. (2012). Assessing impact of climate change on forest cover type shifts in Western Himalayan Eco-region. J. For. Res., 23, 75–80.

Kannan, M.; Saranathan E.; Anbalagan, R. (2015). Comparative analysis in GIS-based landslide hazard zonation—a case study in Bodi-Bodimettu Ghat section, Theni District, Tamil Nadu. India. Arab J. Geosci., 8, 691-699.

Kanungo, D. P.; Arora, M. K.; Sarkar, S.; Gupta, R. P. (2006). A comparative study of conventional, ANN black box, fuzzy and combined neural and fuzzy weighting procedures for landslide susceptibility zonation in Darjeeling Himalayas. Engineering Geology, 85 (3–4), 347–366.

Karsli, F.; Atasoy, M.; Yalcin, A.; Reis, S.; Demir, O.; Gokceoglu, C. (2009). Effects of land-use changes on landslides in a landslide-prone area (Ardesen, Rize, NE Turkey). Environ Monit Assess., 156, 241–255.

Kayastha, P.; Dhital, M. R.; and De, S. F. (2012). Landslide susceptibility mapping using the weight of evidence method in the Tinau watershed, Nepal. Nat. Hazards, 63, 479–498.

Keefer, D. K. (1984). Landslides caused by earthquakes. Geol. Soc. Am. Bull., 95, 406–421.

Keefer, D. V. (2000). Statistical analysis of an earthquake-induced landslide distribution—the 1989 Loma Prieta, California event. Eng. Geol., 58, 231–249.

Khan, S. M.; Page, S.; Ahmad, H.; Harper, D. (2012). Anthropogenic influences on the natural ecosystem of the naran valley in the Western Himalayas. Pakistan J. Bot., 44, 231–238.

Kittur, S.; Sathyakumar, S. (2010). Assessment of spatial and habitat use overlap between Himalayan tahr and livestock in Kedarnath Wildlife Sanctuary, India. Eur. J. wildllife Res., 56, 195–204.

Klein, G. (2001). Estimating global land use change over the past 300 years, the HYDE data base. Global Biogeochemical Cycles, 15, 417–433.

Kumar, G. (2005). *Geology of Uttar Pradesh and Uttaranchal; Geological Society of India*. Bangalore, India.

Kumar, G.; Agrawal, N. C. (1975). *Geology of the Srinagar-Nandprayag Area (Alakananda Valley), Chamoli, Garhwal and Tehri Garhwal Districts, Kumaun Himalaya, Uttar Pradesh*. Himalayan Geology, 5, 29–59.

Lambin, E. F.; Geist, H. J.; Lepers, E. (2003). Dynamics of land-use and land-cover change in tropical Regions. Annu. Rev. Environ. Resour., 28, 205–241.

Lambin, E. F.; Turner, B. L.; Geist, H. J.; Agbola, S. B.; Angelsen, A.; Folke, C.; Bruce, J. W.; Coomes, O. T.; Dirzo, R.; George, P. S.; Homewood, K.; Imbernon, J.; Leemans, R.; Li, X.; Moran, E. F.; Mortimore, M.; Ramakrishnan, P. S.; Richards, J. F.; Steffen, W.; Stone, G. D.; Svedin, U.; Veldkamp, T. A. (2001). The causes of land-use and land-cover change : moving beyond the myths. Global Environ. Chang., 11, 261–269.

Lasch, P.; Lindner, M.; Erhard, M.; Suckow, F.; Wenzel, A. (2002). Regional impact assessment on forest structure and functions under climate change - The Brandenburg case study. For. Ecol. Manage., 162, 73–86.

Leal, I. R.; Filgueiras, B. K. C.; Gomes, J. P.; Iannuzzi, L.; Andersen, A. N. (2012). Effects of habitat fragmentation on ant richness and functional composition in Brazilian Atlantic forest. Biodivers. Conserv., 21, 1687–1701.

Lee, S.; Choi, J. (2004). Landslide susceptibility mapping using GIS and weight of evidence model. International Journal Geographical Information Science, 18, 789–814.

Lele, N.; Joshi, P. K. (2009). Analyzing deforestation rates, spatial forest cover changes and identifying critical areas of forest cover changes in North-East India during 1972–1999. Environ. Monit. Assesmenttal., 1999, 159–170.

Li, M.; Huang, C.; Zhu, Z.; Wen, W.; Xu, D.; and Liu, A. (2009). Use of remote sensing coupled with a vegetation change tracker model to assess rates of forest change and fragmentation in Mississippi, USA. International Journal of Remote Sensing, 30, 6559–6574.

Liu, J.; Daily, G. C.; Ehrich, P. R.; Luck, G. W. (2003). Effects of household dynamics on resource consumption and biodiversity. Nature, 421, 530–533.

Lung, T.; Schaab, G. (2010). A comparative assessment of land cover dynamics of three protected forest areas in tropical East Africa. Environmental Monitoring and Assessment, 161, 531–548.

Macchi, M.; ICIMOD. (2010). *Mountains of the world- ecosystem services in a time of global and climate change.* Kathmandu: ICIMOD, Nepal.

Magliulo, P.; Di, L. A.; Russo, F. et al. (2008). Geomorphology and landslide susceptibility assessment using GIS and bivariate statistics: a case study in southern Italy. Nat Hazards, 47, 411.

Malamud, B. D.; Turcotte, D. L.; Guzzetti, F.; Reichenbach, P. (2004). Landslide inventories and their statistical properties. Earth Surf. Process. Landforms, 29, 687–711.

Malek, Z.; Boerboom, L.; Glade, T. (2015). Future Forest Cover Change Scenarios with Implications for Landslide Risk: An Example from Buzau Subcarpathians, Romania. Environmental Management, 56 (5), 1228–1243.

Mario, P. M.; Jibson, R. W. (2000). A seismic landslide susceptibility rating of geologic units based on analysis of characteristics of landslides triggered by the 17 January, 1994 Northridge, California earthquake. Eng. Geol., 58, 251–270.

Martha, T. R.; Vinod, K. K. (2013). September, 2012 landslide events in Okhimath, India—an assessment of landslide consequences using very high resolution satellite data. Landslides, 10, 469–479.

Mathew, J.; Jha, V.K.; Rawat, G. S. (2007). Weights of evidence modeling for landslide hazard zonation mapping in part of Bhagirathi valley, Uttarakhand. Current Science, 92, 628–638.

Meusburger, K.; Alewell, C. (2008). Impacts of anthropogenic and environmental factors on the occurrence of shallow landslides in an alpine catchment (Urseren Valley, Switzerland). Nat Hazards Earth Syst Sci., 8, 509–520.

Meyer, B.; Turner II. (1992). Human population growth and global land-use / cover change. Annu. Rev. Ecol. Syst., 23, 39–61.

Miehe, G.; Miehe, S.; Schlütz, F. (2009). Early human impact in the forest ecotone of southern High Asia (Hindu Kush, Himalaya). Quat. Res., 71, 255–265.

Misra, S.; Maikhuri, R. K.; Dhyani, D.; Rao, K. S. (2009). Assessment of traditional rights, local interference and natural resource management in Kedarnath Wildlife Sanctuary. International Journal of Sustainable Development & World Ecology, 16, (6), 404–416.

Mondal, S.; Sharma, N.; Kappas, M.; Garg, P. K. (2015). Critical assessment of land use land cover dynamics using multi-temporal satellite images. Environments, 2, 61–90.

Munsi, M.; Malaviya, S.; Oinam, G.; Joshi, P. K. (2009). A landscape approach for quantifying land-use and land-cover change (1976–2006) in middle Himalaya. Reg. Environ. Chang., 10, 145–155.

Nagendra, H.; Munroe, D.K.; South worth, J. (2004). From pattern to process: landscape fragmentation and the analysis of land use/cover change. Agriculture, Ecosystems and Environment, 101, 111–115.

Naithani, A. K. (2001). The August, 1998 Okhimath tragedy in Rudraprayag district of Garhwal Himalaya, Uttaranchal, India. GAIA, 16, 145–156.

Naithani, A. K.; Kumar, D.; Prasad, C. (2002). The catastrophic landslide of 16 July 2001 in Phata Byung area, Rudrapryag district, Garhwal Himalaya, India. Current Science, 82 (8), 921–923.

Nandi, A.; and Shakoor, A. (2009). A GIS-based landslide susceptibility evaluation using bivariate and multivariate statistical analyses, Eng. Geol., 110, 11–20.

Nandy, S.; Kushwaha, S. P. S.; Dadhwal, V. K. (2011). Forest degradation assessment in the upper catchment of the river Tons using remote sensing and GIS. Ecol. Indic., 11, 509–513.

National Innovations in Climate Resilient Agriculture (NICRA). (2009). *District wise agriculture contingency plans*. *Indian* Council of Agricultural Research (ICAR), Ministry of Agriculture, Government of *India.* http://www.nicra-icar.in/nicrarevised/images/statewiseplans/Uttarakhand/UKD10-Rudraprayag 10.07.14.pdf (accessed on 10 July 2017).

National Remote Sensing Centre (NRSC). (2012). *Report on Okhimath landslides in 2012-satellite based study*. National Remote Sensing Centre (NRSC), Hyderabad, India (accessed on 10 July 2017).

Onojeghuo, A. O.; and Blackburn, G. A. (2011). Forest transition in an ecologically important region: patterns and causes for landscape dynamics in the Niger Delta. Ecological Indicators, 11, 1437–1446.

O'Neill, R.V.; Krummel, J. R.; Gardner, R. H.; Sugihara, G.; Jackson, B.; DeAngelis, D. L.; Milne, B. T.; Turner, M. G.; Zygmunt, B.; Christensen, S.W.; Dale, V. H.; Graham, R. L. (1988). Indices of landscape pattern. Landsc. Ecol., 1, 153–162.

O'Neill, R.V.; Riitters, K. H.; Wickham, J. D.; Jones, K. B. (1999). Landscape patterns metrics and regional assessment. Ecosyst. Health, 5, 233–255.

Pan, X.; Nakamura, H.; Nozaki, T.; Huang, X. (2008). A GIS-based landslide hazard assessment by multivariate analysis. Landslides – J. Jpn. Landslide Soc., 45 (3), 187–195.

Pandit, M. K.; Sodhi, N. S.; Koh, L. P.; Bhaskar, A.; Brook, B. W. (2007). Unreported yet massive deforestation driving loss of endemic biodiversity in Indian Himalaya. Biodivers. Conserv., 16, 153–163.

Pandit, M.; Kumar, V. (2013). Land-use change and conservation challenges in the Indian Himalaya: past, present, and future. In: Navjot, S.S., Gibson, L., Raven, P.H. (Eds.), *Conservation Biology: Voices from the Tropics*. Wiley, Chichester, UK.

Paolini, L.; Grings, F.; Sobrino, J. A.; Jiménez Muñoz, J. C.; Karszenbaum, H. (2006). Radiometric correction effects in landsat multi-date/multi-sensor change detection studies. Int. J. Remote Sens., 27, 685–704.

Papathoma-Kohle, M.; Glade, T. (2013). The role of vegetation cover change for landslide hazard and risk. In: Renaud FG, Sudmeier- Rieux K, Estrella M (eds) *The role of ecosystems in disaster risk reduction.* UNU-Press, Tokyo, 293–320.

Pauchauri, A. K; and Pant, M. (1992). Landslide hazard mapping based on geological attributes, Engg. Geol., 32, 81–100.

Perez, M. J.; Kobayashi, H.; Matsumura, I. (2005). Analysis of land use change in Comayagua County, Honduras, based on remote sensing and field survey data. J.JASS., 21, 199–208.

Pradhan, B., (2010). Landslide susceptibility mapping of a catchment area using frequency ratio, fuzzy logic and multivariate logistic regression approaches. J. Indian Soc. Remote Sens., 38 (2), 301–320.

Pradhan, B.; Pirasteh, S. (2010). Comparison between prediction capabilities of neural network and fuzzy logic techniques for landslide susceptibility mapping. Disaster Adv., 3 (3), 26–35.

Promper, C.; Puissant, A.; Malet, J. P.; Glade, T. (2014). Analysis of land cover changes in the past and the future as contribution to landslide risk scenarios. Journal of Applied Geography, 53, 11–19.

Puyravaud, J. P. (2003). Standardizing the calculation of the annual rate of deforestation. For. Ecol. Manage., 177, 593–596.

Qasim, M.; Hubacek, K.; Termansen, M.; Khan, A. (2011). Spatial and temporal dynamics of land use pattern in District Swat, Hindu Kush Himalayan region of Pakistan. Appl. Geogr., 31, 820–828.

Raghuvanshi, T. K.; Ibrahim, J.; Ayalew, D. (2014). Slope stability susceptibility evaluation parameter (SSEP) rating scheme – an approach for landslide hazard zonation. J. Afr. Earth Sci., 99, 595–612.

Rao, K. S.; Pant, R. (2001). Land use dynamics and landscape change pattern in a typical micro watershed in the mid elevation zone of central Himalaya, India. Agriculture Ecosystem Environment, 86, 113–124.

Rasul, G. (2010). The role of the Himalayan mountain systems in food security and agricultural sustainability in South Asia. International Journal of Rural Management, 6 (1), 95–116.

Rautela, P.; Rakshit, R.; Jha, V.K.; Gupta, R. K.; and Munsi, A. (2002). GIS and remote sensing-based study of the reservoir-induced land-use/land-cover changes in the catchment of Tehri dam in Garhwal Himalaya, Uttarakhand (India). Current Science, 83 (3), 308–311.

Rautela, P.; Sajwan, K. S.; Khanduri, S.; Ghildiyal, S.; Rawat, C.; Rawat, A. (2014). *Geological investigations in Rudraprayag district with special reference to mass instability*; Dehradun, India.

Rautela, P.; Thakur, V.C. (1999). Landslide hazard zonation in Kaliganga and Madhyamaheshwar valleys of Garhwal Himalaya: A GIS based approach Himalayan. Geology, 20 (2), 31–44.

Regmi, N. R.; Giardino, J. R.; Vitek, J.D. (2010). Modeling susceptibility to landslides using the weight of evidence approach: western Colorado, USA. Geomorphology, 115, 172–187.

Reichenbach, P.; Busca, C.; Mondini, A.C.; Rossi, M. (2015). Land use change scenarios and landslide susceptibility zonation: the Briga Catchment Test Area (Messina, Italy). In: Lollino G, Manconi A, Clague J et al (eds) *Engineering Geology for Society and Territory, Springer International Publishing,* 1, 557–561.

Richards, J. A. (2006). *Remote Sensing Digital Image Analysis*. Fifth Edit., Springer, Heidelberg.

Roy, P. S.; Behera, M. D.; Murthy, M. S. R.; Roy, A.; Singh, S.; Kushwaha, S. P. S.; Jha, C. S.; Sudhakar, S.; Joshi, P. K.; Reddy, C. S. et al. (2015). New vegetation type map of India prepared using satellite remote sensing: comparison with global vegetation maps and utilities. International Journal of Applied Earth Observation and Geoinformation, 39, 142–159.

Roy, P. S.; Tomar, S. (2000). Biodiversity characterization at landscape level using geospatial modelling technique. Biol. Conserv., 95, 95–109.

Saha, A. K.; Gupta, R. P.; Arora, M. K. (2002). GIS based landslide hazard zonation in the Bhagirathi (Ganga) Valley, Himalaya. Int. J. Remote Sensing, 23 (2), 357–369.

Sarkar, S.; Kanungo, D. P. (2004). An integrated approach for landslide susceptibility mapping using remote sensing and GIS. Photogramm Eng Remote Sens., 70 (5), 617–625.

Sarkar, S.; Kanungo, D. P.; Patra, A. K. (2005). Landslides in the Alaknanda Valley of Garhwal Himalaya. Quarterly Journal of Engineering Geology and Hydrogeology, 39, 79–82.

Sati, V. P. (2012). Agricultural Diversification in the Garhwal Himalaya: A spatio-temporal analysis. Sustain. Agric. Res., 1, 77–86.

Sato, H.; Harp, E. (2009). Interpretation of earthquake-induced landslides triggered by the 12 May 2008, M7. 9 Wenchuan earthquake in the Beichuan area, Sichuan Province, China using satellite imagery and Google Earth. Landslides, 6, 153–159.

Schuster, R. L.; Fleming, R. W. (1986). Economic losses and fatalities due to landslides. Bull. Am. Assoc. Eng. Geol., 23 (Zˇ1), 11–28.

Shalaby, A.; Tateishi, R. (2007). Remote sensing and GIS for mapping and monitoring land cover and land-use changes in the Northwestern coastal zone of Egypt. Appl. Geogr., 27, 28–41.

Sharma, M.; Areendran, G.; Raj, K.; Sharma, A.; Joshi, P. K. (2016). Multitemporal analysis of forest fragmentation in Hindu Kush Himalaya: A case study from Khangchendzonga Biosphere Reserve, Sikkim, India. Environ. Monit. Assess., 188 (10), 596.

Sharma, S.; Palni, L. M. S. and Roy, P. S. (2001). Analysis of fragmentation and anthropogenic disturbances in the Himalayan forests: use of remote sensing GIS. Asian Journal of Geoinformatics, 2(4), 63–69.

Sharma, S.; Roy, P. S. (2007). Forest fragmentation in the Himalaya: A Central Himalayan case study. Int. J. Sustain. Dev. World Ecol., 14, 201–210.

Shrestha, U. B.; Gautam, S.; Bawa, K. S. (2012). Widespread climate change in the Himalayas and associated changes in local ecosystems. PLoS One, 7, 1–10.

Shrivastava, Kumar, S. Maximum devastation occurred in areas of maximum forestland diversion. http://www.downtoearth.org.in/news/maximum-devastation-occurred-in-areas-of-maximum-forestland-diversion-41483 (accessed on 10 Feburary 2017).

Singh, J. (2006). Sustainable development in Indian Himalayan region: linking ecological and economic concerns. Curr. Sci., 90(6), 784–788.

Singh, S. (1981). Soil conservation and afforestation for moderating/ mitigating floods. Indian National Science Academy, New Delhi, 114.

Singh, S. P.; Sharma, C. (2009). Tropical ecology: an overview. Trop. Ecol., 50 (1), 7–21.

Singh, S. P.; Singh, J. S. (1991). Analytical conceptual plan to reforest central Himalaya for sustainable development. Environ. Manage., 15, 369–379.

Sivrikaya, F. G.; Cakir, A. I.; Kadiogullari, S.; Keles, E. S.; Baskent, T. S. (2007). Evaluating land use/land cover changes and fragmentation in the Camli Forest Planning Unit of north-eastern Turkey from 1972 to 2005. Land Degradation and Development, 18, 383–396.

Sterlacchini, S. et. al. (2011). Spatial agreement of predicted patterns in landslide susceptibility maps. Geomorphology, 125 (1), 51–61

Sundriyal, R. C.; Sharma, E. (1996). Anthropogenic pressure on tree structure and biomass in the temperate forest of Mamlay watershed in Sikkim. For. Ecol. Manage., 81, 113–134.

Tang, J.; Wang, L.; Yao, Z. (2008). Analyses of urban landscape dynamics using multi-temporal satellite images: acomparison of two petroleum-oriented cities. Landscape and Urban Planning, 87, 269–278.

Tasser, E.; Mader, M.; Tappeiner, U. (2003). Effects of land use in alpine grasslands on the probability of landslides. Basic Appl. Ecol. 4, 271–280.

Thomas, E. D.; Jason, S. S.; Franco, B. (2015). A Weights-of-Evidence model for mapping the probability of fire occurrence in Lincoln County, Nevada, Annals of the Association of American Geographers, 99, (4), 712–727.

Tiwari, P. (2008). Land use changes in Himalaya and their impacts on environment, society and economy: A study of the lake region in Kumaon Himalaya, India. Adv. Atmos. Sci., 25, 1029–1042.

Tiwari, P. C. (2000). Land-use changes in Himalaya and their impact on the plains ecosystem: Need for sustainable land use. Land use policy, 17, 101–111.

Tiwari, P. C.; Joshi, B. (2014). Environmental Changes and their impact on rural water, food, livelihood, and health security in Kumaon Himalayas. J. Urban Reg. Stud. Contemp. India, 1, 1–12.

Tropeano, D.; Turconi, L. (2004). Using historical documents for landslide, debris flow and stream flood prevention. Applications in northern Italy. Natural Hazards, 31 (3), 663–679.

Uddin, K.; Chaudhary, S.; Chettri, N.; Kotru, R.; Murthy, M.; Prasad, R.; Ning, W.; Man, S.; Krishna, S. (2015). The changing land cover and fragmenting forest on the roof of the World : A case study in Nepal's Kailash Sacred Landscape. Landsc. Urban Plan., 141, 1–10.

Vakhshoori, V.; and Zare, M. (2016). Landslide susceptibility mapping by comparing weight of evidence, fuzzy logic, and frequency ratio methods, Geomatics, Natural Hazards and Risk, 7 (5), 1731–1752.

Van Beek, L. P. H.; Van Asch, T. W. J. (2004). Regional assessment of the effects of land-use change on landslide hazard by means of physically based modelling. Nat Hazards, 31, 289–304.

Van Den E. M. P. J.; Van, G. M.; Van, R. A.; Vandekerckhove, L. (2009). How do humans interact with their environment in residential areas prone to landsliding? A case study from the Flemish Ardennes. In: Proceedings of the international conference on ''landslide processes: from geomorphologic mapping to dynamic modelling,'' Strasbourg, France, 6–7 February 2009, 19–24.

Van Westen, C. J.; Castellanos, E.; Kuriakose, S. L. (2008). Spatial data for landslide susceptibility, hazard, and vulnerability assessment: An overview. Engineering Geology, 102, 112-131.

Van, Westen, C. J.; Rengers, N.; Soeters, R. (2003). Use of geomorphological information in indirect landslide susceptibility assessment. Nat Hazards, 30 (3), 399–419.

Vanacker, V.; Vanderschaeghe, M.; Govers, G.; Willems, E.; Poesen, J.; Deckers, J.; De, B. B. (2003). Linking hydrological, infinite slope stability and land-use change models through GIS for assessing the impact of deforestation on slope stability in high Andean watersheds. Geomorphology, 52, 299–315.

Vogt, P.; Riitters, K. H.; Estreguil, C.; Kozak, J.; Wade, T. G.; Wickham, J. D. (2007). Mapping spatial patterns with morphological image processing. Landsc. Ecol., 22, 171–177.

Wakeel, A.; Rao, K. S.; Maikhuri, R. K.; Saxena, K. G. (2005). Forest management and land use/cover changes in a typical micro watershed in the mid elevation zone of Central Himalaya, India. Forest Ecology and Management, 213, 229–242.

Wang, X.; Niu, R. (2009). Spatial forecast of landslides in three gorges based on spatial data mining. Sensors, 9, 2035–2061.

Xu, C.; Xu, X.; Dai, F., Saraf, A. (2012). Comparison of different models for susceptibility mapping of earthquake triggered landslides related with the 2008 Wenchuan earthquake in China. Comput. Geosci., 46, 317–329.

Xu, C.; Xu, X.; Lee, Y. H.; Tan, X.; Yu, G.; and Dai, F. (2012). The 2010 Yushu earthquake triggered landslide hazard mapping using GIS and weight of evidence modeling, Environ. Earth Sci., 66, 1603–1616.

Yalcin, A. (2008). GIS-based landslide susceptibility mapping using analytical hierarchy process and bivariate statistics in Ardesen (Turkey): comparisons of results and confirmations. Catena, 72, 1–12.

Yesilnacar, E.; Topal, T. (2005). Landslide susceptibility mapping: A comparison of logistic regression and neural networks methods in a medium scale study, Hendek region (Turkey). Eng. Geology, 79, 251–266.

Yi, J.; Bin, Y.; Jingtao, C.; Jianwu, H.; Gaoliao, J. (2010). Analysis of landslides susceptibility to different land use patterns in Enshi. In: Proceedings of the 2nd

conference on environmental science and information application technology, 17–18 July 2010, Wuhan, China.

Yu, H.; Joshi, P. K.; Das, K. K.; Chauniyal, D. D.; Melick, D. R.; Yang, X. (2007). Land use /cover change and environmental vulnerability analysis in Birahi Ganga sub-watershed of the Garhwal Himalaya, India. Trop. Ecol., 48, 241–250.

Zeng, Y.; Schaepman, M. E.; Wu, B.; Clevers, J.; and Bregt, A. K. (2008). Scaling based forest structural change detection using an inverted geometric-optical model in the three Gorges region of China. Remote Sensing of Environment, 112, 4261–4271.

Zomar, R. J.; Ustin, S. L.; Carpenter, C. C. (2016). Land cover change along tropical and subtropical Riparian Corridors within the Makalu Barun national park and conservation area. International Mountain Society. Mt. Res. Dev., 21, 175–183.

Appendices

Appendix 1. Forest fragmentation causative factors, forest fragmentation causative factor classes, number of factor class pixels and patch forest pixels and weights of the factor classes

Factors	Sub-categories of factors	Factor in pixels	Patch forest in pixel	Weight positive (W^+)	Weight negative (W^-)	Weighted contrast $(C = W^+ - W^-)$
Slope angle	Very gentle slope (<15)	575782	11988	0.18	-0.07	0.25
	Gentle slope (16–25)	903786	16785	0.07	-0.05	0.12
	Moderately steep slope (25–35)	550607	7778	-0.21	0.06	-0.27
	Steep slope (36–45)	205845	2496	-0.36	0.03	-0.39
	Very steep slope (46–65)	40137	536	-0.27	0.00	-0.27
	Escarpment/cliff (> 65)	3335	38	-0.43	0.00	-0.43
Slope aspect	North (0–22.5) (337.5–360)	318461	4149	-0.29	0.04	-0.33
	Northeast (22.5–67.5)	268993	4646	-0.01	0.00	-0.01
	East (67.5–112.5)	271970	5433	0.14	-0.02	0.16
	Southeast (112.5–157.5)	282497	5024	0.02	-0.00	0.02
	South (157.5–202.5)	362493	6855	0.08	-0.02	0.10
	Southwest (202.5-247.5)	262630	5389	0.17	-0.02	0.19
	West (247.5–292.5)	260253	5019	0.10	-0.01	0.11
	Northwest (292.5–337.5)	252195	3106	-0.35	0.03	-0.38
Distance to streams	<100 m	122674	3662	0.55	-0.04	0.59
	100–500 m	465023	11548	0.36	-0.12	0.48
	500–1000 m	510838	10222	0.14	-0.04	0.18
	>1000 m	1180957	14189	-0.37	0.29	-0.66
Distance to roads	<100 m	187787	9661	1.12	-0.19	1.31
	100–500 m	446530	15436	0.71	-0.27	0.98
	500–1000 m	299332	5765	0.10	-0.02	0.12
	>1000 m	1345843	8759	-0.99	0.64	-1.63
Altitudes zone based on rainfall	<1000 m (<200 to 300 cm)	145488	4823	0.66	-0.06	0.72
	1000–2000 m (200 to 300 cm or More)	837147	26509	0.61	-0.65	1.26
	2000–3000 m (200 to 300 cm)	678327	1648	-1.98	0.31	-2.29
	>3000 m (<100 to 200 cm)	618530	6641	-0.49	0.13	-0.62
Distance to agriculture land	<100 m	158806	9879	1.32	-0.21	1.53
	100–500 m	567515	20539	0.75	-0.44	1.19
	500–1000 m	370273	1609	-1.40	0.13	-1.53
	>1000 m	1182898	7594	-1.01	0.52	-1.53

Appendix 1 (continued). Forest fragmentation causative factors, forest fragmentation causative factor classes, number of factor class pixels and patch forest pixels and weights of the factor classes

Factors	Sub-categories of factors	Factor in pixels	Patch forest in pixel	Weight positive (W^+)	Weight negative (W^-)	Weighted contrast $(C = W^+ - W^-)$
Distance to built-up area	<100 m	129662	8039	1.32	-0.19	1.51
	100–500 m	570851	21215	0.78	-0.48	1.26
	500–1000 m	307558	2625	-0.72	0.08	-0.80
	>1000 m	1271421	7742	-1.06	0.60	-1.66

Appendix 2. Landslide causative factors, landslide factor classes, number of factor class pixels and landslide pixels and weights of the factor classes

Factors	Sub-categories of factor	Factor in pixel	Landslide inventory pixel	Weight positive (W⁺)	Weight negative (W⁻)	Weighted contrast (C = W⁺ - W⁻)
	Garnetiferous gneiss, Schist, Migmatite	690727	4424	0.64	-0.49	1.13
	Porphyritic gneiss and Mica schist	222299	1224	0.49	-0.07	0.56
	Gneiss, Garnetiferous schist and cale zone	328929	608	-0.60	0.07	-0.67
	Granite gneiss, Mica schist and cale zone	150999	701	0.32	-0.03	0.35
	Granite	171812	122	-1.56	0.06	-1.62
Geology	Schistose quartzite	35237	17	-1.95	0.01	-1.96
	Phyllite	57147	21	-2.22	0.02	-2.24
	Phyllite slate	20578	11	-1.84	0.01	-1.85
	Quartzite and Phyllite	152909	121	-1.45	0.05	-1.50
	Quartzite	407792	367	-1.32	0.15	-1.47
	Dolomite limestone	5304	7	-0.94	0.00	-0.94
	Metabasics	35759	81	-0.40	0.01	-0.41
	Shallow colluvium zone	389679	1267	-0.04	0.01	-0.05
	Thick Colluvium zone	961000	1888	-0.54	0.27	-0.81
Geomorphology	Colluvium terrace	259494	559	-0.45	0.05	-0.50
	Alluvium zone	495930	3022	0.59	-0.25	0.84
	Alluvium terrace	49132	798	1.57	-0.09	1.66
	Glacier	120865	28	-2.70	0.05	-2.75
	Glacier terrace	3392	142	2.52	-0.02	2.54

Appendix 2 (continued). Landslide causative factors, landslide factor classes, number of factor class pixels and landslide pixels and weights of the factor classes

Factors	Sub-categories of factor	Factor in pixel	Landslide inventory pixel	Weight positive (W⁺)	Weight negative (W⁻)	Weighted contrast (C = W⁺ - W⁻)
Slope angle	Very gentle slope (<15)	575782	1407	-0.32	0.09	-0.41
	Gentle slope (16–25)	903786	2927	-0.04	0.03	-0.07
	Moderately steep slope (25–35)	550607	2115	0.13	-0.04	0.17
	Steep slope (36– 45)	205845	984	0.35	-0.04	0.39
	Very steep slope (46–65)	40137	266	0.67	-0.02	0.69
	Escarpment/cliff (> 65)	3335	5	-0.81	0.00	-0.81
Slope aspect	North (337.5–22.5)	318461	254	-1.44	0.12	-1.56
	Northeast (22.5–67.5)	268993	270	-1.21	0.10	-1.31
	East (67.5–112.5)	271970	914	-0.01	0.00	-0.01
	Southeast (112.5–157.5)	282497	1972	0.73	-0.16	0.89
	South (157.5–202.5)	362493	1826	0.40	-0.10	0.50
	Southwest (202.5–247.5)	262630	832	-0.06	0.01	-0.07
	West (247.5–292.5)	260253	924	0.05	-0.01	0.06
	Northwest (292.5–337.5)	252195	712	-0.18	0.02	-0.20
Soil type	Loamy skeletal	141470	550	0.14	-0.01	0.15
	Loamy	540229	355	-1.64	0.22	-1.86
	Fine loamy	1063036	5238	0.38	-0.51	0.89
	Coarse loamy	335880	946	-0.18	0.03	-0.21
	Sandy skeletal	198877	615	-0.09	0.01	-0.10

Appendix 2 (continued). Landslide causative factors, landslide factor classes, number of factor class pixels and landslide pixels and weights of the factor classes

Factors	Sub-categories of factor	Factor in pixel	Landslide inventory pixel	Weight positive (W^+)	Weight negative (W^-)	Weighted contrast ($C = W^+ - W^-$)
Soil depth	Very shallow	445956	294	-1.63	0.18	-1.81
	Shallow	547231	3392	0.61	-0.31	0.92
	Moderate shallow	791487	1202	-0.80	0.26	-1.06
	Moderate deep	91624	484	0.46	-0.02	0.48
	Deep	403194	2332	0.54	-0.17	0.71
Distance to thrusts	<100 m	30599	120	0.15	-0.00	0.15
	100–500 m	121140	439	0.08	-0.00	0.08
	500–1000 m	144499	332	-0.39	0.02	-0.41
	>1000 m (rest of the area)	1983254	6813	0.02	-0.12	0.13
Distance to faults	<100 m	15462	168	1.17	-0.01	1.18
	100–500 m	63013	372	0.56	-0.02	0.58
	500–1000 m	79237	581	0.77	-0.04	0.81
	>1000 m (rest of the area)	2121780	6583	-0.09	0.74	-0.83
Distance to lineaments	<100 m	33209	95	-0.17	0.00	-0.17
	100–500 m	162592	478	-0.14	0.01	-0.15
	500–1000 m	234322	716	-0.10	0.01	-0.11
	>1000 m (rest of the area)	1849369	6415	0.03	-0.12	0.15

Appendix 2 (continued). Landslide causative factors, landslide factor classes, number of factor class pixels and landslide pixels and weights of the factor classes

Factors	Sub-categories of factor	Factor in pixel	Landslide inventory pixel	Weight positive (W⁺)	Weight negative (W⁻)	Weighted contrast (C = W⁺ - W⁻)
	Water bodies	7681	000	0.00	0.00	0.00
	Snow and glaciers	57494	000	0.00	0.00	0.00
	Dense forest	1059185	707	-1.62	0.53	-2.15
	Open forest	531247	1093	-0.49	0.11	-0.60
Land use/ cover	Pasture land	235587	2066	0.95	-0.20	1.15
	Built-up area	9980	118	1.25	-0.01	1.26
	Agriculture land	167871	683	0.19	-0.02	0.21
	Scrub land	66930	1762	2.05	-0.23	2.28
	Barren land	143517	1145	0.85	-0.11	0.96
	<100 m	122674	1027	0.91	-0.09	0.10
Distance to streams	100–500 m	465023	2750	0.56	-0.21	0.77
	500–1000 m	510838	2203	0.24	-0.08	0.32
	>1000 m (rest of the area)	1180957	1724	-0.84	0.48	-1.32
	<900 m	782287	1308	-0.71	0.23	-0.94
Relative relief	900–1200 m	885815	3115	0.04	-0.03	0.07
	1200–1500 m	483683	3172	0.66	-0.29	0.95
	>1500 m	127707	109	-1.38	0.04	-1.42

Appendix 2 (continued). Landslide causative factors, landslide factor classes, number of factor class pixels and landslide pixels and weights of the factor classes

Factors	Sub-categories of factor	Factor in pixel	Landslide inventory pixel	Weight positive (W^+)	Weight negative (W^-)	Weighted contrast ($C = W^+ - W^-$)
Distance to roads	<100 m	187787	1026	0.48	-0.06	0.54
	100–500 m	446530	1500	-0.01	0.00	-0.01
	500–1000 m	299332	880	-0.14	0.02	-0.16
	>1000 m (rest of the area)	1345843	4298	-0.06	0.08	-0.14
Altitude zone based on rainfall	< 1000 m (<200 to 300 cm)	145488	435	-0.12	0.01	-0.13
	1000-2000 m (200 to 300 cm or more)	837147	2748	-0.03	0.02	-0.05
	2000–3000 m (200 to 300 cm)	678327	1647	-0.33	0.11	-0.44
	>3000 m (<100 to 200 cm)	618530	2874	0.32	-0.15	0.47

Appendix 3. Area of potential change of forest fragmentation in zone of landslide susceptibility

		Landslide susceptibility (Area in km^2)				
	Classes	Very low	Low	Medium	High	Total
Forest fragmentation probability (Area in km^2)	**Very low**	619.23	313.10	249.70	21.69	1203.72
	Low	191.09	22.08	7.60	2.67	223.44
	Medium	247.63	57.31	16.40	2.29	323.63
	High	134.42	37.97	11.82	1.06	185.27
	Total	1192.37	430.46	285.52	27.71	1936.06